Explicit Bound states and Resonance fields in Effective Field Theories

Jaume Tarrús Castellà

Explicit Bound States and Resonance fields in Effective Field Theories

by

Jaume Tarrús Castellà

Memòria presentada a la
UNIVERSITAT DE BARCELONA
per a optar al títol de Doctor

Tesi dirigida per:
Joan Soto Riera and Pere Talavera Sànchez

Programa de Doctorat de Física
DEPARTAMENT DE ESTRUCTURA I CONSTITUENTS DE LA MATÈRIA

Barcelona, 2012

To my family

ACKNOWLEDGEMENTS

Vull agrair a en Joan Soto i a en Pere Talavera la oportunitat de fer la meva tesi Doctoral sota la seva direcció. En especial vull agrair-los la seva paciència, per haver-me guiat, i per tenir sempre la porta oberta per discutir i per resoldre el meus dubtes (que n'hi ha hagut molts!). He aprés molta física treballant amb ells. També vull agrair els seu encoratjament i suport per a viatjar a escoles, congressos, workshops i estàncies.

I would like to thank Aneesh Manohar and Gilberto Colangelo for hosting my stays abroad. They were both very kind. I'm very grateful they proposed me very interesting projects and the time they spend guiding me through them. I learn a lot from them. I also want to express my deepest gratitude to Andreas Fuhrer and Massimiliano Procura who made my stays (at San Diego and Bern respectively) so much more enjoyable. Working with them has been a pleasure, and they taught me many little things I would have been embarrassed to ask anyone else. I want to thank my office mate in San Diego, Grigor Aslanyan, for being so welcoming.

Haig d'agrair també a l'Assumpta Parreño per convidar-me a fer un seminari, i a en Federico Mescia per les útils discussions sobre estadística i guiar-nos en els articles de Lattice.

Als meus companys de despatx al llarg dels anys, Carlos, Míriam, Alessandro, Jose Maria, Arnau, Marc i Juan, agrair-los l'exel·lent convivència i per totes les vegades que m'han ajudat a resoldre dubtes de LaTeX, beques, i burocràcies vàries.

Als companys de Llicenciatura, Master i Doctorat, amb qui he compartit discussions, dubtes, problemes ja fos a l'aula, la biblioteca o al bar, gràcies per mantenir la meva motivació en l'estudi de la física, i compartir els moments meravellosos que succeïxen quan finalment entens alguna cosa!

In the writting of the theoretical background of this thesis I made extensive use of the reviews in Refs.[1, 2, 3, 4, 5].

Finalment, vull donar les gràcies a en Francesc Sunyol per deixar-me fer servir la seva plantilla de LaTeXper a aquesta tesi.

Financial support from *Agència de Gestió d'Ajuts Universitaris I de Recerca* under a predoctoral FI fellowship and from *Ministerio de Educación* under a predoctoral FPU program fellowship is acknowledged.

Jaume Tarrús Castellà
Barcelona, April 2012

CONTENTS

LIST OF FIGURES

LIST OF TABLES

BREU RESUM EN CATALÀ

La Cromodinàmica Quàntica (QCD) és la teoria de les interaccions fortes [6, 7, 8]. La QCD tracta de interaccions entre quarks i gluons, i és part del Model Estàndard. La QCD és una teoria gauge no Abeliana and el grup de color $SU(3)$ com a grup gauge. La naturalesa no Abeliana de la teoria es manifesta de forma dramàtica. Mentres que la interacció entre objectes amb carrega de color és dèbil a curtes distàncies, o a alts moments de transferència (llibertat asimptòtica [6, 9, 10]); és forta a distancies llargues ($\lesssim$ 1fm) o a baixes energies, el que condueix al confinament del quarks en objectes sense color, el hadrons [11]. En conseqüència la QCD permet un anàlisis perturbatiu a altes energies, mentres que a baixes energies és altament no pertorbativa.

Una idea important que és implícita en totes les descripcions de fenòmens físics és la de teoria efectiva [12]. La premisa bàsica de les teories efectives és que la dinàmica a baixes energies (o distancies llarges) no depen dels detalls de la dinàmica d'altes energies (o distàncies curtes). Com a resultat, la física de baixes energies pot ser descrita per un Lagrangià efectiu que contingui només els graus de llibertat rellevants a baixes energies, sense tenir en compte de manera explicita possibles graus de llibertat addicionals presents a altes energies. És important adonar-se que els graus de llibertat de baixes energies no tenen per què ser els graus de llibertat fonamentals de la teoria original. Per exemple a QCD, els graus de llibertat fonamentals són els quarks i gluons, però els graus de llibertat més adequats per descriure la física de baixes energies són els hadrons.

Una teoria efectiva descriu la física de baixes energies en termes d'uns pocs paràmetres. Aquest paràmetres de baixa energia poden ser, en principi, calculats en termes de la teoria fonamental d'altes energies. Aquest càlcul es pot portar a terme quan la teoria d'altes energies és pertorbativa, com per exemple Electrodinàmica Quàntica, però quan la teoria està fortament acoblada, com és el cas de QCD, s'han de fer servir tècniques no pertorbatives com per exemple càlculs numèrics en el reticle. En tots els casos els paràmetres de baixes energies es poden ajustar a les dades experimentals. Els efectes de la dinàmica d'altes energies en la teoria de baixes energies estan codificats en els acoblaments de baixes energies i en forma de lligams de simetria sobre la teoria de baixes energies.

Teoria de Pertorbacions Quiral (χPT), és una teoria efectiva de QCD [13, 14]. Els graus de llibertat de χPT són els estats de menor massa de QCD, l'octet de mesons pseudoescalars (π , K, η). χPT está basada en el mecansime de ruptura espontánia de simetria Quiral, explotant d'aquesta manera la naturalesa dels mesons com a bosons de Goldstone. La ruptura explícita de simetria, deguda a les masses finites dels quarks, es tradueix en el mecanisme de alineament del buit i és responsable de la generació de les masses dels mesons [15]. S'ha de desenvolupar un comptatge de potencies per tal determinar quins termes del Lagrangià i quins diagrames de Feynamn són necessaris per calcular les amplituds fins a una determinada precisió. Els resulats es poden organitzar en potencies p/Λ_χ, on p és el moment extern, que pren valors de l'ordre de la massa del pió $p \sim m_\pi$. Λ_χ és el cut–off de la teoria, i normalment es pren de l'ordre de la massa del primer estat de QCD que no és un bosó de Goldstone, el mesó ρ.

χPT pot ser aplicada a les interaccions dels bosons de Goldstone amb altres partícules [16, 17, 18], a les que ens referirem com a camps de matèria. La clau per introduir els camps de matèria al Lagrangià Quiral, és que tots els estats de QCD transformen com representacions irreductibles del subgrup no trencat de la simetria Quiral. La introducció de camps pesats introdueix un problema addicional al introduir una nova escala gran, la massa del camp pesat, que trenca el comptatge de potències. Una forma possible de solucionar el problema és utilitzar la Heavy Baryon expansion [19, 20], o tècniques alternatives que mantenen la simetria Lorentz explícita, com per exemple Infrared Renormalization [21]. Una aplicació particularment interessant d'aquest formalisme és la teoria efectiva per descriure les interaccions nuclears, acoblant el doblet dels nucleons al Lagrangià Quiral [22, 23]. Inclús usant el formalisme de la Heavy Baryon expansion pel Lagrangià per pions i nucleons el comptatge de potencies Quiral presenta problemes degut a l'aparició de singularitats que punxen el camí d'integració. En el sector de dos nucleons. Es pot argumentar que els propagadors dels nucleons s'han de contar com $\sim m_N/m_\pi^2$ (on m_N és la massa dels nucleons) en determinades situacions en comptes de la estimació naïf $\sim 1/m_\pi$. En el primer cas la energia cinètica s'ha de resumar als propagadors dels nucleons.

Com hem mencionat abans, en la construcció de un teoria efectiva de camps és crucial la determinació del graus de llibertat rellevants. Una situació interessant es presenta quan els graus de llibertat de baixes energies poden formar estats lligats, estats virtuals o ressonàncies pròximes al llindar. Com que aquest estats estan a prop del llindar afecten a les amplituds de dispersió, però tan-

mateix no poden ser descrites utilitzant teoria de pertorbacions, ja que les series polinòmiques finites en el moment no poden generar un pol en l'amplitud. Aquest pols es poden obtenir resumant certes classes de diagrames, per exemple usant tècniques d'unitarització, que no són consistents amb el comptatge de la teoria efectiva, o alternativament assumint un augment de l'importància de certs acoblaments, com per exemple a Ref.[76]. En aquest últim cas s'han de calcular les equacions del grup de renormalització per a tots els acoblaments per tal de determinar-ne el tamany correcte, el que dificulta mantenir la sèrie pertorbativa sota control. És una vella observació de Weinberg [24, 25, 26] que la inclusió explícita d'estats lligats i ressonàncies com a graus de llibertat de la teoria efectiva millora la convergència de la teoria de pertorbacions. Es pot entendre fàcilment aquesta millora de la convergencia ja que les amplituds de dispersió tindran la estructura analítica correcta. Un dels temes principals d'aquesta tesi ha sigut explorar aquest fet dins d'un marc modern de teories efectives.

La teoria de camps al reticle és un marc matemàtic ben definit per a la formulació no pertorbativa de QCD [27]. La idea és remplaçar l'espai–temps de Minkowsky quadri–dimensional per un reticle discret en un espai quadri– dimensional Euclidià. La teoria de camps al reticle introdueix un cut–off ultravi-olat d'entrada i dona una definició no pertorbativa de l'integral funcional. Els camps fermiònics viuen als nusos del reticle i el camps de gauge als enllaços. Com que l'acció dels quarks és quadràtica, la integral es pot dur a terme exactament, després els gluons es poden integrar numèricament utilitzant mètodes de Monte Carlo. A part dels efectes sistemàtics deguts al espaiat no nul del reticle i al seu volum finit, les simulacions de QCD al reticle produeixen resultats exactes en el reticle donat, exepte errors estadístics.

És natural combinar χPT i QCD al reticle. QCD al reticle, tot i que té una alt grau de precisió, encara s'esta calculant fent servir valors de la massa dels quarks més grans que els valors físics. χPT es pot fer servir per descriure la dependència en la massa dels quarks dels observables de QCD de baixa energia que es calculen amb QCD al reticle. Per tant χPT proporciona les fórmules per les extrapolacions Quirals dels resultats de QCD al reticle des de valors alts no físics de les masses dels quarks fins al valors físics. Així doncs, combinant QCD al reticle amb χPT, podem obtenir prediccions de QCD per la física de baixes energies de les interaccions fortes. D'altra banda, les masses dels quarks poden ser variades de forma contínua en els cálculs al reticle, això permet un mètode alternatiu per determinar les constants de baixa energia de χPT. Al costat del mètode tradicional d'extraure el valor de les constants de baixa energia ajustant

les expressions de χPT a les dades experimentals, les constants de baixa energia es poden obtenir ajustant a dades de simulacions al reticle per a diferents valors de les masses dels quarks.

El treball original d'aquesta tesi està als capítols 4 i 5. Al capítol 4 hem construït una teoria efectiva Quiral pel sistema nucleó–nucleó que conté camps dibariònics com a graus de llibertat fonamentals. Les longituds de dispersió grans en els canals ${}^1S_0$ i ${}^3S_1$ forcen les masses residuals dels dibarions a ser molt més petites que la massa del pió. Hem organitzat els cálculs en una sèrie de teories efectives, que s'obtenen de forma seqüencial integrant les escales d'alta energia i moments alts. Primer integrem les escales d'energia de la massa del pió. Això porta a una teoria efectiva amb només nucleons i dibarions, pNNEFT. Per tri–moments molt més petits que la massa del pió, és convenient també integrar els moments de l'ordre de la massa del pió, el que duu a $\not\pi$NNEFT.

Hem calculat les amplituds de dispersió nucleó–nucleó per energies inferiors a la massa del pió pels canals ${}^1S_0$ i ${}^3S_1$–${}^3D_1$ fins a tercer ordre. Per tri–moments de l'ordre de la massa del pió, les amplituds de dispersió han estat calculades en pNNEFT, per moments molt més petits que la massa del pió en $\not\pi$NNEFT. Els resultats numèrics dels desfasaments i de l'angle de mescla són similars a aquells obtinguts amb el mètode de Kaplan, Savage i Wise [76]. S'observa una bona descripció pel canal ${}^1S_0$, però pel canal ${}^3S_1$–${}^3D_1$ les nostres expressions també fallen a descriure les dades. El motiu s'ha de buscar en l'iteració del potencial d'intercanvi d'un pió. Això pot ser interpretat com una indicació que els pions potencials han de ser iterats fins a tots els ordres, tal com va proposar originalment Weinberg [22]. La proposta de Weinberg però, no pot acomodar de forma natural els tamanys de les longituds de dispersió i presenta problemes de renormalització.

Hem calculat les masses residuals dels dibarions i els acoblaments nucleó–dibarió fins a segon order (NLO). Hen demostrat que certes classes de diagrames que contribueixen a la massa residual, involucrant n pions potencials i pions de radiació, han de ser resumats. En el canal ${}^3S_1$ això és possible ja que la resumació dels diagrames amb qualsevol nombre de n pions potencials és possible. En el canal ${}^1S_0$ aquesta resumació no és possible, però és molt probable que les contribucions dels loops siguin igualment grans. Fent servir els resultats obtinguts per les masses residuals dels dibarions i els acoblaments nucleó–dibarió per $\not\pi$NNEFT hem donat formules d'extrapolació Quiral per les inverses de les longituds de dispersió dels canals ${}^1S_0$ i ${}^3S_1$ fins a correccions d'ordre $\mathcal{O}\left(m_\pi^3/\Lambda_\chi^2\right)$ que depenen de tres paràmetres independents lliures. Hem ajustat aquestes expres-

sions a dades de simulacions al reticle i hem comparat els resultats amb estudis previs de la dependència en la massa dels quarks de les longituds de dispersió.

La teoria efectiva per al sistema nucleó–nucleó amb camps dibariònics que es presenta en aquesta tesi té un comptatge de potències simple i és renormalitzable. Com que cap contraterme ha sigut augmentat, com en [76], l'analisi dimensional naïf és suficient per estimar el tamany del les constants de baixa energia, mantenint l'expansió pertorbativa sota control. Les masses residuals petites permeten acomodar de forma natural els valors grans de les longituds de dispersió. La mala convergencia del canal ${}^3S_1$ és deguda a que l'interacció del pions de potencial és important en aquest canal, el que indica que s'haurien de resumar. Fins que no es sàpiga fer aquesta resumació, la descripció de les interaccions nuclears a a partir de QCD a través de QCD serà incompleta. Creiem que, un cop formulat un mètode per resumar els pions potencials, NNEFT amb camps dibariònics és un formalisme natural per a la descripció de les forces nuclears.

Al capítol 5 hem considerat la possiblitat que l'espectre de QCD en el limit Quiral contingui un isosinglet escalar amb massa molt mes petita que l'escala hadroníca típica Λ_χ, i hem construït una teoria efectiva que l'inclou conjuntament amb els pseudo–bosons de Goldstone, χPT_S. En el sector purament escalar de la teoria hem argumentat que les autointeraccions de la l'escalar poden ser ignorades. Imposant que l'escalar no es mescla amb el buit conjuntament amb la simetria Quiral, resulta en que dues de les constants de baixa energia s'han de agafar com a zero.

El model sigma lineal té els mateixos graus de llibertat que χPT_S. Tanmateix hem apuntat dos diferències claus. El mecanisme de la ruptura espontània de la simetria Quiral està contingut en el model sigma lineal, el que produeix lligams entre els acoblaments de baixa energia. D'altra banda a χPT_S la ruptura espontània de simetria succeïx a una escala d'alta energia desconeguda, el que dona com a resultat que els acoblaments de baixa energia són independents entre ells. Com a conseqüència χPT_S té més llibertat per descriure les dades de simulacions al reticle. La segona diferència important és que χPT_S és una teoria efectiva i com a tal hi ha un forma consistent de millorar la precisió dels càlculs.

Hem presentat el càlcul de la constant de decaïment i de la massa del pió a NLO. El camp escalar dinàmic introdueix noves no analicitats en les dependències de les masses dels quarks d'aquest observables, i requereix la renormalització de B_0 i F_0, que és absent a χPT. Hem fet servir dades de simulacions en el reticle de Ref.[125] per ajustar les constants de baixa energia. Els $\chi^2_{d.o.f}$ obtinguts pels ajustos de χPT_S són similars als de χPT, el que indica que les dades de sim-

ulacions en el reticle no afavoreixen una teoria sobre l'altra. Tanmateix, quan extraiem el valor de el promig de les masses dels quarks lleugers del ajust, χPT$_S$ produeix valors que són més pròxims als obtinguts de simulacions en el reticle que els extrets usant χPT.

Les expressions de χPT$_S$ per les longituds de dispersió pió–pió de ona S són diferents de les de χPT a primer ordre. A més a més χPT$_S$ permet el càlcul de l'amplitud de decaïment de la sigma. Fent servir els valors de la massa i l'amplitud de decaïment de la sigma de Ref.[121] en la formula que hem obtingut de l'amplitud de decaïment podem obtenir el valor de l'únic paràmetre lliure de les expressions de les longituds de dispersió. Utilitzant aquest valor a podem obtenir els valors de les longituds de dispersió. Els valors obtinguts tant per a la longitud de dispersió del canal d'espin i isospin zero (a_0^0) com per la del canal d'espin zero i isospin dos (a_0^2) no són pròxims als valors experimentals. Tanmateix el valor de a_0^0 és lleugerament més pròxim al obtingut a nivell arbre utilitzant χPT, mentres que el valor de a_0^2 és molt més llunyà. Hem argumentat, usant el limit de desacoblament, que això és degut importants correccions de NLO degudes a valors grans de ℓ_1. També hem mostrat que es pot extreure els valors la massa i l'amplitud de decaïment de la sigma a partir de les dades de les simulacions al reticle, fent servir els valors dels paràmetres obtinguts de l'ajust de les expressions de les longituds de dispersió, deixant tots els paràmetres lliures.

INTRODUCTION

Quantum Chromodynamics (QCD) is the theory of strong interactions [6, 7, 8]. It deals with quarks, gluons and their interactions and is part of the Standard Model of Particle Physics. QCD is a non–Abelian gauge field theory with color $SU(3)$ the underlying gauge group. The non–Abelian nature of the theory has dramatic consequences. While the interaction between colored objects is weak at short distances or high momentum transfer (asymptotic freedom [6, 9, 10]); it is strong at long distances, ($\lesssim$ 1fm) or low energies, leading to the confinement of quarks into colorless objects, the hadrons [11]. Consequently, QCD allows for a perturbative analysis at large energies, whereas it is highly non–perturbative in the low–energy regime.

An important idea that is implicit in all descriptions of physical phenomena is that of an effective theory [12]. The basic premise of effective theories is that dynamics at low–energies (or large distances) does not depend on the details of the dynamics at high energies (or short distances). As a result, low–energy physics can be described using an effective Lagrangian that contains only the relevant degrees of freedom at low energy, without explicitly taking into account additional degrees of freedom present at higher energies. It is important to note that the low–energy degrees of freedom do not necessarily have to be the fundamental degrees of freedom of the theory, as it is the case in QCD, where the fundamental degrees of freedom, quarks and gluons, are not the best suited to describe low–energy physics.

An effective field theory describes low–energy physics in terms of a few parameters. These low energy parameters can be computed in terms of parameters in a more fundamental high energy theory. This computation can be done explicitly in perturbation theory when the high energy theory is weakly coupled. In QED, for example, one can predict low energy parameters such as the magnetic moment of the electron which can be used in the Schrödinger equation. If the high energy theory is strong coupled, as in QCD, one needs to use non-pertubative calculation techniques, for example numerical lattice simulations. However, the low–energy parameters can allways be treated as free parameters that are fit to experiment. The effects of high energy dynamics on the

low–energy effective field theory are encoded in the coupling constants of the low–energy theory, or are present in the form of symmetry constraints on the low–energy theory.

Chiral Perturbation Theory is an effective field theory of QCD [13, 14]. The degrees of freedom of Chiral Perturbation Theory are the lowest mass states of QCD, the octet of pseudoscalar mesons (π, K, η). Chiral Perturbation Theory is based on the mechanism of spontaneous Chiral symmetry breaking, exploiting in this way the Golstone boson nature of the mesons. The explicit symmetry breaking provided by the finite quark masses translate into the mechanism of vacuum alignment and generates masses for the pseudoscalar mesons mentioned above [15]. A power counting can be devised allowing to determine which terms in the Lagrangian, and which Feynman diagrams are required to compute amplitudes in Chiral Perturbation Theory up to a certain precision. The results can be organized in powers of p/Λ_χ, where p is the external momentum, taken to be of the order of the pion mass $p \sim m_\pi$. Λ_χ is the cut–off of the theory, and is usually taken to be of the order of the mass of the first non–Goldstone boson state of QCD, the ρ meson.

Chiral perturbation theory can also be applied to the interactions of the Goldstone bosons with all other particles [16, 17, 18], which we will refer to as matter fields. The key to introduce matter fields to the Chiral Lagrangian, is that all states of QCD transform as irreducible representations of the unbroken Chiral symmetry subgroup. The introduction of heavy fields poses an additional challenge by introducing a new heavy scale, the heavy field mass, that breaks the power counting. A possible method to solve this problem is the use of the Heavy Baryon expansion [19, 20], or alternative approaches that keep the Lorentz symmetry of the Lagrangian explicit as, for example, Infrared Renormalization [21]. A particularly remarkable application of this framework is the effective field theory description of nuclear interactions by coupling nucleon doublets to the Chiral Lagrangian [22, 23].

As stated above, in the construction of an effective field theory it is crucial the determination of all of the relevant degrees of freedom. An interesting problem arises when the low–energy degrees of freedom can form bound states, a virtual state or a resonance close to threshold. Since these states are close to threshold, they affect the scattering amplitudes, yet they can not be described by means of perturbation theory because finite polynomical series of the momentum can not generate a pole in the amplitude. These poles can be obtained by resummating certain classes of diagrams, for example using unitarization methods, which are

not consistent with the effective field theory power counting, or assuming an enhancement in certain couplings, like in Ref.[76]. In the later case renormalization group equations for all low–energy constants involved have to be calculated to determine the correct scaling.

It is an old observation by Weinberg [24, 25, 26] that the explicit inclusion of bound states or resonances as degrees of freedom in a Hamiltonian improves the convergence of perturbation theory. This improved convergence it is easy to understand since the scattering amplitudes will have the right analytical structure. One of the main objectives of this thesis has been to explore this issue in the modern framework of effective field theories.

Lattice field theory provides a mathematically well–defined framework for a formulation of non–perturbative QCD [27]. The idea is to replace the four–dimensional Minkowski space–time continuum with a discrete lattice in a four–dimensional Euclidean space. Lattice field theory introduces an ultraviolet cut-off at the outset and gives a non–perturbative definition of the functional integral. The fermion fields live on lattice sites and the gauge fields live on links. Since the quark action is a quadratic form, the integral can be carried out exactly, then the gluons can be numerically integrated with a Monte Carlo method (see Appendix A for more details). Apart from systematic effects due to non–zero lattice spacing and finite volume, lattice QCD simulations produce results that are exact on the given lattice, up to statistical errors.

It is natural to combine both Chiral Perturbation Theory and lattice QCD. Lattice QCD calculations, although of a remarkable degree of accuracy, are still being carried out at unphysically large quark masses. Chiral Perturbation Theory can be used to describe the dependence on the quark masses of the low–energy QCD observables computed in lattice QCD. Thus Chiral Perturbation Theory provides formulas for the Chiral extrapolations of lattice QCD results from unphysically high quark masses to the physical value. Thus, combining lattice QCD with Chiral Perturbation Theory, we can obtain predictions for low–energy strong interaction physics from QCD. On the other side, the quark masses can be varied continuously in a lattice computation, this allows for an alternative method to determine the low–energy constants of Chiral Perturbation Theory. Alongside the traditional method of extracting the low–energy constants from a fit of the Chiral Perturbation Theory expressions to experimental data, low–energy constants can be obtained from fits of lattice data for different values of the quark masses.

The thesis is organized as follows. The first three chapter are devoted to the

theoretical background of this thesis. In chapter 1 the general features of the Chiral symmetry of the QCD Lagrangian and its consequences are introduced. In chapter 2 we briefly review Chiral Perturbation Theory. In chapter 3 we outline how to introduce matter fields to the Chiral Lagrangian, with special focus in the nucleon doublet. A large portion of chapter 3 is also devoted to discuss the power counting of the Chiral Lagrangian including nucleons. Chapters 4 and 5 comprise the novel work of this thesis. Chapter 4 deals with the inclusions of dibaryon fields into nucleon–nucleon effective field theories, based in the works presented in Refs. [31, 32, 33, 34]. In Chapter 5 we present and extension of Chiral Perturbation Theory including a light isosinglet scalar field, presented in Refs.[35, 36]. The thesis is completed with a conclusions and outlook chapter.

CHAPTER

1

CHIRAL SYMMETRY IN THE QCD LAGRANGIAN

1.1 The QCD Lagrangian

Quantum Chromodynamics (QCD) is the theory that describes strong interactions [6, 7, 8]. It is a Yang–Mills theory [37] invariant under gauge transformations of the color group $SU(3)_C$. The matter fields interacting through strong interactions are the quarks. The quarks belong to the fundamental representation of the color group and are spin-1/2 fermions with six different flavors (see Table 1.1). The gauge fields, the so–called gluons, are in the adjoint representation and are spin-1 particles. Quarks and gluons are the fundamental degrees of freedom of QCD. The QCD Lagrangian reads

$$\mathcal{L}_{QCD} = \sum_f \bar{q}_f \left(i\not{D} - m_f \right) q_f - \frac{1}{4}\mathcal{G}_{\mu\nu,a}\mathcal{G}_a^{\mu\nu} + \bar{\theta}\frac{g^2}{64\pi^2}\epsilon^{\mu\nu\rho\sigma}\mathcal{G}_{\mu\nu,a}\mathcal{G}_{\rho\sigma,a}\,, \tag{1.1}$$

were f stands for the different quark flavors, up (u), down (d), strange (s), charm (c), botom (b) and top (t). The color indices have been omitted for the quark fields, but it should be kept in mind that each quark flavor field consists of a color triplet. The covariant derivative

$$D_\mu q_f = \partial_\mu q_f - ig\sum_{a=1}^{8}\frac{\lambda_a^C}{2}\mathcal{A}_{\mu,a}q_f\,, \tag{1.2}$$

contains eigth gauge fields, $\mathcal{A}_{\mu,a}$, because $SU(3)_C$ is an eigth–parameter group. The strength of the interaction between quarks and gluons is regulated by the coupling constant g, which is the same for all quark flavors. λ_a^C are the Gell–Mann matrices (see Appendix B). The QCD Lagrangian (1.1) also contains gen-

flavor	u	d	s
charge[e]	$2/3$	$-1/3$	$-1/3$
mass[MeV]	$1.7 - 3.1$	$4.1 - 5.7$	100^{+30}_{-20}
flavor	c	b	t
charge[e]	$2/3$	$-1/3$	$2/3$
mass[GeV]	$1.29^{+0.05}_{-0.11}$	$4.19^{+0.18}_{-0.06}$	$172.9 \pm 0.6 \pm 0.9$

Table 1.1: Quark flavors and their charges. Values from PDG(2010)[38]

eralized field strength tensor for non-Abelian gauge groups

$$\mathcal{G}_{\mu\nu,a} = \partial_\mu \mathcal{A}_{\nu,a} - \partial_\nu \mathcal{A}_{\mu,a} + g f_{abc} \mathcal{A}_{\mu,b} \mathcal{A}_{\nu,c} \,, \tag{1.3}$$

the structure constants, f_{abc}, for $SU(3)$ can be found in Appendix B.

The last term in (1.1) is the so–called θ term. It explicitly violates the P and CP discrete symmetries, and hence does not have to be taken into account if these symmetries are enforced in the construction of the Lagrangian. However nature is known to violate P and CP. The θ term should give a large contribution to an electric dipole moment for the neutron, nevertheless this is known accurately to be very small. The current upper bound to the $\bar{\theta}$ parameter given by the neutron electric dipole moment is $\|\bar{\theta}\| \lesssim 10^{-10}$ [38], therefore we will not consider it further.

The β function determining how the renormalized coupling g changes with the running scale μ is defined as

$$\beta \equiv 4\pi\mu \frac{d\alpha_s}{d\mu} \,. \tag{1.4}$$

For small $g(\mu)$ we can compute $\beta(g)$ in perturbation theory. The leading term in the perturbative expansion is of order g^3

$$\beta(g) = -\beta_0 \frac{g^3}{(4\pi)^2} \,, \quad \beta_0 = \frac{1}{3}(11N_c - 2N_f) \,, \tag{1.5}$$

where N_c is the number of colors and N_f is the number of flavors below the energy scale under consideration. Eq.(1.5) shows that in the ultraviolet limit, for small positive value of the coupling g, $N_c = 3$ colors and $N_f = 6$ flavors, the β

function is negative [6]. Using Eq.(1.5) in Eq.(1.4) and integrating one obtains

$$\alpha_s(\mu) \equiv \frac{g^2}{4\pi} = \frac{4\pi}{\beta_0 \log\left(\mu^2/\Lambda^2_{QCD}\right)}\,, \tag{1.6}$$

where Λ_{QCD} is an integration constant. The calculation at three–loop together with the Particle Data Group average for α_s at the mass of he Z boson, gives $\Lambda_{QCD} = 217^{+25}_{-23}$MeV for 5 active quark flavors, in the $\overline{MS}$ [39] substraction scheme and using dimensional regularization [40]. It is justified in (1.5) to neglect higher–order contributions to the β–function only if the running coupling constant is small; accordingly, the above representation of the scale dependence of the coupling constant only holds $\mu \gg \Lambda_{QCD}$. Moreover, for small values of the scale, the perturbative approach is no longer valid. The negative sign in the QCD β–function at high energies means that the coupling constant becomes smaller the higher the energy is, as a result the quarks behave like asymptotic free states in the ultraviolet limit. This property is known as **asymptotic freedom**[9, 6, 10]. As a consequence perturbation theory in powers of α_s can be applied in the calculations of the Green functions. When the energies involved are small the color interaction between quarks and gluons becomes non-pertubative, to study QCD in this regime we have to use effective field theories or do numerical calculations using formulations of QCD on the lattice.

The last crucial property of QCD is the so–called **color confinement** [11]. In a theory like Quantum Electrodinamics two charged particles forming a bound state can be separated an infinite distance with a finite amount of energy. On the other hand the porperty of color confinement of QCD means that to infinitely split a bound state of two strong charged particles an infinite amount of energy is needed. Since QCD is a non–Abelian $SU(3)_C$ gauge theory all asymptotic states must be color singlets (mesons and barions). There is no analytical prove of color confinement.

1.2 Chiral Symmetry

In order to visualize the global symmetries of the QCD Lagrangian let us introduce the right– and left–handed components of the quark fields

$$q_{f,R} = P_R q_f\,, \quad q_{f,L} = P_L q_f\,, \tag{1.7}$$

the right–hand and left–hand projectors are defined as

$$P_{R,L} = \frac{1}{2}\left(1 \pm \gamma_5\right) . \tag{1.8}$$

The projector operators have the following properties: completeness: $P_L + P_R = 1$, idempotent: $P_{R,L}^2 = P_{RL}$, orthogonality: $P_R P_L = P_L P_R = 0$.

Let the Chiral limit be the limit where the n_f light quarks are massless. The Lagrangian for the light quarks in the Chiral limit then contains no terms that connect the right– and left–handed components of the quark fields

$$\mathcal{L}^0_{QCD} = \sum_f \left(i\bar{q}_{f,R} \not{D} q_{f,R} + i\bar{q}_{f,L} \not{D} q_{f,L} \right) - \frac{1}{4} \mathcal{G}_{\mu\nu,a} \mathcal{G}_a^{\mu\nu} . \tag{1.9}$$

Due to the flavor independence of the covariant derivative $\mathcal{L}^0_{QCD}$ is invariant under independent global rotations of the right– and left–handed quark fields

$$q_R \to V_R q_R , \quad q_L \to V_L q_L , \quad V_R, V_L \in U(N_f) \tag{1.10}$$

where $q_R = \left(q_{R,1}, \ldots, q_{R,N_f}\right)^T$ and the same for left-handed quarks. $\mathcal{L}^0_{QCD}$ has a classical global $U(N_f)_L \times U(N_f)_R$ [8].

The Noether theorem establishes the connection between continuous symmetries of a dynamical system and conserved currents. A conserved current fulfills the following condition:

$$\partial^\mu J_\mu = 0 . \tag{1.11}$$

The Noether currents associated with the symmetry transformations of (1.10) are given by:

$$J^\mu_{R,a} = \bar{q}_R \gamma^\mu \frac{\lambda^a}{2} q_R , \quad J^\mu_{L,a} = \bar{q}_L \gamma^\mu \frac{\lambda^a}{2} q_L , \quad a = 1, \ldots, N_f^2 - 1 , \tag{1.12}$$

$$J^\mu_R = \bar{q}_R \gamma^\mu q_R , \quad J^\mu_L = \bar{q}_L \gamma^\mu q_L , \tag{1.13}$$

where the matrices λ_a form a complete set of traceless, Hermitian $N_f \times N_f$ matrices that generate $SU(N_f)$. Instead of the Chiral transformations in Eq.(1.10) often one uses the linear combinations $V_V = V_R + V_L$ and $V_A = V_R - V_L$, which

correspond to the currents

$$J^{\mu}_{V,a} = \bar{q}\gamma^{\mu}\frac{\lambda^a}{2}q\,, \quad J^{\mu}_{A,a} = \bar{q}\gamma^{\mu}\gamma_5\frac{\lambda^a}{2}q\,, \quad a = 1,\ldots,N_f^2-1\,, \tag{1.14}$$

$$J^{\mu}_{V,0} = \bar{q}\gamma^{\mu}q\,, \quad J^{\mu,0}_{A} = \bar{q}\gamma^{\mu}\gamma_5 q\,, \tag{1.15}$$

transforming as a vector and an axial–vector respectively. The Chiral symmetry of QCD can thus be written as the direct product

$$\begin{aligned} U(N_f)_R \times U(N_f)_L =& SU(N_f)_R \times SU(N_f)_L \times U(1)_R \times U(1)_L \\ =& SU(N_f)_R \times SU(N_f)_L \times U(1)_V \times U(1)_A\,. \end{aligned} \tag{1.16}$$

The singlet axial current fails to be conserved at the quantum level [41, 42, 43] (axial $U_A(1)$ anomaly). The factor $U(1)_V$ is generated by the charge associated to the singlet vector current $J^{\mu}_{V,0}$, the baryon number. It is therefore the symmetry group associated to baryon number conservation.

Each Noether current has associated a charge, defined as

$$Q(x^0) = \int d^3\vec{x}J^0(x)\,. \tag{1.17}$$

If the current is conserved, then the charge is time independent, $dQ/dx^0 = 0$. The conserved charges of Chiral symmetry form the following algebras

$$\begin{aligned} \left[Q^{\alpha}_{L,R}, Q^{\beta}_{L,R}\right] &= if_{\alpha\beta\gamma}Q^{\gamma}_{L,R}\,, \\ \left[Q^{\alpha}_{R}, Q^{\beta}_{L}\right] &= 0\,, \\ \left[Q^{\alpha}_{V}, Q^{\beta}_{V}\right] &= if_{\alpha\beta\gamma}Q^{\gamma}_{V}\,, \\ \left[Q^{\alpha}_{A}, Q^{\beta}_{A}\right] &= if_{\alpha\beta\gamma}Q^{\gamma}_{V}\,, \\ \left[Q^{\alpha}_{V}, Q^{\beta}_{A}\right] &= if_{\alpha\beta\gamma}Q^{\gamma}_{A}\,. \end{aligned} \tag{1.18}$$

Note that Q^{α}_{A} does not form a closed algebra.

1.3 Chiral Symmetry as a Nambu–Goldstone Symmetry

A global symmetry G of a classical Lagrangian can be realized in two different ways in the corresponding quantized theory. The type of realization depends on the behavior of the ground state (or vacuum state) under symmetry transformations. The generators of the symmetry transformations for the quantum states corresponding to symmetry group G of the Lagrangian are the Noether charges Q associated to the conserved currents. If the charges annihilate the vacuum, $Q|0\rangle = 0$, then the symmetry is **Wigner–Weyl** realized. If, on the contrary, the charges do not annihilate the vacuum, $Q|0\rangle \neq 0$, the symmetry is **Nambu–Goldstone** realized. Note that vacuum symmetries are always symmetries of the Lagrangian, but not viceversa. It is also common to refer Nambu–Goldstone realized symmetries as spontaneously broken symmetries.

To visualize the effects of a symmetry of the theory in the Lagrangian lets consider the following example; let $|p\rangle$ be a particle eigenstate of the Hamiltonian H with momentum $\vec{p}$ and mass m

$$H|p\rangle = \sqrt{\vec{p}^2 + m^2}|p\rangle\,, \tag{1.19}$$

and Q^α the set of conserved charges associated to G and. Using the Heisenberg equation of motion for the conserved charge operator

$$0 = \frac{d}{dt}Q^\alpha = -i\left[Q^\alpha, H\right]\,, \tag{1.20}$$

we find that conserved charges commute with the Hamiltonian. It follows that

$$HQ^\alpha|p\rangle = \sqrt{\vec{p}^2 + m^2}Q^\alpha|p\rangle\,. \tag{1.21}$$

In words, this means that the state $Q^\alpha|p\rangle$ has the same energy as $|p\rangle$. In order to see the consequences of this on the particle spectrum, let $\left(a_p^\alpha\right)^\dagger$ be a set of creation operators that form a representation of G. Then write

$$Q^\alpha|p\rangle = Q^\alpha\left(a_p^\beta\right)^\dagger|0\rangle = \left[Q^\alpha, \left(a_p^\beta\right)^\dagger\right]|0\rangle + \left(a_p^\beta\right)^\dagger Q|0\rangle\,, \tag{1.22}$$

since the creation operators form a representation of G the commutator with the

charge can be written as a linear combination of creation operators

$$Q^\alpha|p\rangle = t^{\alpha\beta}\left(a_p^\beta\right)^\dagger|0\rangle + \left(a_p^\beta\right)^\dagger Q|0\rangle\,, \tag{1.23}$$

If the conserved charge annihilates the vacuum, i.e the symmetry is Wigner-Weyl realized, then $t^{\alpha\beta}\left(a_p^\beta\right)^\dagger|0\rangle$ represents a one particle state. This implies a multiplet of equal mass particles, generated by continual application of all the charge generators. There particles are physical states in the Fock space, they are constructed upon the vacuum and are all classified according to the irreducible (linear) representations of G. This kind of symmetry realization is called manifest because it has a direct translation in the particle spectrum, forcing it to split into degenerate sets of particles according to multiplets of G. If the vacuum is not annihilated by the charge, i.e the symmetry is Nambu-Goldstone realized, then the argument above by which the degenerate particle multiplets are generated does no longer apply due to the presence of a second tern in (1.23).

Now, let G be the Chiral symmetry group, and the Hamiltonian eigenstate $|p\rangle$ to be also a parity eigenstate with eigenvalue n_p (with $n_p^2 = 1$)

$$P|p, n_p\rangle = n_p|p, n_p\rangle\,, \tag{1.24}$$

then consider the state resulting of applying Q_A^α to this state, $Q_A^\alpha|p, n_p\rangle$, the party eigenvalue of this state is

$$PQ_A^\alpha|p, n_p\rangle = PQ_A^\alpha P^{-1}P|p, n_p\rangle = -n_p Q_A^\alpha|p, n_p\rangle\,. \tag{1.25}$$

Combining this result with (1.23) implies that if Q_A^α annihilates the vacuum the spectrum of QCD has to consist of pairs of degenerate multiplets with opposite parity. However this degenerate multiplets of opposite parity are not present in nature, which leads to the conclusion that the QCD vacuum at low energies is not annihilated by the conserved charge associated to the axial Chiral transformations. As a consequence Chiral symmetry $SU(n_f)_L \times SU(n_f)_R$ is spontaneously broken to the subgroup $SU(n_f)_V$.

1.4 Goldstone Theorem

The Goldstone theorem states that for any broken generator of the continuous symmetry, the theory must contain a massless particle [44, 45, 46, 47]. Consider a local field theory with a global symmetry given by a Lie group G. Let the ground

state of the quantum theory, $|0\rangle$, be invariant only under a subgroup $H \subset G$. The conserved charges Q^α do not annihilate the vacuum. The index α links each of the conserved charges with the elements of the left cosets $(G/H)_L = \{gH; g \in G\}$. Assume the existence of an operator $\mathcal{O}(x)$ that satisfies

$$\langle 0|[Q^\alpha, \mathcal{O}(0)]|0\rangle = v\,, \quad v \neq 0\,. \tag{1.26}$$

The left–hand side of (1.26) is called an order parameter of the spontaneously broken symmetry G. Note that for the order parameter to be different of zero the conserved charge cannot annihilate the vacuum. Inserting a complete set of states $\mathbf{1} = \sum\!\!\!\!\!\!\int_n |n,\vec{p}\rangle\langle n,\vec{p}|$ in (1.26) and using the definition for the conserved charges we obtain

$$\sum\!\!\!\!\!\!\int_n \int d^3\vec{x}\left(\langle 0|J^{0,\alpha}(x)|n,\vec{p}\rangle\langle n,\vec{p}|\mathcal{O}(0)|0\rangle - \langle 0|\mathcal{O}(0)|n,\vec{p}\rangle\langle n,\vec{p}|J^{0,\alpha}(x)|0\rangle\right) = v\,, \tag{1.27}$$

Making use of translational invariance, $J^\alpha(x) = e^{iP\cdot x}J^\alpha(0)e^{-iP\cdot x}$,

$$\begin{aligned}\sum\!\!\!\!\!\!\int_n (2\pi)^3\delta^3(\vec{p})\Big(e^{-iE_n x^0}\langle 0|\ J^{0,\alpha}(0)|n,\vec{p}\rangle\langle n,\vec{p}|\mathcal{O}(0)|0\rangle \\ -e^{iE_n x^0}\langle 0|\mathcal{O}(0)|n,\vec{p}\rangle\langle n,\vec{p}|J^{0,\alpha}(0)|0\rangle\Big) = v\,,\end{aligned} \tag{1.28}$$

now, the Dirac delta only selects states with zero momentum from the complete set

$$\begin{aligned}\sum_n (2\pi)^3\Big(e^{-iE_n x^0}\langle 0|\ J^{0,\alpha}(0)|n,0\rangle\langle n,0|\mathcal{O}(0)|0\rangle \\ -e^{iE_n x^0}\langle 0|\mathcal{O}(0)|n,0\rangle\langle n,0|J^{0,\alpha}(0)|0\rangle\Big) = v\,,\end{aligned} \tag{1.29}$$

the states with $E_n > 0$ carry a dependence on the time, but (1.26) is time independent, thus the sum of the states with $E_n > 0$ has to vanish. States with zero energy and momentum have to be necessarily massless. Then we conclude that the existence on a non–zero order parameter implies the existence of massless states in the theory spectrum with the defining property,

$$\langle 0|J^{0,\alpha}(0)|\pi\rangle\langle\pi|\mathcal{O}(0)|0\rangle \neq 0\,, \tag{1.30}$$

where $|\pi\rangle$ denote the massless states, to which we will refer to as Goldstone states from now on. The properties of these Goldstone states can be obtained from the fact that both terms in (1.30) cannot vanish. Consider the first matrix

element,

$$\langle 0|J^{0,\alpha}(0)|\pi\rangle \neq 0\,, \tag{1.31}$$

The conserved current matrix element, $J^{0,\alpha}$, links the Goldstone states with the vacuum, then the internal quantum numbers and parity of the Goldstone states correspond to those of the conserved charge Q^{α}. The second matrix element in (1.30),

$$\langle \pi|\mathcal{O}(0)|0\rangle \neq 0\,, \tag{1.32}$$

forces the Golstone states to have the same spin as the state $\mathcal{O}(0)|0\rangle$. The conserved charges are linearly independent by construction and so are the currents, thus the states $J^{0,\alpha}(0)|0\rangle$ are also linearly independent, as a consequence there must be a Golstone state for each broken symmetry generator, or in other words the physical spectrum contains $dim\,(G/H)_L = dimG - dimH$ Goldstone states.

Now, from (1.31) we can see that a Goldstone boson state can be created from the vacuum trough a symmetry current, which is nothing more than a local space–time dependent symmetry transformation in the space generated by the broken generators. In the zero–momentum limit, the $Q^{\alpha}|0\rangle$ states have the same energy as the vacuum state since the conserved charges commute with the Hamiltonian. This means that in the zero–momentum limit the $Q^{\alpha}|0\rangle$ states are indistinguishable from the vacuum. Since the space generated by the broken generators is $(G/H)_L$ there is a set of equivalent vacuum states in a one–to–one correspondence with the elements of $(G/H)_L$. For this reason $(G/H)_L$ is often called the vacuum manifold. Since there is no preferred vacuum state every space–time point can have a different vacuum state. This can be parametrized by a field of symmetry transformations of $(G/H)_L$ that transforms an arbitrarily chosen standard vacuum state to the vacuum state of each space–time point. Such fields are the Goldstone fields. Since, only the variation of the Goldstone fields is relevant, it follows that the Goldstone fields can only interact through derivatives. Since derivatives are small at small energies the interactions of Goldstone fields should be weak at low energies.

In the particular case at hand, QCD, G is Chiral symmetry and H is the vector subgroup. If we choose the number of light quarks to be $n_f = 3$, there are eight broken axial symmetry generators that correspond to eight Goldstone states with negative parity. This Goldstone states can be identified to the eigth lightest hadronic states $(\pi^+, \pi^-, \pi^0, \eta, K^+, K^-, K^0, \bar{K}^0)$. If we choose $n_f = 2$, only three pseudoscalar Golstone boson states have to be identified (π^+, π^-, π^0). In nature this particles have small non–zero masses, this is due to a small explicit

symmetry breaking. We will explore this further in the next section. The corresponding $\mathcal{O}$ has to be a pseudoscalar operator, meaning that the Goldstone state will be spin zero bosons. The simplest possibilities are $\mathcal{O}^a = \bar{q}\gamma_5\lambda^a q$, which satisfy in the $n_f = 3$ case

$$\langle 0|[Q_A^a, \bar{q}\gamma_5\lambda_b q]|0\rangle = -\frac{1}{2}\langle 0|\bar{q}\{\lambda_a, \lambda_b\}q|0\rangle = -\frac{2}{3}\delta_{ab}\langle 0|\bar{q}q|0\rangle\,. \tag{1.33}$$

The natural order parameter for the spontaneous Chiral symmetry breaking is then the quark condensate. The quark condensate in the Chiral limit fulfills

$$\langle 0|\bar{u}u|0\rangle = \langle 0|\bar{d}d|0\rangle = \langle 0|\bar{s}s|0\rangle \neq 0\,. \tag{1.34}$$

The matrix element of the axial-vector current between the vacuum and the Goldstone boson states can be parametrized thanks to Lorenz covariance as

$$\langle 0|J_V^{\alpha,\mu}(x)|\pi^\beta(p)\rangle = ip_\mu F_0\delta^{\alpha\beta}e^{ip\cdot x}\,, \tag{1.35}$$

where $F_0 \sim 93$MeV is the so–called pion decay constant in the Chiral limit.

1.5 Explicit Chiral Symmetry breaking

Up until now we have been disregarding the fact that in the QCD Lagrangian the light quark fields do have non–zero mass terms. When taking into account those terms the divergences of the conserved currents will no longer be zero, meaning the currents will not be conserved anymore. Lets consider the quark mass matrix for $n_f = 3$ and the $n_f = 2$ cases

$$n_f = 3\,,\quad \mathcal{M} = \begin{pmatrix} m_u & 0 & 0 \\ 0 & m_d & 0 \\ 0 & 0 & m_s \end{pmatrix};\quad n_f = 2\,,\quad \mathcal{M} = \begin{pmatrix} m_u & 0 \\ 0 & m_d \end{pmatrix}. \tag{1.36}$$

We can rewrite the mass terms in (1.1) in terms of $\mathcal{M}$

$$\mathcal{L}_\mathcal{M} = -\bar{q}\mathcal{M}q\,, \tag{1.37}$$

note that $\mathcal{M}$ is a $SU(n_f)$ matrix. Using the right– and left– hand projectors, introduced in (1.8), to split the quark fields into left and right components we

obtain

$$\mathcal{L}_M = -\left(\bar{q}_R \mathcal{M} q_L + \bar{q}_L \mathcal{M} q_R\right) . \tag{1.38}$$

Thus the quark mass terms mix the left and right components of the quark fields and are not symmetric under Chiral symmetry. The quark mass terms induce the following divergences to the Noether currents

$$\begin{aligned}
\partial_\mu J_V^{\mu,a} &= i\bar{q}\left[\mathcal{M}, \frac{\lambda_a}{2}\right] q \,, \\
\partial_\mu J_A^{\mu,a} &= i\bar{q}\left\{\frac{\lambda_a}{2}, \mathcal{M}\right\} \gamma_5 q \,, \\
\partial_\mu J_V^{\mu} &= 0 \,, \\
\partial_\mu J_A^{\mu} &= i2\bar{q}\mathcal{M}\gamma_5 q + \frac{3g^2}{32\pi^2}\epsilon_{\mu\nu\rho\sigma}\mathcal{G}_a^{\mu\nu}\mathcal{G}_a^{\rho\sigma} \,.
\end{aligned} \tag{1.39}$$

The last term in $\partial_\mu J_A^\mu$ is the $U_A(1)$ anomaly. The existence of explicit symmetry breaking terms in the Lagrangian means that the set of states of the vacuum manifold are no longer of the same energy. As a result there will be a minimum energy state that naturally will be the preferred vacuum state. This phenomenon is known as vacuum alignment. Let Q^α be the set of conserved charges corresponding to the broken symmetry generators. We can now write any vacuum state as

$$|0,\pi\rangle = e^{-i\pi^\alpha Q^\alpha}|0,0\rangle \,, \tag{1.40}$$

where $|0,0\rangle$ is an arbitrary reference vacuum state. If we assume that the light quark mass terms (1.37) in the QCD Lagrangian are a small perturbation we can use time independent perturbation theory to obtain the vacuum states energy variation. First let us define κ as the small variational parameter as

$$k\mathcal{H} = -\mathcal{L}_\mathcal{M} \,, \tag{1.41}$$

then the energy variation is

$$\Delta E(\pi) = \kappa\langle 0,\pi|\mathcal{H}(0)|0,\pi\rangle + \mathcal{O}(\kappa^2) \,. \tag{1.42}$$

The perturbative expansion in κ has to be performed about the minimal energy vacuum to avoid paradoxical results [48]. Since we must have a minimum at

$\pi = 0$ the following two conditions have to be met

$$\begin{aligned} \left.\frac{\partial \Delta E(\pi)}{\partial \pi_\alpha}\right|_{\pi_\alpha=0} &= i\kappa\langle 0,0|\left[\lambda_\alpha^B,\mathcal{H}\right]|0,0\rangle = 0\,, \\ \left.\frac{\partial^2 \Delta E(\pi)}{\partial \pi_\alpha \partial \pi_\beta}\right|_{\pi_\beta,\pi_\alpha=0} &= -\kappa\langle 0,0|\left[\lambda_\beta^B,\left[\lambda_\alpha^B,\mathcal{H}\right]\right]|0,0\rangle > 0\,. \end{aligned} \tag{1.43}$$

As a result now to move among the states of the vacuum manifold costs energy. Identifying the π parameter with the Goldstone boson field we can read the second derivative of the energy variation as the Golstone boson field mass times an unknown positive constant

$$m_{\alpha\beta}^2 = -\frac{\kappa}{\omega_G}\langle 0,0|\left[\lambda_\beta^B,\left[\lambda_\alpha^B,\mathcal{H}\right]\right]|0,0\rangle\,. \tag{1.44}$$

Therefore the explicit symmetry breaking due to the finite light quark masses generates masses for the Goldstone bosons [49].

CHAPTER

2

CHIRAL PERTURBATION THEORY

2.1 Effective Field Theories

Chiral perturbation theory is an effective field theory. The basic premise of an effective field theory is that dynamics at low energies (or large distances) does not depend on the details of the dynamics at high–energies (or short distances). Therefore the physics below a specific cut–off can be described by an effective Lagrangian containing only the relevant degrees of freedom present at low energies, ignoring additional degrees of freedom present at high–energies. The relevant degrees of freedom at low energy might not be the fundamental degrees of freedom of the underlying theory. For example the fundamental degrees of freedom of QCD are the quarks and gluons, but for Chiral perturbation theory they are pions, kaons, the eta meson.

It is crucial that between the typical energy scale of the physics we want to study and the high–energy cut-off there is a large energy gap with no additional degrees of freedom because this will determinate how fast the theory will converge. Effective field theories have only a limited momentum range of applicability, as its convergence will slow down as the momentum approaches the cut–off, but, as long as the momentum stays well below it, the effective field theory is designed to give an appropriate description up to a finite accuracy.

The theoretical basis of effective field theories can be formulated as a theorem [12]: *For a given set of asymptotic states, perturbation theory with the most general Lagrangian containing all terms allowed by the assumed symmetries will yield the most general S–matrix elements consistent with analicity, perturbative unitarity, cluster decomposition and the assumed symmetries*.

The following important ingredient, together with the effective Lagrangian,

is a method that allows to decide which terms contribute in a calculation up to a certain accuracy. We will see that we can organize the calculations in a pertubative series incorporating new operators from the Lagrangian at each order. This is crucial for the renormalizability of the calculations. Since an effective field theory contains all terms compatible with the symmetries, it will contain non–renormalizable operators too, making it non-renormalizable in a traditional sense. However the new operators appearing at each order allow for all the divergences to be absorbed. The price to be paid for such order by order renormalizability is that each new operator introduces an unknown low–energy constants, as a result as we increase the accuracy, more low–energy constants have to be considered and more experimental input is needed to determine them. Thus as the precision augments the theory loses predictability.

2.2 Non-linear realization of Goldstone Bosons

In the previous chapter, in section 1.4, we have argued that in a theory with a spontaneously broken symmetry the vacuum state is not unique, but instead there exist a set of equivalent vacuum states generated by the broken symmetry generators. The set of vacuum states is called the vacuum manifold, and is given by the coset space G/H where G is the global symmetry and H is the subgroup to which it is spontaneously broken. In our case G is Chiral symmetry, $SU(n_f)_L \times SU(n_f)_R$, and $H = SU(n_f)_V$. Each point in space–time can be in any particular state of the vacuum manifold, to take this into account we introduced the Goldstone fields which give the symmetry transformation of G that rotates an arbitrarily chosen standard vacuum to the local vacuum orientation. We would like to choose a set of coordinates which describe the local orientation of the vacuum for small fluctuations about the standard vacuum configuration. The general formalism for effective Lagrangians for spontaneously broken symmetries was worked out by Callan, Coleman, Wess and Zumino [16, 17, 18]. Let $\Xi(x) \in G$ be the rotation matrix that transforms the standard vacuum configuration to the local field configuration. The matrix u is not unique, uh where $h \in H$, gives the same field configuration, since the standard vacuum is invariant under transformations of H. The prescription of [16, 17] is to pick a set of broken generators X and choose

$$\Xi = e^{i X \cdot \pi(x)} . \tag{2.1}$$

Under a global symmetry transformation $g \in G$, the matrix $\Xi(x)$ is transformed to the new matrix $g\Xi$. The new matrix is no longer in the prescribed form 2.1, but can be written as

$$g\,\Xi = \Xi'\,h\,, \tag{2.2}$$

since the two matrices $g\Xi$ and Ξ', which describe the same field configuration, are related by a unique element of H. Although the g matrix is independent of x, since it is a global transformation, the matrix h is not, because it depends on g and $\Xi(x)$. The matrix h is also non-trivial because the vacuum manifold G/H is curved. The transformation is usually written as

$$\Xi \to g\,\Xi\,h^{-1}\,(g, u(x))\ . \tag{2.3}$$

Equations (2.1) and (2.3) give the choice for the Goldstone boson field, and its transformation properties, of Refs.[16, 17]. Any other choice is also possible and gives the same results for all observables, such as the S–matrix, but does not give the same off–mass–shell green functions.

Let T^α be the generators of $SU(n_f)$, then the generators of G are T^α_L and T^α_R which act on the left and right handed quarks respectively, and the generators of H are the flavor generators $T^\alpha_V = T^\alpha_L + T^\alpha_R$. There are two commonly used bases for Chiral Perturbation Theory, the u–basis and the U–basis.

The u–basis

Pick the broken generators as $X^\alpha = T^\alpha_L - T^\alpha_R$. Let the $SU(n_f)_L \times SU(n_f)_R$ transformation be represented in block diagonal form

$$g = \begin{pmatrix} L & 0 \\ 0 & R \end{pmatrix}, \tag{2.4}$$

where L and R are $SU(n_f)_L$ and $SU(n_f)_R$ transformations respectively. The unbroken transformations have the form (2.4) with ($L = R = V$)

$$h = \begin{pmatrix} V & 0 \\ 0 & V \end{pmatrix}. \tag{2.5}$$

The u field is then defined using the prescription (2.1)

$$\Xi(x) = e^{i\,X\cdot\pi(x)} = \exp i \begin{pmatrix} T\cdot\pi & 0 \\ 0 & -T\cdot\pi \end{pmatrix} = \begin{pmatrix} u(x) & 0 \\ 0 & u(x)^\dagger \end{pmatrix}, \tag{2.6}$$

where

$$u(x) = e^{i\,T\cdot\pi(x)} \tag{2.7}$$

denotes the upper block of $\Xi(x)$. Using the transformation law for Ξ (2.3)

$$\begin{pmatrix} u(x) & 0 \\ 0 & u(x)^\dagger \end{pmatrix} \to \begin{pmatrix} R & 0 \\ 0 & L \end{pmatrix} \begin{pmatrix} u(x) & 0 \\ 0 & u(x)^\dagger \end{pmatrix} \begin{pmatrix} K^{-1} & 0 \\ 0 & K^{-1} \end{pmatrix}, \tag{2.8}$$

we can derive the transformation law for $u(x)$

$$u(x) \to Ru(x)K^{-1}(x) = K(x)u(x)L^\dagger\,, \tag{2.9}$$

which defines V in terms of L, R and u.

The U–basis

The U–basis can be obtained from (2.1) using $X^\alpha = T_L^\alpha$ for the broken generators. In this case we have

$$\Xi(x) = e^{i\,X\cdot\pi'(x)} = \exp i \begin{pmatrix} T\cdot\pi'(x) & 0 \\ 0 & 0 \end{pmatrix} = \begin{pmatrix} U(x) & 0 \\ 0 & 1 \end{pmatrix}, \tag{2.10}$$

where

$$U(x) = e^{i\,T\cdot\pi'(x)}\,, \tag{2.11}$$

denotes the upper block of $\Xi(x)$. The transformation law (2.3) is

$$\begin{pmatrix} U(x) & 0 \\ 0 & 1 \end{pmatrix} \to \begin{pmatrix} R & 0 \\ 0 & L \end{pmatrix} \begin{pmatrix} U(x) & 0 \\ 0 & 1 \end{pmatrix} \begin{pmatrix} V^{-1} & 0 \\ 0 & V^{-1} \end{pmatrix} \tag{2.12}$$

which gives $V = R$ and thus the transformation law for $U(x)$ is

$$U(x) \to RU(x)L^\dagger\,. \tag{2.13}$$

Comparing the transformation laws in both basis, one can see that u and U are related by

$$U(x) = u^2(x) \tag{2.14}$$

2.3 The lowest–order Chiral Lagrangian

The Goldstone boson fields parametrize the Chiral transformations that pick the vacuum state, they are the analog to angles in rotations. Goldstone boson fields are thus dimensionless, however in order to write down an effective Lagrangian it is convenient to make Goldstone boson fields to have mass dimension one, as for any other spin–zero boson field. The standard choice is to redefine the Goldstone boson fields as $\pi \to \pi/F_0$, were F_0 is a mass dimension one constant. As result we have

$$u = e^{i\,T\cdot\pi/F_0}\,, \quad U = e^{2i\,T\cdot\pi/F_0}\,, \tag{2.15}$$

later we will show that F_0 can be identified as the pion decay constant in the Chiral limit. The π^α are the Goldstone boson fields in the isospin basis, nevertheless often we will want to work in the charge basis. Taking the up, down and strange quarks as light, that is $n_f = 3$, we have

$$\boldsymbol{\pi} \equiv \pi^\alpha \lambda^\alpha = 2\pi^\alpha T^\alpha = \begin{pmatrix} \pi^0 + \frac{1}{\sqrt{3}}\eta & \sqrt{2}\pi^+ & \sqrt{2}K^+ \\ \sqrt{2}\pi^- & -\pi^0 + \frac{1}{\sqrt{3}}\eta & \sqrt{2}K^0 \\ \sqrt{2}K^- & \sqrt{2}\bar{K}^0 & -\frac{2}{\sqrt{3}}\eta \end{pmatrix}, \tag{2.16}$$

where λ^α are the Gell–Mann matrices (see Appendix B). In the case of $n_f = 2$, were only the up and down quarks are considered light, we have

$$\boldsymbol{\pi} \equiv \pi^\alpha \tau^\alpha = 2\pi^\alpha T^\alpha = \begin{pmatrix} \pi^0 & \sqrt{2}\pi^+ \\ \sqrt{2}\pi^- & -\pi^0 \end{pmatrix}, \tag{2.17}$$

where τ^α are the Pauli matrices.

The Goldstone bosons are the lowest energy states in the QCD spectrum and it exist an energy gap between them and the next non-Goldstone boson state, the ρ meson. Therefore the Goldstone bosons are going to be the degrees of freedom of the effective theory. The low energy effective Lagrangian for QCD is the most general possible Lagrangian consistent with spontaneously broken $SU(n_f)_L \times SU(n_f)_R$ symmetry. It is easy to construct the most general Lagrangian under the transformation $U \to LUR^\dagger$. The most general invariant term with no derivatives must be the product of terms of the form $\mathrm{Tr}\,UU^\dagger \ldots UU^\dagger$, however $UU^\dagger = 1$, so all such terms are constant and independent of the Goldstone boson fields. This means that, as we expected, the Goldstone boson fields have to couple derivatively. Derivatives have to go in pairs due to Lorentz in-

variance and the only invariant with two derivatives is

$$\mathcal{L}^{(2)} = \frac{F_0^2}{4}\mathrm{Tr}\,\partial_\mu U \partial^\mu U^\dagger \,. \tag{2.18}$$

In order to have the kinetic terms for the π fields, that appear when the exponential in U is expanded, properly normalized the low–energy constant multiplying this operator has to be fixed at $\frac{F_0^2}{4}$.

The Noether theorem can be used to obtain the conserved currents associated to Chiral symmetry of the Lagrangian on (2.18). The left current is

$$J_L^{\mu,\alpha} = \frac{i}{2}F_0^2 \mathrm{Tr}\, T^\alpha U \partial^\mu U^\dagger \,, \tag{2.19}$$

the right current can be obtained by a parity transformation $\pi(x) \to -\pi(-x)$, or by an infinitesimal $SU(n_f)_R$ transformation

$$J_R^{\mu,\alpha} = \frac{i}{2}F_0^2 \mathrm{Tr}\, T^\alpha U^\dagger \partial^\mu U \,. \tag{2.20}$$

The axial current is obtained by subtracting the left current from the right current, expanding it in powers of the π fields

$$J_A^{\mu,\alpha} = J_R^{\mu,\alpha} - J_L^{\mu,\alpha} = -F_0 \partial^\mu \pi^\alpha + \ldots \tag{2.21}$$

Taking the matrix element of the axial current between the standard vacuum and a Goldstone boson state

$$\langle 0|J_A^{\mu\alpha}|\pi^\beta\rangle = iF_0 p^\mu \,. \tag{2.22}$$

If we compare (2.22) with (1.35) we see that introducing F_0 in (2.15) was justified.

2.4 Power counting

The Chiral Lagrangian can be organized according to the number of derivatives of the operators

$$\mathcal{L}_\chi = \sum_{n=1}^{\infty} \mathcal{L}^{(2n)} \,, \tag{2.23}$$

the number of derivatives is always an even number due to Lorentz invariance requirements. Consider an arbitrary loop graph, for example the one in Fig.2.1,

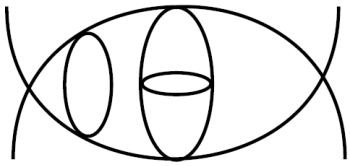

Figure 2.1: Arbitrary loop diagram

with m_2 interaction vertices that come from $\mathcal{L}^{(2)}$, m_4 interaction vertices that come from $\mathcal{L}^{(4)}$, and so on. The general form of this diagram is

$$\mathcal{A} \sim \int \left(d^4p\right)^L \frac{1}{\left(p^2\right)^I} \prod_n \left(p^{2n}\right)^{m_{2n}} , \tag{2.24}$$

where L is the number of loops, I is the number of internal lines, and p stands for the momentum running in the loop. There is a d^4p for each loop, and each boson propagator contributes a factor $1/p^2$. Each vertex from $\mathcal{L}^{(2n)}$ gives a factor of p^{2n}. In the mass subtraction scheme the only dimensional parameters are the momenta p. Thus the amplitude has to have the form $\mathcal{A} \sim p^D$, where D is given by

$$D = 4L - 2I + \sum_n 2n\, m_{2n} , \tag{2.25}$$

For any Feymann diagram one can show that the number of vertices, loops and internal lines are not independent quantities

$$V - I + L = 1 , \tag{2.26}$$

where V is the number of vertices. The relation in (2.26) can be used to write (2.25) in terms of the number of vertices instead in number of the internal lines, then using $V = \sum_n m_{2n}$ one gets

$$D = 2 + 2L + \sum_n 2\left(n-1\right) m_{2n} . \tag{2.27}$$

The Chiral Lagrangian starts at order p^2, so $n \geq 1$, and all terms in (2.27) are positive. As a result, only a finite number of terms in the effective Lagrangian are needed to work to a fixed order in p. For example to compute scattering amplitudes at order p^4, we set $D = 4$ in (2.27) and find out which combinations of L, n and m_{2n} fulfill the constrain. The solutions are $L = 0\,, m_4 = 1\,, m_{2n>4} = 0$,

and $L = 1, m_{2n>2} = 0$. This mean that to compute amplitudes to order p^4 one only needs to consider tree level diagrams with insertions of vertices from $\mathcal{L}^{(4)}$ and one loop diagrams with vertices from the $\mathcal{L}^{(2)}$ [12].

2.5 Naive Dimensional Analysis

The question of how large is the convergence radius of the low–energy expansion was explored by Georgi and Manohar in [50]. Since higher order terms are required as counterterms for loops involving lower order interactions, it is inconsistent to assume that the size of these terms is smaller than the typical loop corrections. Any running low–energy constant $L(\mu)$ in a counterterm should be at least as big as its anomalous dimension $\mu dL(\mu)/d\mu$.

Take, for example, the π–π scattering amplitude at order p^4. The power counting argument tells us that there is a tree level graph with an insertion of $\mathcal{L}^{(4)}$ and a loop graph with vertexes from $\mathcal{L}^{(2)}$. The loop diagram is of order

$$I \sim \int \frac{d^4k}{(2\pi)^4} \frac{k^2}{F_0^2} \frac{k^2}{F_0^2} \frac{1}{k^4}, \tag{2.28}$$

where $\frac{1}{k^4}$ is from the two internal propagators, and each four pion vertex contributes by k^2/F_0^2. Estimating the integral gives

$$I \sim \frac{p^4}{16\pi^2 F_0^4} \log(p/\mu), \tag{2.29}$$

where μ is the $\overline{MS}$ renormalization scale, and p represents a generic external momentum. A four derivative operator in the Lagrangian of the form

$$l \,\mathrm{Tr} \partial_\mu U \partial^\mu U^\dagger \partial_\nu U \partial^\nu U^\dagger, \tag{2.30}$$

produces a four pion interaction of order lp^4/F_0^4 when U is expanded in powers of $\boldsymbol{\pi}/F_0$. The total four pion amplitude, which is the sum of the tree and loop diagrams, is μ–independent. A shift in the renormalization scale μ is compensated for by a corresponding shift in l. A change in μ of order one produces a shift in l of $\delta l \sim 1/16\pi^2$. Generically, l must be at least as δl,

$$|l| \gtrsim |\delta l| \sim \frac{1}{16\pi^2}, \tag{2.31}$$

because a shift in the renormalization point of order one produces a shift in L of this size.

Now, the quantum field theory action must be dimensionless, which means all the terms in the Lagrangian have to be of mass dimension four. Therefore the low–energy constants associated with a given operator must have the size

$$\mathcal{L}_\chi = \frac{F_0^2}{4}\left[\mathrm{Tr}\partial_\mu U \partial^\mu U^\dagger + \frac{1}{\Lambda_\chi^2}\mathcal{L}^{(4)} + \frac{1}{\Lambda_\chi^4}\mathcal{L}^{(6)} + \cdots\right]. \tag{2.32}$$

This naturally gives an expansion for the amplitudes in powers of p/Λ_χ. The expansion is going to converge as long as $p/\Lambda_\chi \ll 1$, which is true for momentum of the order of the pion and the kaon mass. Combining the estimate from (2.31) with the Lagrangian in the form of (2.32) one finds

$$\Lambda_\chi \leq 4\pi F_0 \sim 1\mathrm{GeV} \tag{2.33}$$

Numerous calculations suggest that in QCD, this inequality can be replaced by $\Lambda_\chi \sim 4\pi F_0$, and be used as the expansion parameter for the effective theory.

2.6 Coupling to external fields

The effective theory technique becomes much more powerful if one introduces couplings to externals fields. Following Gasser and Leutwyler [13, 14], we introduce in the QCD Lagrangian in the Chiral limit (1.9) the couplings of the conserved of the vector and axial–vector currents as well as the scalar and pseudoscalar quark densities to the external c–numbers fields $v^\mu(x)\,, a^\mu(x)\,, s(x)$ and $p(x)$

$$\mathcal{L}_{QCD} = \mathcal{L}^0_{QCD} + \mathcal{L}_{ext}\,, \tag{2.34}$$

with

$$\mathcal{L}_{ext} = \bar{q}\gamma^\mu\left(v_\mu + \gamma_5 a_\mu\right)q - \bar{q}\left(s - i\gamma_5 p\right)q\,. \tag{2.35}$$

The external fields are color-neutral, Hermitian $n_f \times f$ matrices in the flavor space and commute with the Dirac matrices. Since we are not concerned with the effects of the axial $U(1)$ anomaly, we omit the coupling to the singlet axial current and set $\mathrm{Tr}\, a_\mu = 0$. The ordinary n_f–flavor QCD Lagrangian is recovered by setting $v_\mu = a_\mu = p = 0$ and $s = \mathcal{M}$, where $\mathcal{M}$ is the quark mass matrix defined in (1.36). The external fields can be used to incorporate the electromagnetic and

semileptonic weak interactions

$$\begin{aligned} r_\mu &\equiv v_\mu + a_\mu = eQA_\mu \\ l_\mu &\equiv v_\mu - a_\mu = eQA_\mu + \frac{e}{\sqrt{2}sin\theta_W}\left(W_\mu^\dagger T_+ + h.c.\right) + \ldots \end{aligned} \tag{2.36}$$

Here Q denotes the quark–charge matrix and T_+ is a matrix containing the relevant Cabibbo-Kobayashi-Maskawa factors, for example for $n_f = 2$, $Q = \mathrm{diag}\,(2/3, -1/3)$ and

$$T_+ = \begin{pmatrix} 0 & V_{ud} \\ 0 & 0 \end{pmatrix}. \tag{2.37}$$

Let us define the generating functional $Z\,[v, a, s, p]$ by

$$\begin{aligned} \exp\left(iZ\,[v, a, s, p]\right) =& \langle 0\,out|0\,in\rangle_{v,a,s,p} \\ =& \int \mathcal{D}q\mathcal{D}\bar{q}\mathcal{D}G_\mu^\alpha \exp\left[i\int d^4x \mathcal{L}_{QCD}\left(q, \bar{q}, G_\mu^\alpha, r_\mu, l_\mu, s, p\right)\right], \end{aligned} \tag{2.38}$$

where the external fields play the role of classical auxiliary variables. The expansion of the generating functional in powers of the external fields determines the Green functions of the theory. The quantity $\exp\left(iZ\,[v, a, s, p]\right)$ is the vacuum–to–vacuum transition amplitude in presence of external fields and describes the response of the system to the perturbations generated by them. The external field method has an important advantage: in the absence of anomalies, the Ward identities obeyed by the Green functions of the currents (the so–called Chiral Ward identities) are equivalent to the statement that the generating functionals is invariant under local transformations of the external fields [12, 51]. The Lagrangian in (2.34) is invariant under local Chiral group transformations if the external fields transform according to

$$\begin{aligned} r_\mu &\to V_R r_\mu V_R^\dagger + iV_R\partial_\mu V_R^\dagger \\ l_\mu &\to V_L l_\mu V_L^\dagger + iV_L\partial_\mu V_L^\dagger \\ s + ip &\to V_R(s + ip)V_L^\dagger \\ s - ip &\to V_R(s - ip)V_L^\dagger. \end{aligned} \tag{2.39}$$

The derivatives in (2.39) serve the same purpose as in the construction of gauge theories, they cancel terms originated from the kinetic parts of the Lagrangian. The defining property of Chiral perturbation theory as an effective field theory

of QCD is that the low–energy Green functions coincide with those of QCD, that is that the generating functionals are equivalent

$$\exp\left(iZ\left[v,a,s,p\right]\right) = \int \mathcal{D}U \exp\left[i\int d^4x \mathcal{L}_\chi\left(U,r_\mu,l_\mu,s,p\right)\right]. \tag{2.40}$$

The most remarkable property of this method is that no information of the underlying theory is lost, the effective field theory is just a convenient way to work out the low–energy expansion, within its radius of convergence, at any desired order. Since both the underlying theory and the effective fields theory have to fulfill the same Ward identities, the effective theory has to be invariant under the local transformations of the external fields given in (2.39). The transformations (2.39) determine how the external fields couple to the Goldstone boson fields. We can use this local symmetry to build a generalized Lagrangian for the Goldstone boson in the presence of external fields. To respect local invariance of the Gauge fields r_μ and l_μ we have to define the covariant derivatives

$$D_\mu U = \partial_\mu U - ir_\mu U + iUl_\mu\,, \quad D_\mu U^\dagger = \partial_\mu U^\dagger - iU^\dagger r_\mu + il_\mu U^\dagger\,, \tag{2.41}$$

and the field strength tensors

$$F_L^{\mu\nu} = \partial^\mu l^\nu - \partial^\nu l^\mu - i\left[l^\mu, l^\nu\right] \quad F_R^{\mu\nu} = \partial^\mu r^\nu - \partial^\nu r^\mu - i\left[r^\mu, r^\nu\right]. \tag{2.42}$$

Note that $D_\mu U$ transform a like U under Chiral transformations, and that the field strength tensors are traceless in the flavor space. At the lowest order in momentum, the more general effective Lagrangian consistent with Lorentz invariance and local Chiral symmetry coupled to external fields is of the form

$$\mathcal{L}^{(2)} = \frac{F_0^2}{4}\mathrm{Tr}\left[D_\mu U^\dagger D^\mu U + U^\dagger\chi + \chi^\dagger U\right], \tag{2.43}$$

where

$$\chi = 2B_0(s+ip)\,, \tag{2.44}$$

and B_0 is a low–energy constant, like F_0, not fixed by symmetry requirements. In order to build (2.43) we need to generalize the power counting defined in section 2.4 to include the external fields. The prescription we will use is to count the gauge fields as $l_\mu \sim r_\rho \sim p$ and $\chi \sim p^2$, where p is here a generic external momentum.

The physical meaning of B_0 can be understood as follows. Take derivatives

of the generating functional with respect to the external scalar and pseudoscalar sources

$$\begin{aligned}\bar{q}_L^\alpha q_R^\beta &= -\frac{\delta\mathcal{L}_\chi}{\delta(s-ip)^{\alpha\beta}} = -\frac{F_0^2}{2}U^{\alpha\beta}(\pi)\,,\\ \bar{q}_R^\alpha q_L^\beta &= -\frac{\delta\mathcal{L}_\chi}{\delta(s+ip)^{\alpha\beta}} = -\frac{F_0^2}{2}U^{\alpha\beta}(\pi)\,,\end{aligned} \tag{2.45}$$

adding them up and summing for n_f flavors, and at first order in $\pi = 0$

$$\langle 0|\bar{q}q|0\rangle = -n_f F_0^2 B_0\,. \tag{2.46}$$

In section 1.4 we showed that $\langle 0|\bar{q}q|0\rangle$ is related to the order parameter associated to the spontaneous breaking of Chiral symmetry, B_0 is thus related to the value of this order parameter. The Goldstone bosons, parametrized by the matrix $U^{\alpha\beta}(\pi)$, correspond to excitations over this vacuum condensate. Taking $s = \mathcal{M}$, and $p = 0$, the explicit Chiral symmetry breaking in the original QCD Lagrangian is introduced to the effective Lagrangian. As anticipated in section 1.5 the Goldstone bosons acquire masses, and thus we will refer to them as pseudo–Goldstone bosons. The χ term in (2.43) gives rise to the pseudogoldstone bosons mass terms plus additional interaction proportional to the quark masses. The relation between the peudoscalar meson masses and the quark masses is,

$$\begin{aligned}&m_{\pi^\pm}^2 = 2B_0\hat{m}\,, \quad m_{\pi^0}^2 = 2B_0\hat{m} - \epsilon + \mathcal{O}\left(\epsilon^2\right)\,,\\ &m_{K^\pm}^2 = B_0\left(m_u + m_s\right)\,, \quad m_{K^\pm}^2 = B_0\left(m_d + m_s\right)\,,\\ &m_\eta^2 = \frac{2}{3}B_0(\hat{m} + 2m_s) + \epsilon + \mathcal{O}\left(\epsilon^2\right)\,,\end{aligned} \tag{2.47}$$

where

$$\hat{m} = \frac{1}{2}\left(m_u + m_d\right)\,, \quad \epsilon = \frac{B_0\left(m_u - m_d\right)^2}{4\left(m_s - \hat{m}\right)}\,. \tag{2.48}$$

The ϵ parameter indicates how much isospin symmetry is broken. The physical value of ϵ is small and frequently is be taken as zero, corrections proportional to ϵ can be taken as suppressed by an additional Chiral order. The order ϵ corrections to $m_{\pi^0}^2$ and m_η^2 originate from a small mixing term between the π^0 and η fields

$$-\frac{B_0}{\sqrt{3}}(m_u - m_d)\pi^0\eta\,. \tag{2.49}$$

The diagonalization of the quadratic π^0, η mass matrix, gives the eigenvalues shown in (2.47).

2.7 The Chiral Lagrangian up to next–to–leading order

The construction of the Chiral Lagrangian proceeds by writing down all Lorentz invariants (products of) traces of Chiral symmetry, in addition one has to implement the discrete symmetries P and C and hermiticity on the Lagrangian. This is straightforward with the help of the transformation properties given in (2.13) and (2.39). The real difficulty is to find the minimal set of terms for those Lagrangians. The corresponding low–energy constants then parametrize the most general solutions of the Chiral Ward Identities. To obtain the minimal set of independent dimension four monomials [13, 14], we should use the following relations or procedures: partial integration, equations of motion of the lowest order Lagrangian and the Cayley–Hamilton relations. In the case of $n_f = 2$ there are further simplifications because in $SU(2)$ the antisymmetric structure constants vanish, while this does not happen in $SU(3)$, thus the Lagrangians for $n_f = 2$ and $n_f = 3$ are different. For the purpose of this work we will only need $n_f = 2$. The Cayley–Hamilton theorem states that any n–dimensional matrix obeys its own characteristic equation. For two arbitrary two–dimensional matrices, A_1 and A_2, Cayley–Hamilton theorem implies the following relation

$$A_1A_2 + A_2A_1 - A_1\mathrm{Tr}\left[A_2\right] - A_2\mathrm{Tr}\left[A_1\right] + \mathrm{Tr}\left[A_1\right]\mathrm{Tr}\left[A_2\right]I_{2\times2} - \mathrm{Tr}\left[A_1A_2\right]I_{2\times2} = 0\,. \tag{2.50}$$

The next–to–leading Chiral Lagrangian for $n_f = 2$ [13, 52] is

$$\begin{aligned}
\mathcal{L}^{(4)} =& \frac{l_1}{4}\mathrm{Tr}\left[D_\mu U^\dagger D^\mu U\right]^2 + \frac{l_2}{4}\mathrm{Tr}\left[D_\mu U^\dagger D^\nu U\right]\mathrm{Tr}\left[D_\mu U^\dagger D^\nu U\right] \\
&+ \frac{l_3}{16}\mathrm{Tr}\left[\chi^\dagger U + U^\dagger\chi\right]^2 + \frac{l_4}{4}\mathrm{Tr}\left[D_\mu U^\dagger D^\nu\chi + D_\mu U D^\nu\chi^\dagger\right] \\
&+ l_5\mathrm{Tr}\left[F_R^{\mu\nu}UF_L^{\mu\nu}U^\dagger\right] + \frac{il_6}{2}\mathrm{Tr}\left[F_R^{\mu\nu}D^\mu UD^\nu U^\dagger + F_L^{\mu\nu}D^\mu U^\dagger D^\nu U\right] \\
&- \frac{l_7}{16}\mathrm{Tr}\left[\chi^\dagger U - U^\dagger\chi\right]^2 + \frac{1}{4}\left(h_1 + h_3\right)\mathrm{Tr}\left[\chi^\dagger\chi\right] \\
&+ \frac{1}{2}\left(h_1 - h_3\right)\mathrm{Re}(\det\chi) - h_2\mathrm{Tr}\left[F_R^{\mu\nu}F_{R\,\mu\nu} + F_L^{\mu\nu}F_{L\,\mu\nu}\right]\,.
\end{aligned} \tag{2.51}$$

The numerical values of the low–energy constants $l_i\,, i = 1,7$ and $h_i\,, i = 1,3$ is not determined by Chiral symmetry and needs to be fixed using experimental input or lattice QCD data. Meson–resonance saturation is a theoretical way of estimating these low-energy constants.

When calculating loop diagrams, using vertices from $\mathcal{L}^{(2)}$, ultraviolet divergences appear, in the framework of dimensional regularization these divergences appear as poles at space–time dimension $d = 4$. The loop diagrams are renormalized by absorbing the infinite parts into redefinitions of the fields and the parameters of the Lagrangian. Since $\mathcal{L}^{(2)}$ is not renormalizable in a traditional sense, the infinities are absorbed by the low–energy constants of $\mathcal{L}^{(4)}$. The fact that all the terms allowed by symmetries are included assures the necessary counterterms to absorb all possible divergences. The low–energy constants in (2.51) renormalize as follows

$$l_i := l_i^r + \gamma_i \lambda \quad (i = 1, \ldots, 7)\,, \qquad h_j := h_j^r + \delta_j \lambda \quad (j = 1, 2, 3)\,, \tag{2.52}$$

with

$$\lambda = \frac{1}{16\pi^2}\left(\frac{1}{d-4} - \frac{1}{2}\left[\ln 4\pi + \Gamma'(1) + 1\right]\right). \tag{2.53}$$

If the theory only includes the pseudo–Goldstone bosons the γ are

$$\begin{aligned} &\gamma_1 = \frac{1}{3} \quad \gamma_2 = \frac{2}{3} \quad \gamma_3 = -\frac{1}{2} \quad \gamma_4 = 2 \quad \gamma_5 = -\frac{1}{6} \\ &\gamma_6 = -\frac{1}{3} \quad \gamma_7 = 0 \quad \delta_1 = 2 \quad \delta_2 = \frac{1}{12} \quad \delta_3 = 0 \quad . \end{aligned} \tag{2.54}$$

CHAPTER

3

PION–NUCLEON CHIRAL EFFECTIVE THEORIES

3.1 Transformation properties of matter fields

Chiral perturbation theory can also be used to describe the interactions of pseudo–Goldstone bosons with matter fields: baryons, heavy mesons, etc. As we have seen in Chapter 1 Chiral symmetry is spontaneously broken to $SU_V(n_f)$. Therefore the particle spectrum of QCD can be organized in multiplets of the remaining unbroken symmetry group of the theory, $SU_V(n_f)$, transforming according to its irreducible linear realizations. Additionally we have argued in Chapter 2 that Goldstone boson degrees of freedom transform according to non-linear realization of the Chiral symmetry group. Matter fields do not have a preferred realization of the Chiral symmetry group, any transformation law that reduces to the adjoint transformation law for $SU_V(n_f)$ is acceptable [18, 16, 17]. To be specific, lets consider the following examples; for $n_f = 3$ the octet of the $\frac{1}{2}^+$ baryons B, see Fig.3.1, and for $n_f = 2$ the proton–neutron doublet ψ

$$B = \begin{pmatrix} \frac{1}{\sqrt{2}}\boldsymbol{\Sigma}^0 + \frac{1}{\sqrt{6}}\Lambda & \boldsymbol{\Sigma}^+ & p \\ \boldsymbol{\Sigma}^- & -\frac{1}{\sqrt{2}}\boldsymbol{\Sigma}^0 + \frac{1}{\sqrt{6}}\Lambda & n \\ \boldsymbol{\Xi}^- & \boldsymbol{\Xi}^0 & -\frac{2}{\sqrt{6}}\Lambda \end{pmatrix}, \quad \psi = \begin{pmatrix} p \\ n \end{pmatrix}, \tag{3.1}$$

in Chapter 5 we will consider the case of a $SU_V(2)$ singlet 0^+. Using the notation of section 2.2, the transformations under the unbroken subgroup H are

$$B \to VBV^\dagger, \quad \psi \to V\psi\,. \tag{3.2}$$

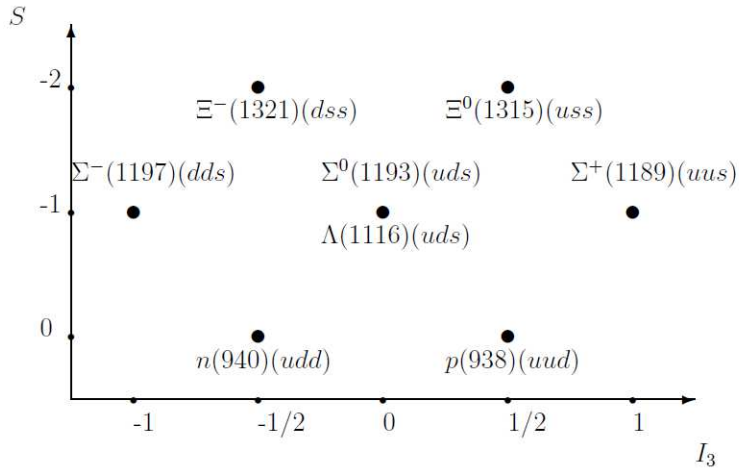

Figure 3.1: The Baryon octet in a (I_3, S). In parenthesis the masses in MeV and the quark content

Any Chiral symmetry transformations that reduces to these is valid, for example one can chose the following transformations for B and ψ

$$B \to RBR^\dagger\,, B \to KBR^\dagger\,, \psi \to K\psi\,, \psi \to R\psi\,, \text{etc}\,. \tag{3.3}$$

The different choices are all equivalent, and correspond to redefining the baryon fields. For example, assuming the second transformation law in (3.3) for B, then $\tilde{B} = uB$ transforms like the first transformation law in (3.3). The prescription of [16, 17] for matter fields is that under a Chiral symmetry group transformation, the transformation law is

$$B \to KBK^\dagger\,, \quad \psi \to K\psi\,, \tag{3.4}$$

which turns out to be the most convenient when constructing a Chiral Lagrangian for matter fields.

3.2 Lowest order Lagrangian and the power counting breakdown

The Chiral Lagrangian for matter fields is the most general invariant Lagrangian written in terms of the matter fields of (3.1) and the Goldstone bosons fields consistent with Chiral symmetry, Lorentz invariance and the discrete symmetries C, P and T. As in the mesonic sector the Chiral Ward identities for the baryonic sector will be satisfied if the Chiral symmetry in the effective Lagrangian is promoted to a local symmetry [53]. The local character of the transformations implies that we need to introduce a covariant derivative $\nabla_\mu\psi\,(\nabla_\mu B)$ that transforms with the same transformation law as $\psi\,(B)$

$$\nabla_\mu B = \partial_\mu B + [\Gamma_\mu, B]\,, \quad \nabla_\mu\psi = \partial_\mu\psi + \Gamma_\mu\psi\,, \tag{3.5}$$

where Γ_μ is

$$\Gamma_\mu = \frac{1}{2}\left(u^\dagger\left(\partial_\mu - ir_\mu\right)u + u\left(\partial_\mu - il_\mu\right)u^\dagger\right)\,, \tag{3.6}$$

and transforms like a connection in the coset space. It is also useful to introduce another Hermitian building block, the so–called veilbein

$$u_\mu = i\left(u^\dagger\left(\partial_\mu - ir_\mu\right)u - u\left(\partial_\mu - il_\mu\right)u^\dagger\right)\,, \tag{3.7}$$

which transforms like an axial vector and under Chiral symmetry

$$u_\mu \to K u_\mu K^\dagger \tag{3.8}$$

Now we are in position to write the most general Lagrangian with the smallest number of derivatives. For $n_f = 3$ [53]

$$\mathcal{L}_B^{(1)} = \mathrm{Tr}\left[\bar{B}\left(i\not{\nabla} - m_B\right)B\right] + D\mathrm{Tr}\left[\bar{B}\gamma^\mu\gamma_5\left\{u_\mu, B\right\}\right] + F\mathrm{Tr}\left[\bar{B}\gamma^\mu\gamma_5\left[u_\mu, B\right]\right]\,. \tag{3.9}$$

The low–energy constants D and F are not constrained by Chiral symmetry, and can determined by fitting the semileptonic decays $B \to B' + e^- + \bar{\nu}_e$. For $n_f = 2$ [54]

$$\mathcal{L}_\psi^{(1)} = \bar{\psi}\left(i\not{\nabla} - m_N + \frac{g_A}{2}\gamma^\mu\gamma_5 u_\mu\right)\psi\,. \tag{3.10}$$

The only low–energy constant is the axial–vector coupling $\mathring{g}_A$, which is related to D and F by $\mathring{g}_A = D + F$, and obviously $m_B \sim m_N$.

As in the mesonic Lagrangian the higher dimension terms are suppressed by inverse powers of Λ_χ however there is no longer a consistent derivative expansion for processes involving baryons. Consider the kinetic term in (3.9) or (3.10), even for low–momentum processes this produces a factor of m_B/Λ_χ, because of the time derivative in ∂_μ. Now consider the next operator in number of derivatives, it will produces a factor m_B^2/Λ_χ^2 which is not small compared with the kinetic term because $m_B \sim \Lambda_\chi$. Thus a computation, for example, of low–momentum baryon–pion scattering amplitudes requires that one first sum all the time derivatives in the effective Lagrangian; it is not consistent to use only the lowest term. A similar problem occurs in the loop expansion. The power counting argument fails because m_B is a dimensionful parameter of order $\Lambda\chi$ that does not vanish in the Chiral limit. Higher order loops diagrams involving baryon propagators can produce amplitudes which are only suppressed by factors of $m_B/\Lambda_\chi \sim 1$ and therefore as important as lower order amplitudes. The renormalization of divergences also may requier the tuning of low–energy constants appearing at lower order. In this framework it is complicated to establish a systematic method of assessing the relative importance of diagrams generated by the Chiral Lagrangian with matter fields. In the next section a formalism relying in a non–relativistic formulation of the heavy fields is developed to circumvent these problems. There are alternative approaches that keep the heavy fields relativistic, the so–called Infrared Regularization [21] and the Extended On–mass–shell renormalization [55, 56].

3.3 Heavy Baryon Chiral Perturbation Theory

The heavy baryon perturbation theory describes the interactions of a heavy baryon with low momentum pseudo–Goldstone bosons. Jenkins and Manohar formulated heavy baryon perturbation theory [19, 20] expanding the explicitly covariant Lagrangian about nearly on–shell baryons, so that one has a Lagrangian that can be expanded in inverse powers of the heavy baryon mass. This approach follows closely the techniques originally developed by Georgi [57] for the study of heavy quark systems. The approach is also analogous to the Foldy–Wouthuysen non-relativistic reduction [58] which provides a systematic procedure to block–diagonalize a relativistic Dirac Hamiltonian in powers of the inverse mass M of the Dirac field. In the rest of this section we will work out the heavy baryon expansion for the nucleon Lagrangian (3.10) because it is the one we will need in chapter 4, but the procedure is analogous for any heavy matter field coupled to

the Chiral Lagrangian. For a explicit Lorentz covariant description of the pion–nucleon system see [59].

The velocity of the nucleons is nearly unchanged when it exchanges some small momentum with the pions, as a result a nearly on–shell nucleon with velocity v^μ has a momentum

$$p^\mu = m_N v^\mu + k^\mu \,, \tag{3.11}$$

where k^μ is a small momentum compared to m_N. The velocity four–vector has the properties $v^2 = 1\,, v^0 \geq 1$. Consider the projectors

$$P_v^\pm = \frac{1}{2}\left(1 \pm \not{v}\right) \,, \tag{3.12}$$

which fulfill the properties: completeness $P_v^+ + P_v^- = 1$, idempotent $(P_v^\pm)^2 = P_v^\pm$ and orthogonal $P_v^\pm P_v^\mp = 0$. The nucleon field ψ can be decomposed using this projector operators

$$\psi = e^{-im_N v\cdot x}\left[H_v + h_v\right] \,, \tag{3.13}$$

with

$$H_v = \exp\left[im_N v\cdot x\right] P_v^+ \psi \,, \quad h_v = \exp\left[im_N v\cdot x\right] P_v^- \psi \,. \tag{3.14}$$

In the nucleon rest frame, $v = (1,0,0,0)$, $H_v(h_v)$ corresponds to the particle (antiparticle) part of the spinor and subtracting the nucleon mass from all energies. If we are interested in processes with only nucleons and no antinucleons as asymptotic states, the h_v field parts of the Lagrangian can be eliminated by using the equations of motion or by Gaussian integration of the h_v fields in the generating functional. Writing the Lagrangian (3.10) in terms of H_v and h_v and then integrating out the later with either of the proposed methods we obtain

$$\begin{aligned}\mathcal{L}_\psi^{(1)} =& \bar{H}_v\left(iv\cdot\nabla + \frac{g_A}{2}\not{u}_\perp\gamma_5\right)H_v + \bar{H}_v\left(i\not{\nabla}_\perp + \frac{g_A}{2}v\cdot u\gamma_5\right)\\ &\times\left(2m_N + iv\cdot\nabla - \frac{g_A}{2}\not{u}_\perp\gamma_5\right)^{-1}\left(i\not{\nabla}_\perp - \frac{g_A}{2}v\cdot u\gamma_5\right)H_v \,,\end{aligned} \tag{3.15}$$

where the perpendicular component of a quantity A^μ is defined as $A_\perp^\mu = A^\mu - v\cdot A v^\mu$. In the second term the $2m_N$ factor dominates the denominator and thus can be expanded in series of the inverse powers of m_N

$$\mathcal{L}_{H_v}^{(1)} = \bar{H}_v\left(iv\cdot\nabla + \frac{g_A}{2}\not{u}_\perp\gamma_5\right)H_v + \mathcal{O}\left(\frac{1}{m_N}\right) \,. \tag{3.16}$$

The derivatives on the H_v fields produce factors k, rather than p, so that higher derivative terms in the Lagrangian are suppressed by powers of k/Λ_χ, which is small. Thus, the effective Lagrangian has a consistent derivative expansion as long as the pion momentum and the off–shellness of the baryon is small compared with Λ_χ. The heavy baryon formulation of the Chiral nucleon Lagrangian does not contain the nucleon mass term thus it does not appear in the nucleon propagator which avoids the power counting breaking m_N/Λ_χ factors coming from loop integrals. The heavy nucleon Lagrangian also has an expansion in $1/m_N$. The $1/m_N$ effects in the original Dirac theory can be reproduced in the effective theory by including higher dimension operators suppressed by inverse powers of m_N. The resultant Chiral expansion is valid regardless of the relative size of m_N and Λ_χ, although in practice it is true that $m_N \sim \Lambda_\chi$. However it has been argued by the authors of [61] that the convergence of the Heavy Baryon expansion is slow in certain observables.

3.4 The non–relativistic pion–nucleon Lagrangian up to next-to-leading order

In section 2.7 we constructed the next–to–leading order Lagrangian for pseudo–Goldstone bosons, in that case we saw that all next–to–leading order operators are dimension six, and in general operators always have even dimension. In the nucleon sector due to the fermionic spin–$1/2$ nature of nucleons the effective Lagrangian operators can be of odd as well as even dimension. Hence the next–to-leading nucleon–pion Lagrangian is composed of operators of dimension five. We should construct the effective Lagrangian directly in a non–relativistic form, constructing it from the relativistic formulation is not consistent because the Lagrangian with relativistic nucleons does not have a well defined counting. In the non-relativistic Lagrangian Lorentz symmetry is realized in the form of reparametrization invariance [62]. Reparametrization invariance fixes some of the low–energy constants of the theory. The next–to–leading Lagrangian in the heavy baryon limit [60] can, thus be broken up into two pieces, the first with the low–energy constants fixed by reparametrization invariance

$$\mathcal{L}^{(2)}_{H_v\,,fixed} = \frac{1}{2m_N}\bar{H}_v\left((v\cdot\nabla)^2 - \nabla^2 - ig_A\left\{\vec{S}\cdot\vec{\nabla}, v\cdot u\right\}\right)H_v\,, \tag{3.17}$$

where $S_\mu = \frac{i}{2}\gamma_5\sigma_{\mu\nu}v^\nu$ is the covariant spin–operator. The second piece has free low–energy constants

$$\mathcal{L}^{(2)}_{H_v,ct} = \bar{H}_v\left(c_1\,\mathrm{Tr}\left[\chi_+\right] + \frac{c_2}{2}\mathrm{Tr}\left[(v\cdot u)^2\right] + \frac{c_3}{2}\mathrm{Tr}\left[u^\mu u_\mu\right] + i\frac{c_4}{2}\left[S^\mu, S^\nu\right]\left[u^\mu, u^\nu\right]\right.$$
$$\left. + c_5\tilde{\chi}_+ - i\frac{c_6}{4m_N}\left[S^\mu, S^\nu\right]F^+_{\mu\nu} - i\frac{c_7}{4m_N}\left[S^\mu, S^\nu\right]\mathrm{Tr}\left[F^+_{\mu\nu}\right]\right)H_v\,, \tag{3.18}$$

where

$$\chi_+ = u^\dagger\chi u^\dagger + u\chi^\dagger u\,, \quad \tilde{A} = A - \mathrm{Tr}\left[A\right]\,,$$
$$F^+_{\mu\nu} = u^\dagger F^{\mu\nu}_R u + uF^{\mu\nu}_L u^\dagger\,. \tag{3.19}$$

The $c_i\,, i = 1,\ldots,5$ carry the dimension of an inverse mass and should be of the order $1/\Lambda_\chi$. In the particular cases of c_6 and c_7 we followed the notation of [60] and where these low energy constants are dimensionless and of order one by introducing an inverse power of m_N.

Finally, working in the nucleon reference frame $v = (1,0,0,0)$, only the upper pair component on the Dirac spinor of the H_v is non–zero, which leads to large simplification in the Lagrangian and the calculations. Let us define N as the upper two component spinor of the H_v field, the Lagrangians (3.16), (3.17) and (3.18) reduce to

$$\mathcal{L}^{(1)}_{\pi N} = N^\dagger\left(i\nabla_0 - \frac{g_A}{2}\vec{\sigma}\cdot\vec{u}\right)N\,, \tag{3.20}$$

and

$$\mathcal{L}^{(2)}_{\pi N} = N^\dagger\left(\frac{\vec{\nabla}^2}{2m_N} + \frac{ig_A}{4m_N}\{\vec{\sigma}\cdot\vec{\nabla}, u_0\} + c_1\mathrm{Tr}\left[\chi_+\right] + c_2u_0^2 - c_3\vec{u}\cdot\vec{u}\right.$$
$$\left. + i\frac{c_4}{2}\epsilon^{ijk}\sigma^k u_i u_j + c_5\tilde{\chi}_+ - \frac{c_6}{8m_N}\epsilon^{ijk}F^+_{ij}\sigma_k - \frac{c_7}{8m_N}\epsilon^{ijk}\mathrm{Tr}\left[F^+_{ij}\right]\sigma_k\right)N\,. \tag{3.21}$$

Up until now we have only considered the one nucleon sector. Since the barionic number is conserved the Lagrangian can be splited into pieces with a definite barionic number. Next we are going to consider the two nucleon sector.

Nucleon contact Lagrangian

Two–nucleon contact interactions consist of four nucleon fields. Such terms are need to renormalize loop integrals, and when considering nucleon-nucleon scattering or the nucleon–nucleon potential. Nucleon contact interactions can be interpreted as encoding unresolved short–distance dynamics, for example the exchange of heavy mesons. Because of parity nucleon contact interactions come only in even powers of derivatives, thus

$$\mathcal{L}_{NN} = \sum_{n=1}^{\infty} \mathcal{L}_{NN}^{(2n)} \,. \tag{3.22}$$

The lowest order NN Lagrangian has no derivatives and reads [22, 23]

$$\mathcal{L}_{NN}^{(0)} = -\frac{1}{2} C_S N^\dagger N N^\dagger N - \frac{1}{2} C_T \left(N^\dagger \vec{\sigma} N\right) \cdot \left(N^\dagger \vec{\sigma} N\right) \,. \tag{3.23}$$

A discussion on the next–to–leading Lagrangian can be found in Ref. [63].

3.5 Power Counting

The power counting scheme for an effective field theory for pions and nucleons is not as straightforward as in the theory with only pseudo–Goldstone bosons. Although a power counting rule like (2.27) can be written it is not valid for all sectors of the theory, hence the method we will follow is to estimate the size of a diagram in terms of the relevant scales, and by inspecting all possible diagrams this way determine which one contributes up to a given precision. Obviously higher order terms in the effective Lagrangian will automatically suppress a diagram beyond a given order and should not be considered. In a pion–nucleon effective field theory the expansion of the Lagrangian is in powers of $1/\Lambda_\chi$ and of $1/m_N$, however these two quantities are quite similar and we can safely count them as being of the same size $\Lambda_\chi \sim m_N$ for power counting purposes. In section (2.5) we argued that $4\pi F_0 \sim \Lambda_\chi$, as a result we can relate all heavy scales of the theory to Λ_χ. As in the mesonic sector the light scales will be typical momentum p and the mass m_π of the pions, as well as a new light scale in the form of the residual nucleon momentum k. All of these scales are of the same size $p \sim m_\pi \sim k$. Thus the effective field theory counting can be organized in powers of p/Λ_χ. Now the first step to determine the size of the contribution to the amplitude from a given diagram is to know the sizes of the vertices in it. From the

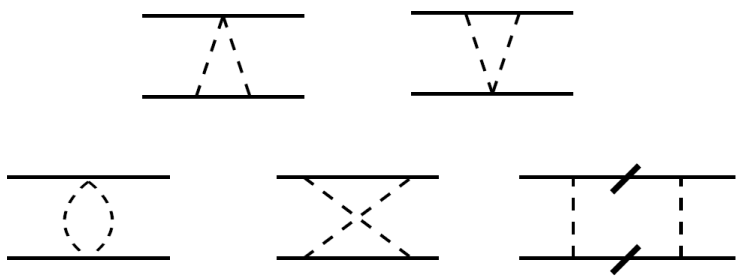

Figure 3.2: The solid lines represent nucleon lines and the dashed ones pion lines. The first four diagrams are irreducible, while the fifth one can be reduced by cutting the two internal nucleon lines.

discussion on sections 2.4 and 2.5 we have that the size of a pion–pion coupling is given by

$$\Lambda_\chi^2 F_0^2 \left(\frac{\pi}{F_0}\right)^{n_\pi} \left(\frac{(\partial, m_\pi)}{\Lambda_\chi}\right)^m , \tag{3.24}$$

where n_π is the number of pion legs of the vertex and m the number of derivatives plus the number of pion mass powers. In the pion sector n_π and m are always even. An equivalent analysis for the one nucleon and two nucleon sectors couplings leads to

$$\Lambda_\chi^4 \left(\frac{\pi}{F_0}\right)^{n_\pi} \left(\frac{(\partial, m_\pi)}{\Lambda_\chi}\right)^m \left(\frac{N}{\Lambda_\chi^{3/2}}\right)^{n_N} , \tag{3.25}$$

where n_N is the number of nucleon legs. In the pion–nucleon sector n_π and m can be both even and odd.

The next step is to assign factors to the pion and nucleon propagators as well as the loop integrals differentials. Following section 2.4 we add a factor of $1/p^2$ for each pion propagator, a p^4 factor for each loop and for the nucleon propagators a $1/p$ factor. Loop integrals also carry a $(4\pi)^2$ factor, that should be taken into account to make the identifications $4\pi F_0 \sim \Lambda_\chi$. Taking all the factors together we can obtain the size of a the contribution from a particular diagram and determine whether it is relevant to our calculation.

This power counting, is the so-called Weinberg's power counting, and only works for irreducible diagrams [22, 23]. A n–nucleon irreducible diagram is a diagram that cannot be splited in two by cutting n–nucleon lines (see Fig.3.2). In particular, in the one nucleon sector all diagrams are irreducible and Weinberg's

power counting applies. Now, to explore the reason why Weinberg's power counting fails, lets consider the reducible diagram in Fig.3.2 from the two nucleon sector. At this point, let us outline how to perform loop integrals with non–relativistic nucleon propagators. From the Lagrangian in (3.20) we obtain that the propagator for non–relativistic nucleons is $i\left(l^0+i\epsilon\right)^{-1}$, where l is the nucleon momentum. The usual techniques will not be useful when non–relativistic nucleon propagators are present. To perform this kind of integrals, first the loop energy is integrated using contour integration, afterwards we are left with a usual integral over a 3 dimensional euclidean space that can be performed with the usual techniques, in particular it can be regularized using dimensional regularization. Let us take the external momentum as zero for simplicity, then the loop integral reads

$$\int \frac{d^4l}{(2\pi)^4}\frac{P(\vec{l})}{\left(l^0+i\epsilon\right)\left(-l^0+i\epsilon\right)\left(l^2-m_\pi^2+i\epsilon\right)^2}\,, \tag{3.26}$$

where l is here the loop momentum, and $P(\vec{l})$ is polynomial in l. The integral over l^0 possesses the so–called pinch singularity due to the poles at $l^0=\pm i\epsilon$. Notice that such pinch singularities only show up in the case of at least two nucleons since for a single nucleon the contour of integration can be contorted to avoid the singularity. This singularities are not "real" but an artifact of the heavy baryon approximation for the nucleon propagators (static nucleons) that is not valid for such diagrams. There are several ways to make sense of pinch singularities [64, 65, 66], we will choose to resummate the kinetic term into the propagator or equivalently treat $\vec{\nabla}^2/2m_N$ as a leading order operator. Doing so the poles in the loop integral are $l^0=\mp\frac{\vec{l}^2}{2m_N}\pm i\epsilon$, as a result the integration path is no longer pinched by the poles when $\epsilon\to 0$, and the contour integral can be performed. We can choose an integration contour going through the upper or lower complex half–plain, regardless there is going to be always a nucleon and a pion pole enclosed in the integration path. Lets us consider first the nucleon pole contribution, choosing a integration path through the upper half–plain we obtain

$$i\int \frac{d^3l}{(2\pi)^3}\frac{-m_N P(\vec{l})}{\vec{l}^2\left(\left(\frac{\vec{l}^2}{2m_N}\right)^2-\vec{l}^2-m_\pi^2+i\epsilon\right)^2}\sim i\int \frac{d^3l}{(2\pi)^3}\frac{m_N P(\vec{l})}{\vec{l}^2\left(\vec{l}^2+m_\pi^2-i\epsilon\right)^2}\,. \tag{3.27}$$

Since $\vec{l}^2 >> (\vec{l}^2/2m_N)^2$ for any value of the momentum, $(\vec{l}^2/2m_N)^2$ can be ig-

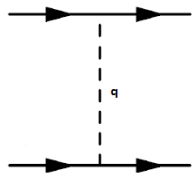

Figure 3.3: Pion exchanged between on-shell nucleons are always potential pions.

nored in a first order approximation in the pion propagators. We will call pion lines in where $l^0 \sim \vec{l}^2/m_N$ potential pion lines. Potential pions do not only occur in loop diagrams, consider for example a pion exchange between two nucleon lines in Fig. 3.3. In the center of mass frame with the external nucleon lines on–shell the pion energy is given by $q^0 = 0$, and thus the energy term can also be ignored. The second pole that contributes to the l^0 integration in (3.26) is the pion pole, $l^0 = \pm\left(\sqrt{\vec{p}^2 + m_\pi^2} - i\epsilon\right)$, that lies inside of the integration contour. In this case, the pion line fulfills $l^0 \sim \vec{l} \sim m_\pi$ and we will call it a radiation pion line. When a pion pole is taken the energy term of the nucleon propagator dominates over the kinetic energy and the latter can be neglected.

$$-i\frac{3}{8}\int \frac{d^3l}{(2\pi)^3}\frac{P(\vec{l})}{\left(\sqrt{\vec{p}^2 + m_\pi^2} - i\epsilon\right)^5}\,. \tag{3.28}$$

It is important to note that the nucleon pole contribution (potential pions) is enhanced by a factor m_N/m_π over the pion pole contribution (radiation pion). Essentially introducing the nucleon kinetic term in the nucleon propagator we have introduced a second mass scale. This implies that the loop integrals are no longer homogeneous, that is, the integral contributes to more than a single power in the expansion parameter. In the next section we will discuss a general method for expanding the loop integrals in homogeneous pieces.

In terms of the power counting we will differentiate already at a diagramatical level between potential and radiation pions, then the nucleon propagator (and loop energy) will be counted accordingly. In the first case the time derivative operator is of the same size as the kinetic energy operator and the nucleon propagator is counted as m_N/m_π^2, in the second the time derivative operator is bigger than the kinetic energy and the nucleon propagator must be counted as $1/m_\pi$.

The original proposal by Weinberg [22, 23] was to compute the nucleon-nucleon potential up to a given order including only the irreducible contributions, where all nucleons are off-shell and are counted as $1/m_\pi$. Then solve the Schrödinger equation with such potential using time ordered perturbation theory or the Lippmann–Schwinger equation. This is essentially equivalent to iterate the potential between two nearly on-shell nucleon states up to certain order in the first case and to all orders in the second. It was shown in Ref. [67] that solving the Schrödinger equation with time ordered perturbation theory leads to the same results as perturbation theory for non–relativistic field theory as long as the kinetic energy term is included in the propagators. The first step has been carried successfully up to next–to–leading order [68, 69] and next-to-next-to–leading order [70, 71, 72, 73]. However when the potential is more that $1/r^2$ singular at the origin then the Schrödinger equation solution is divergent and need to be regularized. This corresponds to divergent diagrams in the field theory. To regularize the Schrödinger equation we need to resort to introducing a cut–off, which cannot be eliminated from the final expressions and breaks Chiral symmetry. On the other hand in field theory in perturbation theory it is well known how to deal with divergences, one merely regularizes the integrals and then renormalizes the couplings on the theory, absorbing terms that diverge into the definitions of the renormalized couplings. Using dimensional regularization and $\overline{MS}$ subtraction scheme the symmetries, including Chiral symmetry, are preserved.

3.6 Threshold Expansions

Many processes in physics, like the ones with pion–nucleon interactions, involve more than one mass scale. Such processes are notoriously difficult to calculate in perturbation theory beyond one–loop level. To proceed one has to resort to approximations, either numerical or analytical. Among the latter finds its place the strategy of the regions [74]. The idea is to perform an asymptotic expansion of the integrals in certain ratios of the mass scales, so that the resulting integrals appearing in the calculation of every term in the expansion are simpler. In particular, this means that the expansion should be manifestly homogeneous The method can be summarized as follows:

1. Determine the large and small scales.

2. Introduce factorization scales μ_i and divide the loop integration domain

into regions in which the loop momentum is of order of one of the scales in the problem.

3. Perform a Taylor expansion in every region in the small parameters of said region and stay at leading order. At this point keep only the relevant regions and discard the rest. The relevant regions are those that maintain the pole structure of the original integral. If we integrate over multiple momenta and the integrand has several propagators, so that we have one or more poles associated with each momentum, after performing the Taylor expansion we should still have at least one pole for each momentum. If we end up loosing all the pole that were associated with one of the variables of integration the region we are considering is irrelevant and must not be taken into account.

4. After the expansion, ignore all factorization scales and integrate over the entire loop integration domain in every relevant region.

The non-trivial point to justify is the last one, which guarantees the homogeneity of the expansion formula. In order for that point to hold is essential to use dimensional regularization to regularize the integral, even if it is finite in four dimensions. Loosely speaking, item 4 follows in dimensional regularization from the property that all integrals without scales vanish, but the truth is that at present day there are no mathematical proofs of the method of the regions. The best we can say is that it has not failed yet, giving asymptotic expansions for any diagram in any limit and having been checked in numerous examples when comparing results of expansions with existing explicit analytical results.

As an example lets apply this method to the two pion box diagram diagram we studied in section 3.5 (the last diagram in Fig. 3.2). The small scale is the pion mass m_π and the large scale is the nucleon mass m_N. The factorization scales correspond to m_π and m_π^2/m_N, the loop energy variable can be of order of one of this two scales, the loop three–momentum can only be of order m_π. There are then only two possible regions. Performing the Taylor expansion of (3.26) we obtain

- $l^0 \sim m_\pi^2/m_N\,, \vec{l} \sim m_\pi$

$$\int -\frac{d^4l}{(2\pi)^4} \frac{P(\vec{l})}{\left(l^0 - \frac{\vec{l}^2}{2m_N} + i\epsilon\right)\left(-l^0 - \frac{\vec{l}^2}{2m_N} + i\epsilon\right)\left(\vec{l}^2 + m_\pi^2 + i\epsilon\right)^2}\,, \tag{3.29}$$

This contributions correspond to two interations of the one pion potential exchange.

- $l^0 \sim \vec{l} \sim m_\pi$

$$\int \frac{d^4 l}{(2\pi)^4} \frac{P(\vec{l})}{(l^0 + i\epsilon)\,(-l^0 + i\epsilon)\,(l^2 - m_\pi^2 + i\epsilon)^2}\,. \tag{3.30}$$

In the second region we are left with four poles. Unfortunately we recover the pinch singularity due to the nucleon poles. However these contributions of the nucleon poles are already included in the first region. Thus, to regularize the pinch singularity in this case, one should subtract (3.29) in the static limit of (3.6).

The two regions correspond to what we have identified as the potential pion and radiation pions contributions in section 3.5. There we already saw, in (3.27) and (3.28), that this two contributions are homogeneous in the power counting, with the potential pion contribution being the leading one.

CHAPTER

4

NUCLEON–NUCLEON EFECTIVE FIELD THEORY WITH DIBARYON FIELDS

4.1 Introduction

In non–relativistic nucleon–nucleon scattering the S–matrix is related to the amplitude scattering amplitude $\mathcal{A}$ by

$$S = 1 + i\frac{pm_N}{2\pi}\mathcal{A}\,, \tag{4.1}$$

where p is the magnitude of the nucleon momentum in the center–of–mass frame, related to the total energy in that frame by $E = p^2/m_N + \ldots$. For S–wave scattering, $\mathcal{A}$ is related to the phase shift, δ, through the relation

$$\mathcal{A} = \frac{4\pi}{m_N}\frac{1}{p\cot\delta - ip}\,. \tag{4.2}$$

From quantum mechanics is well known that it is the quantity $p\cot\delta$ rather than $\mathcal{A}$, which has a well defined expansion for small momenta $p \ll \Lambda$, where Λ is the theory cut–off, which is the scale of the last degree of freedom integrated out. It is the so–called, effective range expansion

$$p\cot\delta = -\frac{1}{a} + \frac{1}{2}\sum_{n=0}^{\infty} r_n p^{2(n+1)}\,, \tag{4.3}$$

where a is the scattering length, and r_0 the effective range. The radius of convergence of momentum expansion of $\mathcal{A}$ depends on the size of the scattering length. In the context of an effective field theory there is only one dimensionfull scale Λ.

Since by dimensional analysis the scattering length has inverse mass dimension, we have to conclude that the size of the scattering length is $a \sim 1/\Lambda$. This means that (4.2) can be expanded in powers of the momentum

$$\mathcal{A} = -\frac{4\pi a}{m_N}\left(1 - iap + \mathcal{O}\left(p^2/\Lambda^2\right)\right). \tag{4.4}$$

At zero external momentum only the first term survives $-\frac{4\pi a}{m_N}$.

Now using the effective field theory for pion–nucleon interactions described in section 3.4 and the power counting developed in section 3.5 we can calculate the nucleon–nucleon scattering amplitude. The leading order (LO) amplitude result for the ${}^1S_0$ plane wave is as follows

$$\mathcal{A} = C_S - 3C_T - \frac{g_A^2}{4F_0^2}\left(-1 - \frac{m_\pi^2}{4p^2}\ln\left(1 + \frac{4p^2}{m_\pi^2}\right)\right). \tag{4.5}$$

Matching both expressions for the amplitude, (4.4) and (4.5), at zero external momentum we can determine the LO contribution of the effective theory to the scattering length

$$a^{^1S_0} = -\frac{m_N}{4\pi}\left(C_S - 3C_T\right) \sim \frac{1}{\Lambda_\chi}. \tag{4.6}$$

Hence we conclude that the effective theory elaborated in sections 3.4 and 3.5 is consistent with scattering lengths of the size $a \sim 1/\Lambda_\chi$.

However, it turns out that in nature the size of the S–wave scattering lengths is of the order $1/a \sim m_\pi^2/\Lambda_\chi$ rather than $1/a \sim \Lambda_\chi$. The actual experimental values are $a^{^1S_0} = -23.714(13)$fm and $a^{^3S_1} = 5.423(5)$fm. This is due to the presence of a shallow virtual state in the ${}^1S_0$ channel and a bound state, the deuteron, in the ${}^3S_1$ channel. The large scattering lengths of this channels indicate that the resonance/bound state are very close to threshold [75]. As a consequence the amplitude (4.2) can not be expanded in positive powers of the momentum.

An alternative approach was proposed by Kaplan, Savage, and Wise [76, 77]. The key ingredient was the use of the power divergence subtraction scheme instead of $\overline{MS}$ scheme to subtract the ultraviolet divergences. Working in the dimensional regularization framework, the $\overline{MS}$ subtraction scheme only the poles appearing at space–time dimension four are subtracted. In power divergence subtraction scheme both the poles appearing at dimension three and four are subtracted. This leads to modified renormalization group equations for the nucleon contact terms of (3.23). Solving this equations for $C^{^1S_0} \equiv C_S - 3C_T$, with

the boundary condition $C^{^1S_0}(\mu = 0) = \frac{4\pi a^{^1S_0}}{m_N}$ leads to

$$C^{^1S_0} = -\frac{4\pi}{m_N}\left(\frac{1}{\mu - \frac{1}{a^{^1S_0}}}\right) \sim -\frac{4\pi}{m_N\mu}\,, \tag{4.7}$$

where μ is the renormalization scale, and in the last step utilizes that the scattering length is large. Choosing $\mu \sim m_\pi \sim p$ results in an enhancement of the contact term from $C^{^1S_0} \sim 1/\Lambda_\chi^2$ to $\sim 1/m_\pi\Lambda_\chi$. As a result the contact terms become the sole contributors to the LO. Furthermore all Feynman diagrams with $C^{^1S_0}$ in each vertex contribute at the same order, and thus have to be resum

$$\mathcal{A}_{LO} = \frac{-C^{^1S_0}}{1 + \frac{C^{^1S_0}m_N}{4\pi}(\mu + ip)}\,, \tag{4.8}$$

which has the nice property of reproducing the pole structure of the $^1S_0$ channel. Matching (4.8) to the effective range expansion we obtain the LO expression in the KSW approach of the scattering length

$$\frac{1}{a^{^1S_0}} = \mu + \frac{4\pi}{m_N C^{^1S_0}}\,. \tag{4.9}$$

The new term introduced by using partial divergence subtraction scheme allows for the fine tuning of the scattering length to its experimental value. The scattering amplitudes in this approach were computed up to next–to–leading order (NLO) in Ref.[76]. However when this calculations were carried out to next–to–next–to–leading order (N^{2}LO) Ref.[85] a bad convergence of the perturbative series was observed, particularly in the $^3S_1$ channel.

The proposal presented in this chapter elaborates on the idea that the difficulties encountered so far in constructing a consistent and useful nucleon–nucleon effective field theory may be a consequence of a misidentification of the low energy degrees of freedom. We will assume the nucleon–nucleon effective field theory (NNEFT) for energy and momentum scales much lower than Λ_χ contains two dibaryon fields, i.e with baryonic number $N_B = 2$, as explicit degrees of freedom each one with the quantum numbers associated to one of the S–wave channels. We will work in the framework of dimensional regularization and $\overline{MS}$ subtraction scheme. The dibaryon residual masses, the difference between the dibaryon mass and the $2m_N$ subtraction due to the non–relativistic approximation, are of the order or smaller than the pion mass. The introduction of a

small free scale in the residual masses allows to naturally accommodate the large scattering lengths presents in these channels. If the dibaryon fields are naively integrated out, one gets the enhanced contact interactions of the KSW approach. We will argue that they must be kept as explicit degrees of freedom.

The relation between dibaryon fields and the KSW approach was noted early [78]. Dibaryon fields have also been used in effective field theory formulations of the three body problem (see [79, 80, 81] and references there in). However, they have mostly been regarded as a convenient trick to carry out calculations (see, for instance, [82]). What it is new in our approach is the assumption that they *must* be included as explicit degrees in the NNEFT. They cannot be integrated out if one wants to keep a natural counting. For a fundamental field theory their introduction should be irrelevant, since one can build the appropriate quantum numbers of the dibaryon out of the nucleon fields, and their inclusion does not affect the symmetries of the theory. For an effective theory, however, where calculations are necessarily organized in ratios of scales, it is extremely important to keep the appropriate degrees of freedom in the Lagrangian, even if they may appear redundant at first sight.

This chapter is based in the work presented in Refs. [31, 32, 33, 34]

4.2 The nucleon–nucleon Chiral effective theory with dibaryon fields

Our starting point is the effective theory for the $N_B = 2$ sector of QCD for non–relativistic energies much smaller than Λ_χ. The distinct feature of this effective field theory is that in addition to the usual degrees of freedom for a NNEFT, namely nucleons and pions, two dibaryon fields, an isovector (D_s^a) with quantum numbers ${}^1S_0$ and an isoscalar ($\vec{D}_v$) with quantum numbers ${}^3S_1$ are also included. Chiral symmetry, and its breaking due to the quark masses in QCD, constrain the possible interactions of the nucleons and dibaryon fields with the pions.

The $N_B = 0$ sector is given by the Chiral Lagrangian which will only be needed at LO (2.43). We will work in the isospin limit, namely $m_u = m_d$, which makes ϵ, defined in (2.48), vanish. For the pion–nucleon interactions we will need the Lagrangian up to NLO, that is (3.20) and (3.21). We will take the value of the axial–vector coupling as $g_A = 1.25$. The $N_B = 2$ sector consist of terms with (local) two nucleon interactions, dibaryons and dibaryon–nucleon interac-

tions. The terms with two nucleon interactions (3.22) can be removed by local field redefinitions [79, 80, 82] of the dibaryon fields and will not be further considered. The terms with dibaryon fields and no nucleons in the rest frame of the dibaryons read

$$\mathcal{L}_D = \mathcal{L}_D^{(1)} + \mathcal{L}_D^{(2)} + \dots \,, \tag{4.10}$$

where $\mathcal{L}_D^{(1)}$ is the $\mathcal{O}(p)$

$$\mathcal{L}_D^{(1)} = \frac{1}{2}\mathrm{Tr}\left[D_s^\dagger\left(-id_0 + \delta'_{m_s}\right)D_s\right] + \vec{D}_v^\dagger\left(-i\partial_0 + \delta'_{m_v}\right)\vec{D}_v + ic_{sv}\left(\vec{D}_v^\dagger \mathrm{Tr}\left[\vec{u}D_s\right] - h.c.\right) , \tag{4.11}$$

where $D_s = D_s^a\tau_a$ and δ'_{m_i}, $i = s, v$ are the dibaryon residual masses, which must be much smaller than Λ_χ, otherwise the dibaryon should have been integrated out as the remaining resonances have. The negative signs of the time derivatives are chosen this way in order to eventually reproduce the signs of the effective range parameters.

The covariant derivative for the scalar (isovector) dibaryon field is defined as $d_0 D_s = \partial_0 D_s + \frac{1}{2}[[u, \partial_0 u], D_s]$. $\mathcal{L}_D^{(2)}$ is the $\mathcal{O}(p^2)$ Lagrangian

$$\begin{aligned}\mathcal{L}_D^{(2)} =& s_1 Tr[D_s(u\mathcal{M}^\dagger u + u^\dagger\mathcal{M}u^\dagger)D_s^\dagger] + s_2 Tr[D_s^\dagger(u\mathcal{M}^\dagger u + u^\dagger\mathcal{M}u^\dagger)D_s] + \\ &+ v_1\vec{D}_v^\dagger\cdot\vec{D}_v Tr[u^\dagger\mathcal{M}u^\dagger + u\mathcal{M}^\dagger u] + \dots\end{aligned} \tag{4.12}$$

s_i, $i = 1, 2$, and v_1, are low–energy constants. We have only displayed here the terms which will eventually contribute in our calculations. The complete list of operators is given in the Appendix D.

The dibaryon–nucleon interactions will also be needed at NLO,

$$\mathcal{L}_{DN} = \mathcal{L}_{DN}^{(1)} + \mathcal{L}_{DN}^{(2)} + \cdots \tag{4.13}$$

At LO they read

$$\begin{aligned}\mathcal{L}_{DN}^{(1)} =& \frac{A_s}{\sqrt{2}}(N^\dagger\sigma^2\tau^a\tau^2 N^*)D_{s,a} + \frac{A_s}{\sqrt{2}}(N^\top\sigma^2\tau^2\tau^a N)D_{s,a}^\dagger + \\ &+ \frac{A_v}{\sqrt{2}}(N^\dagger\tau^2\vec{\sigma}\sigma^2 N^*)\cdot\vec{D}_v + \frac{A_v}{\sqrt{2}}(N^\top\tau^2\sigma^2\vec{\sigma}N)\cdot\vec{D}_v^\dagger \,,\end{aligned} \tag{4.14}$$

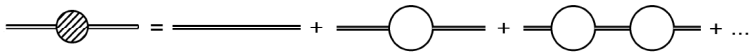

Figure 4.1: The dibaryon propagator gets an important contribution from resuming the bubble self–energy diagrams

where $A_i \sim \Lambda_\chi^{-1/2}$, $i = s, v$, and at NLO

$$\begin{aligned}\mathcal{L}^{(2)}_{DN} =& \frac{B_s}{\sqrt{2}}(N^\dagger\sigma^2\tau^a\tau^2\vec{\nabla}^2N^*)D_{s,a} + \frac{B_s}{\sqrt{2}}(N^\top\sigma^2\tau^2\tau^a\vec{\nabla}^2N)D^\dagger_{s,a} + \\ &+ \frac{B_v}{\sqrt{2}}(N^\dagger\tau^2\vec{\sigma}\sigma^2\vec{\nabla}^2N^*)\cdot\vec{D}_v + \frac{B_v}{\sqrt{2}}(N^\top\tau^2\sigma^2\vec{\sigma}\vec{\nabla}^2N)\cdot\vec{D}^\dagger_v \\ &+ \frac{B'_v}{\sqrt{2}}(\nabla_iN^\dagger\tau^2\sigma^i\sigma^2\nabla_jN^*)D^j_v + \frac{B'_v}{\sqrt{2}}(\nabla_iN^\top\tau^2\sigma^2\sigma^i\nabla_jN)D^{j\dagger}_v\,.\end{aligned} \tag{4.15}$$

Again, we have only displayed here the terms which will eventually contribute in our calculations. The complete list of operators is given in the Appendix D. The dibaryon field propagator gets an important contribution to the self–energy due to the interaction with the nucleons (Fig.4.1), which is always parametrically larger than the energy E. As a consequence the LO expression for the dibaryon field propagator becomes, in dimensional regularization and $\overline{MS}$ subtraction scheme

$$\frac{i}{\delta'_{m_j} + i\frac{A_j^2 m_N p}{\pi}} \qquad j = s, v\,, \tag{4.16}$$

($p = \sqrt{m_N E}$) rather than the tree level expression $i/(-E + \delta'_{m_j} - i\eta)$. The unconventional signs for the time derivatives in (4.11) are chosen in this way in order to correctly reproduce the sign of the effective ranges later on. They do not imply any violation of unitarity because the correct LO expression for the propagator is (4.16) and not the tree level one. The size of the residual mass can be extracted computing the LO amplitude using the propagator (4.16) and matching the result to the effective range expansion

$$\delta'_{m_i} \sim \frac{1}{\pi a_i} \lesssim \frac{m_\pi^2}{\Lambda_\chi} \qquad i = s, v, \tag{4.17}$$

where a_i are the scattering lengths. Therefore for $p \gg \frac{m_\pi^2}{\Lambda_\chi}$ the full propagator can

Figure 4.2: The LO dibaryon propagator for $p \gg \delta_{m_i}$ is the first term in the expansion of the full dibaryon propagator around $(-E + \delta_{m_i}) = 0$. The second term is an effective vertex.

be expanded. The first term of this expansion will be the LO propagator (Fig.4.2)

$$\frac{\pi}{A_i^2 m_N p} \qquad i = s, v, \tag{4.18}$$

the second term will be an effective vertex taking into account the effects due to $i(-E + \delta_{m_i})$. Higher order terms in this expansion will be equivalent to multiple insertions of this vertex. From (4.18) it follows that the leading contribution to the nucleon–nucleon scattering amplitude for energies $\sim m_\pi$ is parametrically $\sim 1/m_\pi \Lambda_\chi$ which is more important than the tree level contribution from the one pion exchange ($\sim 1/\Lambda_\chi^2$).

Furthermore for $p \gg \delta'_{m_i}$ the LO Lagrangian becomes both scale and $SU(4)$ (spin-flavor Wigner symmetric) invariant, if the interactions with pions are neglected [87]. Indeed, concerning $SU(4)$, the single nucleon sector is obviously invariant. Moreover, since all terms in (4.11) become subleading, one can redefine the dibaryon fields in such a way that all couplings in (4.14) are equal. In that case the dibaryon–nucleon interactions become $SU(4)$ invariant if the two dibaryon fields are chosen to form a 6^* representation of $SU(4)$. Scale invariance also holds because the dibaryon fields only appear in (4.14) and their scaling transformations can be chosen such that those terms are invariant. Moreover equation (4.16) implies that the dibaryon field should not be integrated out unless $p \ll \delta'_{m_i}$, instead of $E \ll \delta'_{m_i}$ as the tree level expression suggests. If $\delta'_{m_i} \ll m_\pi$, it should also be kept as an explicit degree of freedom in the $\not\pi$NNEFT, like in Refs. [88, 89, 90]. Nevertheless, if the dibaryon fields are integrated out, one can still organize the calculation in terms of nucleon fields by taking into acount suitable correlated enhancements in the local four–nucleon interactions [86]. This is due to the fact that the path integral over dibaryon fields is Gaussian and can be carried out exactly.

Except for the above mentioned contributions to the self–energy of the dibaryon fields, which become LO, the calculation can be organized perturbatively in powers of $1/\Lambda_\chi$. Hence one expects that any ultraviolet divergence arising in higher order calculations will be absorbed in a low–energy constant of a higher

dimensional operator built out of nucleon, dibaryon and pion fields.

We shall restrict ourselves in the following to energies $E \lesssim m_\pi^2/\Lambda_\chi \ll m_\pi$, which implies nucleon three momenta $\sim m_\pi$. We shall follow the strategy of [91], which was inspired in the formalism of [92], and shall build a lower energy effective field theory, pNNEFT, with no explicit pion fields: the effects due to the pions will be encoded in two nucleon non–local interactions (potentials) and redefinitions of the low–energy constants.

4.3 The potential nucleon–nucleon effective theory with dibaryon fields

For energies $E \sim m_\pi^2/\Lambda_\chi \ll m_\pi$, the pion fields can be integrated out. This integration produces nucleon–nucleon potentials and redefinitions of low energy constants. Since $\delta'_{m_i} \sim m_\pi^2/\Lambda_\chi$ the dibaryon fields must be kept as explicit degrees of freedom in pNNEFT. The Lagrangian in the $N_B = 1$ sector reads

$$\mathcal{L}_N = N^\dagger \left(i\partial_0 - \delta m_N + \frac{\vec{\partial}^2}{2m_N} \right) N \,. \tag{4.19}$$

In the $N_B = 2$ sector further two nucleon interactions (potentials) are induced. They read

$$\mathcal{L}_{NN} = \frac{1}{2} \int d^3\vec{r}\, N^\dagger \sigma^i \tau^\alpha N(x_1) V_{ij;\alpha\beta}(x_1 - x_2) N^\dagger \sigma^j \tau^\beta N(x_2) \,, \tag{4.20}$$

$x_1^0 = x_2^0 = x^0$, $\vec{r} = \vec{x}_1 - \vec{x}_2$ and $x = (x_1 + x_2)/2$ where $V_{ij;\alpha\beta}(x_1 - x_2)$ is a generic potential ($i, j, \alpha, \beta = 1, 2, 3$), which may be calculated in an expansion in $1/\Lambda_\chi$ (in fact, beyond one loop it becomes an expansion in $\sqrt{1/\Lambda_\chi}$ [93]). The terms with dibaryon fields and no nucleons read

$$\mathcal{L}_D^{(1)} = D_{s,a}^\dagger \Big(-i\partial_0 + \delta_{m_s} \Big) D_s^a + \vec{D}_v^\dagger \Big(-i\partial_0 + \delta_{m_v} \Big) \vec{D}_v \,, \tag{4.21}$$

δ_{m_i}, $i = s, v$ are the (redefined) dibaryon residual masses. Note that δm_N in (4.19) can be reshuffled into δ_{m_i} by local field redefinitions. Note also that because of $\delta'_{m_i} \ll m_\pi$ the quark mass dependence of δ_{m_i} is a LO effect. The dibaryon–nucleon interactions remain the same as in (4.13), except for the values of the A_i

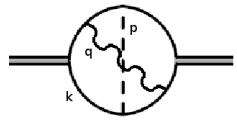

Figure 4.3: Example diagram of enhancement of a potential pion (dashed line) inside a radiation pion loop (wavy line).

which get modified

$$\begin{aligned}\mathcal{L}_{DN}^{(1)} =& \frac{A_s}{\sqrt{2}}(N^\dagger\sigma^2\tau^a\tau^2N^*)D_{s,a} + \frac{A_s}{\sqrt{2}}(N^\top\sigma^2\tau^2\tau^aN)D_{s,a}^\dagger + \\ &+ \frac{A_v}{\sqrt{2}}(N^\dagger\tau^2\vec{\sigma}\sigma^2N^*)\cdot\vec{D}_v + \frac{A_v}{\sqrt{2}}(N^\top\tau^2\sigma^2\vec{\sigma}N)\cdot\vec{D}_v^\dagger\,,\end{aligned} \tag{4.22}$$

$$\begin{aligned}\mathcal{L}_{DN}^{(2)} =& \frac{B_s}{\sqrt{2}}(N^\dagger\sigma^2\tau^a\tau^2\partial^2N^*)D_{s,a} + \frac{B_s}{\sqrt{2}}(N^\top\sigma^2\tau^2\tau^a\partial^2N)D_{s,a}^\dagger + \\ &+ \frac{B_v}{\sqrt{2}}(N^\dagger\tau^2\vec{\sigma}\sigma^2\partial^2N^*)\cdot\vec{D}_v + \frac{B_v}{\sqrt{2}}(N^\top\tau^2\sigma^2\vec{\sigma}\partial^2N)\cdot\vec{D}_v^\dagger \\ &+ \frac{B_v'}{\sqrt{2}}(\partial_iN^\dagger\tau^2\sigma^i\sigma^2\partial_jN^*)D_v^j + \frac{B_v'}{\sqrt{2}}(\partial_iN^\top\tau^2\sigma^2\sigma^i\partial_jN)D_v^{j\dagger}\,.\end{aligned} \tag{4.23}$$

The calculations in pNNEFT can be organized in ratios E/p and p/Λ_χ (recall $m_\pi \sim p$). The ultraviolet divergences arising at higher orders will be absorbed by local terms build out of nucleon and dibaryon fields.

4.4 Potential pions in loops with radiation pions

In this section we discuss a particular class of contributions to the matching calculation between pNNEFT and NNEFT. The former is obtained from the latter by integrating out nucleons of energy $E \gtrsim m_\pi$ and pions. Among the latter there are the so–called radiation pions, namely pions with $q^0 \sim \vec{q} \sim m_\pi$ that interact with nucleons of $E \sim m_\pi$ and $p \sim \sqrt{m_\pi m_N}$.

The lowest order diagrams involving radiation pions are depicted in Fig.4.8. When a so–called potential pion, namely a pion with $q^0 \sim \vec{q}^2/m_N$, is added to one of those diagrams, for instance like in Fig.4.3, the potential pion three–momentum is $\vec{q} \sim \sqrt{m_\pi m_N}$ and thus their energy is $q^0 \sim m_\pi$. A parametric suppression of only $\sqrt{m_\pi/\Lambda_\chi}$ occurs [87, 32], which numerically turns out to be $\mathcal{O}(1)$ [93]. It is then necessary to sum up these kind of contributions.

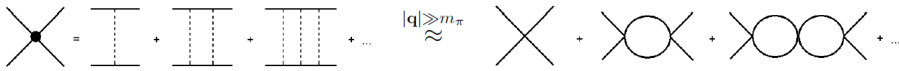

Figure 4.4: Potential pion exchanges in the ${}^1S_0$ channel can be approximated by contact interactions and resummed into an effective vertex when the external momentum is bigger than the pion mass.

4.4.1 Loop resummation

Let us consider the exchange of n potential pions between two nucleon lines. If we project it to the ${}^1S_0$ channel, the three-momenta coming from the vertices of each potential pion exchange contract between themselves. Note that this is not the case if we project to the ${}^3S_1$ channel, where a three-momentum from one of the vertices of a given potential pion exchange may get contracted with a three-momentum of a neighboring potential pion exchange vertex. If these n-pion exchanges are in a loop with a radiation pion, then the three-momentum in the denominator of the potential pion propagators dominates over the pion mass and the pion energy. As a consequence, the potential pion exchanges collapse into a local vertices (contact interactions) with a coupling constant $g_A^2/(4F_0^2)$, where g_A is the axial pion–nucleon coupling constant and F_0 is the pion decay constant. Again, this is not so in the ${}^3S_1$ channel, where even at very large momentum transfer the potential remains non–local (i.e. it does not reduce to a contact interaction). In the left hand side of Fig.4.4 we depicted the first terms in a series of diagrams with an arbitrary large number of potential pion exchanges. Using the previous reasoning we can collapse the potential pion exchanges into local vertices obtaining the diagrams on the right hand side. In dimensional regularization the result for the first few terms is

$$i\frac{g_A^2}{4F_0^2} + i\frac{g_A^2}{4F_0^2}\left(-\frac{\sqrt{q^0-i\epsilon}}{\alpha}\right) + i\frac{g_A^2}{4F_0^2}\left(-\frac{\sqrt{q^0-i\epsilon}}{\alpha}\right)^2 + \dots \tag{4.24}$$

where we have taken the external energy to be $-q^0$ and α is defined as

$$\alpha = \frac{16\pi F_0^2}{g_A^2 m_N^{3/2}}\,. \tag{4.25}$$

Naively we would expect each bubble to suppress the diagram by a factor of $\sqrt{m_\pi/\Lambda_\chi}$. However a more careful analysis shows that the actual size of each bubble is in fact $\sqrt{m_\pi}/\alpha \sim 1.19$ which is of order $\mathcal{O}(1)$, and hence the series

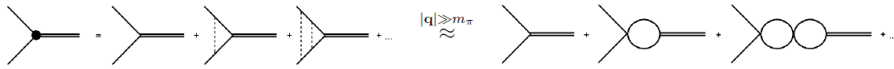

Figure 4.5: Resummation of potential pions in the dibaryon–nucleon vertex.

Figure 4.6: Inside radiation pion loops the ${}^1S_0$ receives an additional self–energy contribution.

should be resummed. The result of the resummation can be casted as an effective energy–dependent four–nucleon vertex with coupling constant

$$C_{eff} = i\frac{g_A^2}{4F_0^2}\frac{\alpha}{\alpha+\sqrt{q^0-i\epsilon}}\,. \tag{4.26}$$

An analogous resummation has to be done for potential pion exchanges in the nucleon–dibaryon vertex of Fig.4.5. Following the same procedure as before we obtain an energy–dependent effective nucleon–dibaryon vertex

$$A_{s,eff} = A_s\frac{\alpha}{\alpha+\sqrt{q^0-i\epsilon}}\,. \tag{4.27}$$

Furthermore using the effective vertex of (4.26) we can construct the self–energy depicted in Fig.4.6, which inside radiation pion loops turns out to be of order $\mathcal{O}(1)$ and thus has to be included in the LO propagator (4.18). The following expression for the ${}^1S_0$ propagator inside radiation pion loops is obtained

$$-\frac{1}{4A_s^2}\frac{g_A^2}{4F_0^2}\left(1+\frac{\alpha}{\sqrt{q^0-i\epsilon}}\right). \tag{4.28}$$

Note that in order to have a ${}^1S_0$ nucleon–nucleon state in a loop with a single radiation pion, the initial nucleon–nucleon state must be in the ${}^3S_1$ channel. This procedure can then be applied to the calculation of δ_{m_v}, but not to the calculation of δ_{m_s}. This is due to the fact that in the last channel the contact interaction is replaced by a non–local potential that turns out to be singular, and therefore cannot be straigtshforwardly used in a Lippmann–Schwinger equation, see [91, 99, 96, 97, 98, 100, 101, 102] for discussions and possible solutions.

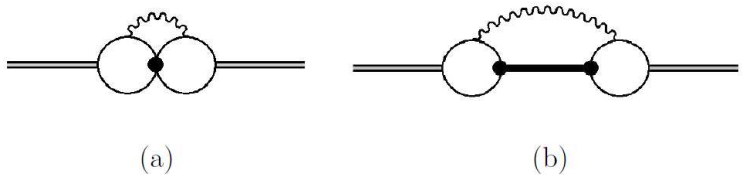

Figure 4.7: Order $O(m_\pi^2/\Lambda_\chi)$ contributions to the dibaryon residual mass. Radiation pions are represented by Wavy lines.

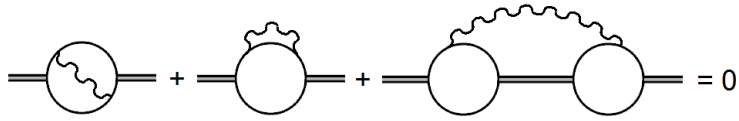

Figure 4.8: Order $O(m_\pi^2/\Lambda_\chi)$ contributions to the dibaryon residual mass with one radiation pion (wavy lines), that cancel due to Wigner symmetry.

4.4.2 Cancellation of the contributions to δ_{m_v}

Making use of the new effective vertices obtained by resumming potential pion exchanges, two new diagrams contributing at LO to δ_{m_v}, shown in Fig.4.7, are found

$$\mathcal{A}_a = 8A_v^2\left(\frac{1}{\alpha}B(1/4,1) - \alpha^2 B(1,1) + \alpha B(3/4,1) - B(1/2,1)\right), \tag{4.29}$$

$$\begin{aligned}\mathcal{A}_b = 8A_v^2\big(&B(1/2,1) - \alpha B(3/4,1) + \alpha^2 B(0,2) - \alpha^3 B(1/4,2) - \alpha^6 B(1,2)\\ &+\alpha^7 B(5/4,2)\big)\,.\end{aligned} \tag{4.30}$$

The definition of $B(\beta_1,\beta_2)$ is the Appendix C. The (4.29) and (4.30) contributions are of the same order as the diagrams in Fig.4.8. Those diagrams can be naively counted as $\mathcal{O}\left(m_\pi^{5/2}/\Lambda_\chi^{3/2}\right)$, however they are proportional to $\sqrt{m_\pi}/\alpha \sim 1$. Then analogously as we did previously we should count diagrams in Fig.4.8 as $\mathcal{O}\left(m_\pi^2/\Lambda_\chi\right)$. The sum of these diagrams is known to cancel due to Wigner symmetry, however since the third one is already included in Fig.4.7b we should add the first two to (4.30) in order to get the complete result at $\mathcal{O}\left(m_\pi^2/\Lambda_\chi\right)$

$$\mathcal{A}_s = -8A_v^2\frac{1}{\alpha}B(5/4,0)\,. \tag{4.31}$$

The sum of these three contributions ($\mathcal{A}_a$, $\mathcal{A}_b$, $\mathcal{A}_s$) adds up to zero, which can be checked by making use of the relation

$$B\left(\beta_1 - 1, \beta_2\right) = B\left(\beta_1, \beta_2 - 1\right) + \alpha^4 B\left(\beta_1, \beta_2\right) . \tag{4.32}$$

This is at first sight a surprising result. The interaction of nucleons with potential pions spoils the arguments that led to the proof that the sum of the diagrams in Fig.4.8 vanishes as a consequence of Wigner symmetry [87]. Yet, since the contact four–nucleon interaction we obtain is only used in the ${}^1S_0$ channel, it could well be replaced by a Wigner symmetric one with no effect in our calculation, and hence the arguments of [87] would still go through. Nevertheless, as it will become clear soon, the actual reason of the cancellation is that the contact four–nucleon interaction can be removed by the following local field redefinition of the dibaryon field

$$D_s^a \to D_s^a - \frac{g_A^2}{4F_0^2 A_s} N^T P_a^{{}^1S_0} N \, , \tag{4.33}$$

where $P_a^{{}^1S_0} = \frac{(i\sigma_2)(i\tau_2\tau_a)}{2\sqrt{2}}$, is the projector to the ${}^1S_0$ partial wave. Indeed, we have checked that the resummation of potential pion exchanges in the diagrams of Fig.4.9, in which Wigner symmetry is violated by the cross and bullet vertices, also vanishes.

As we have mentioned in the previous section the resummation cannot be carried out for the analogous diagrams for δ_{m_s}. However, it is likely that the perturbative expansion also breaks down in this channel due to numerical factors coming from loop integrals. Hence, any prediction for the quark mass dependence of δ_{m_s} in terms of a perturbative expansion has to be taken with caution because it could be missing large corrections.

Part of the reasoning we have used in the ${}^3S_1$ channel can be adapted to discuss the result for the diagrams with a single potential pion exchange in a loop with a radiation pion in the ${}^1S_0$ channel. In this set of diagrams the radiation pion three–momentum in the denominators of the loop integral can be neglected in front of any of the nucleon or potential pion three–momentum, then the potential pion three momenta in the pion–nucleon vertices must end up contracted between themselves, and hence we are left with a situation analogous to the one in the ${}^3S_1$ channel. At this point we can approximate the potential exchange by a four–nucleon contact term, following the same reasoning as for the contributions to δ_{m_v}. The contact term can then be eliminated by a field redefinition analogous to (4.33) for the $\vec{D}_v$ dibaryon field. We then conclude that the sum of

the diagrams in Fig.4.8 with a single potential pion insertion must also vanish in the ${}^1S_0$ channel. This result is in contradiction with those of [84, 32], where this class of diagrams with one potential pion inside a radiation pion loop were found to be non–zero. We believe that this is a consequence of double counting certain diagrams. In particular the last diagram in Fig.17 of [84] is already included in the first one. According to our calculations this error would lead to the result presented in [84, 32].

4.5 Matching NNEFT to pNNEFT

In the one nucleon sector pion loops produce energy independent terms which are $O(m_\pi^2/\Lambda_\chi^2)$ [94] and hence relevant for the N^{2}LO calculation, which together with the contribution $O(m_\pi/\Lambda_\chi)$ from terms proportional to the quark masses make up the nucleon residual mass δm_N in (4.19). We can reshuffle δm_N into the dibaryon residual mass by local field redefinitions. The expression for δm_N can be found [106], and up to $\mathcal{O}\left(m_\pi^3/\Lambda_\chi^2\right)$ contributions it reads

$$\delta m_N = -4c_1 m_\pi^2 - \frac{3g_A^2}{64\pi F_0^2} m_\pi^3 \,. \tag{4.34}$$

In the NLO pion-dibaryon Lagrangian (4.12) the residual mass gets $\mathcal{O}\left(m_\pi^2/\Lambda_\chi\right)$ contributions proportional to the quark mass. Additional $\mathcal{O}\left(m_\pi^3/\Lambda_\chi^2\right)$ contributions come from the diagrams in Fig.4.9. Adding up all the contributions we obtain the formula for the residual mass

$$\begin{aligned}
\delta_{m_v} &= \delta'_{m_v} + 2\frac{v_1}{B_0} m_\pi^2 + 2\delta m_N + \left(\frac{g_A^2}{4F_0^2}\right)\frac{m_\pi^3}{8\pi}\frac{A_v^2}{A_s^2} + c_{sv}\left(\frac{g_A}{2F_0^2}\right)\frac{m_\pi^3}{8\pi}\frac{A_v}{A_s} \,, \\
\delta_{m_s} &= \delta'_{m_s} + 2\frac{s_1+s_2}{B_0} m_\pi^2 + 2\delta m_N + \left(\frac{g_A^2}{4F_0^2}\right)\frac{m_\pi^3}{8\pi}\frac{A_s^2}{A_v^2} + c_{sv}\left(\frac{g_A}{2F_0^2}\right)\frac{m_\pi^3}{8\pi}\frac{A_s}{A_v} \,.
\end{aligned} \tag{4.35}$$

The dibaryon–nucleon vertices may in principle get $O(m_\pi^2/\Lambda_\chi^2)$ contributions from a pion loop, but they turn out to vanish, except for those which reduce to iterations of the one pion exchange potential (see (4.37)) which will already be included in the calculations in pNNEFT and must not be considered in the matching. Note that for this to be so the matching calculation must be done according to the prescriptions of Ref. [65] This prescription gives results which differ from the on-shell prescription of Ref. [84] and are usually simpler. Agreement is eventually recovered at the level of physical amplitudes, in which a

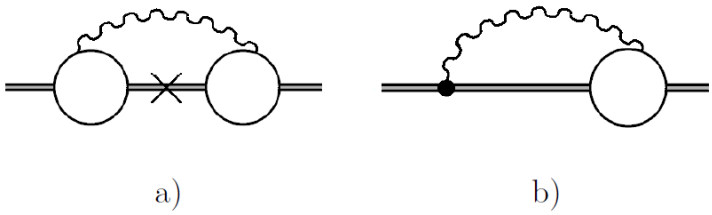

Figure 4.9: Order $O(m_\pi^3/\Lambda_\chi^2)$ contributions to the dibaryon residual mass.

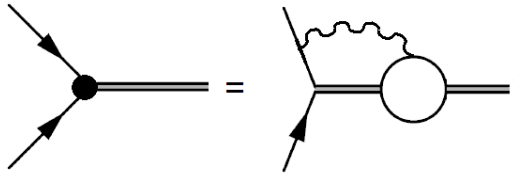

Figure 4.10: Matching of the effective vertex of the pNNEFT theory with the NNEFT vertex diagram.

number of cancellations occur for the on-shell prescription. There is, however, a two loop contribution of this order involving radiation pions from the diagram in Fig.4.10

$$A_i \to A_i\left(1 - 2\frac{g_A^2 m_\pi^2}{(4\pi F_0)^2}\right). \tag{4.36}$$

Finally, in the two nucleon interactions (4.20), the one pion exchange is the only relevant contribution at this order, which produces the well known one pion exchange potential

$$V_{ij;\alpha\beta}(x_1 - x_2) = -\frac{g_A^2}{4F_0^2}\int \frac{d^3q}{(2\pi)^3}\frac{q_i q_j}{\vec{q}^2 + m_\pi^2}\delta^{\alpha\beta}e^{-i\vec{q}\cdot(\vec{x}_1-\vec{x}_2)}\,. \tag{4.37}$$

for $i\,, j\,, \alpha\,, \beta = 1, 2, 3$.

4.6 Calculation in pNNEFT

When $p \sim m_\pi$, we have already integrated out all higher energy and momentum scales in pNNEFT, and hence we already have the optimal EFT to carry out calculations. Moreover, for this momentum both the time derivative and

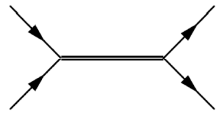

Figure 4.11: LO diagram.

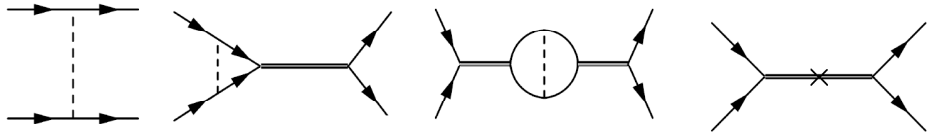

(a) (b)

Figure 4.12: (a) NLO diagrams with one potential pion exchange. (b) NLO diagram with one $i(-E+\delta_{m_i})$ insertion.

the residual mass in the dibaryon Lagrangian are small and can be treated as $O(m_\pi/\Lambda_\chi)$ perturbations.

S–Waves

Let us then focus on the calculation of nucleon–nucleon amplitudes up to N^{2}LO. At LO we get from Fig.4.11 the following S wave scale covariant Wigner symmetric amplitudes

$$\mathcal{A}^j_{LO} = i\frac{4\pi}{m_N p} \qquad j = s, v. \tag{4.38}$$

At NLO we get from the diagrams in Fig.4.12a

$$\mathcal{A}^{i,I}_{NLO} = -\frac{g_A^2}{16F_0^2}\left(\frac{m_N m_\pi}{4\pi}\right)^2 \ln\left(1+\frac{4p^2}{m_\pi^2}\right)(\mathcal{A}^i_{LO})^2 \qquad i = s, v, \tag{4.39}$$

The individual integrals can be found in Appendix C. From the diagram in Fig.4.12b

$$\mathcal{A}^{i,II}_{NLO} = \left(\frac{-E+\delta_{m_i}}{4A_i^2}\right)(\mathcal{A}^i_{LO})^2 \qquad i = s, v. \tag{4.40}$$

At N^{2}LO we obtain the following contributions. From the diagrams in Fig.4.13

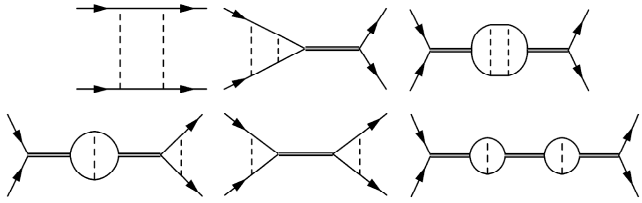

Figure 4.13: N^2LO diagrams with two potential pion exchange.

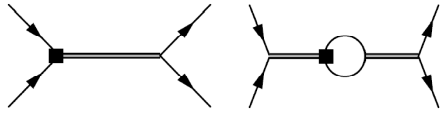

Figure 4.14: Diagrams with one vertex from (4.15).

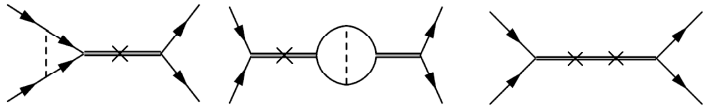

(a) (b)

Figure 4.15: N^2LO diagrams with, (a) one $i(-E + \delta_{m_i})$ insertion and one potential pion, and (b) two $i(-E + \delta_{m_i})$ insertions.

$$\mathcal{A}^{s,I}_{N^2LO} = \left(\frac{g_A^2}{4F_0^2}\right)^2 \left(\frac{m_N m_\pi}{4\pi}\right)^3 \left(\frac{m_\pi}{p}\right)\left[\frac{i}{16}\ln^2\left(1+\frac{4p^2}{m_\pi^2}\right) - \frac{1}{2}\mathrm{Im}\left[\mathrm{Li}_2\left(\frac{-m_\pi}{m_\pi - 2ip}\right)\right] + \right.$$
$$\left. -\frac{1}{4}\mathrm{Im}\left[\mathrm{Li}_2\left(\frac{m_\pi + 2ip}{-m_\pi + 2ip}\right)\right] + \frac{1}{2}\ln\left(1+\frac{4p^2}{m_\pi^2}\right)\arctan\left(\frac{2p}{m_\pi}\right)\right](\mathcal{A}^s_{LO})^2\,, \tag{4.41}$$

$$\mathcal{A}^{v,I}_{N^2LO} = \left(\frac{g_A^2}{4F_0^2}\right)^2 \left(\frac{m_N m_\pi}{4\pi}\right)^3 \left[6\left(\frac{p}{m_\pi}\right)^2 - \frac{3}{4}\left(\frac{m_\pi}{p}\right)^2 + 4 - \left(\frac{9}{4}\left(\frac{m_\pi}{p}\right)^4 + 3\left(\frac{m_\pi}{p}\right)^2\right)\ln 2\right.$$
$$+\frac{i}{16}\left(\frac{m_\pi}{p}\right)\ln^2\left(1+\frac{4p^2}{m_\pi^2}\right) + i\left(\frac{9}{8}\left(\frac{m_\pi}{p}\right)^3 - \left(\frac{3}{2}\left(\frac{m_\pi}{p}\right)^2 + \frac{9}{8}\left(\frac{m_\pi}{p}\right)^4\right)\arctan\left(\frac{2p}{m_\pi}\right)\right.$$
$$\left.+\left(\frac{m_\pi}{2p} + \frac{9}{32}\left(\frac{m_\pi}{p}\right)^5 + \frac{3}{4}\left(\frac{m_\pi}{p}\right)^3\right)\arctan^2\left(\frac{2p}{m_\pi}\right)\right) + \frac{m_\pi}{4p}\ln\left(1+\frac{4p^2}{m_\pi^2}\right)\arctan\left(\frac{2p}{m_\pi}\right)$$
$$+\frac{3}{4}\left(\frac{3}{4}\left(\frac{m_\pi}{p}\right)^4 + \left(\frac{m_\pi}{p}\right)^2\right)\ln\left(1+\frac{4p^2}{m_\pi^2}\right) - \frac{3}{4}\left(\left(\frac{m_\pi}{p}\right)^2 + \frac{3}{4}\left(\frac{m_\pi}{p}\right)^4\right)\ln\left(1+\frac{p^2}{m_\pi^2}\right)$$
$$+\left(6\left(\frac{p}{m_\pi}\right)^3 + \frac{6p}{m_\pi} - \frac{3m_\pi}{4p} - \frac{9}{8}\left(\frac{m_\pi}{p}\right)^3\right)\arctan\left(\frac{p}{m}\right) - \frac{3}{4}\left(\frac{3}{8}\left(\frac{m_\pi}{p}\right)^5 + \left(\frac{m_\pi}{p}\right)^3 + \frac{m_\pi}{p}\right)$$
$$\left.\left(2\mathrm{Im}\left[\mathrm{Li}_2\left(\frac{-m_\pi}{m_\pi - 2ip}\right)\right] + \mathrm{Im}\left[\mathrm{Li}_2\left(\frac{m_\pi + 2ip}{-m_\pi + 2ip}\right)\right] - \ln\left(1+\frac{4p^2}{m_\pi^2}\right)\arctan\left(\frac{2p}{m_\pi}\right)\right)\right](\mathcal{A}^v_{LO})^2\,. \tag{4.42}$$

The individual integrals can be found in Appendix C.

The sum of the diagrams in Fig.4.14 turns out to be zero for the ${}^1S_0$ and ${}^3S_1$ channels (they only contribute to the ${}^3S_1$–${}^3D_1$ mixing, see below). This can be understood as follows: these diagrams involve corrections to the nucleon–dibaryon vertices of order $(\frac{m_\pi}{\Lambda_\chi})^2$. We can redefine the dibaryon fields in order to remove these corrections from nucleon–dibaryon vertices, as a consequence these corrections would appear in the $N_B = 2$ sector (4.19), however, since this sector is subleading, the new operators induced by the field redefinition in this sector are of higher order.

From the diagrams in Fig.4.15

$$\mathcal{A}^{j,II}_{N^2LO} = -\left(\frac{-E+\delta_{m_j}}{4A_j^2}\right)\left(\frac{g_A^2}{4F_0^2}\right)\left(\frac{m_N m_\pi}{4\pi}\right)\frac{m_\pi}{p}\left(\arctan\left(\frac{2p}{m_\pi}\right) + \frac{i}{2}\ln\left(1+\frac{4p^2}{m_\pi^2}\right)\right)(\mathcal{A}^j_{LO})^2$$
$$+\left(\frac{-E+\delta_{m_j}}{4A_j^2}\right)^2(\mathcal{A}^j_{LO})^3 \qquad j = s, v. \tag{4.43}$$

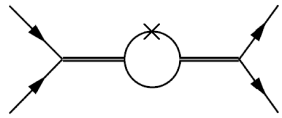

Figure 4.16: The cross in one of the nucleon propagators stands for the use of the relativistic correction. In order to compute this diagram the relativistic correction has been expanded up to first order

Relativistic Corrections

There are two contributions coming from relativistic corrections. The first one comes from using $i/(p^0 - \frac{p^2}{2m_N} + \frac{p^4}{8m_N^3} + i\epsilon)$ instead of $i/(p^0 - \frac{p^2}{2m_N} + i\epsilon)$ as the nucleon propagator. We obtain the contribution in Fig.4.16

$$\mathcal{A}^{j,a}_{N^2LO} = i\left(\frac{5p^3}{32\pi m_N}\right)(\mathcal{A}^j_{LO})^2 \qquad j = s, v. \tag{4.44}$$

Another contribution arise when using the first relativistic correction to the dispersion relation of the nucleons

$$p^0 = \frac{p^2}{2m_N} - \frac{p^4}{8m_N^3}\,, \tag{4.45}$$

in the bubble self–energy diagram of Fig.4.1. This results in the following contribution to the amplitude

$$\mathcal{A}^{j,b}_{N^2LO} = -i\left(\frac{p^3}{32\pi m_N}\right)(\mathcal{A}^j_{LO})^2 \qquad j = s, v. \tag{4.46}$$

However a new normalization of the amplitude that takes into account the new dispersion relation has to be considered

$$S = 1 + \frac{i}{2\pi}\frac{p^2}{dE/dp}\mathcal{A} = 1 + i\frac{m_N p}{2\pi}\left(1 + \frac{p^2}{2m_N^2}\right)\mathcal{A}\,, \tag{4.47}$$

this new normalization induces a new contribution to the S matrix, $i\frac{p^3}{4\pi m_N}\mathcal{A}^j_{LO}$, that exactly cancels the contributions coming from the aforementioned relativistic contributions to the amplitude.

${}^3S_1$–${}^3D_1$ mixing

The ${}^3S_1$–${}^3D_1$ mixing amplitude has no contribution at LO. At NLO the first two diagrams of Fig.4.12a are the only contribution

$$\mathcal{A}^{mix}_{NLO} = \sqrt{2}\left(\frac{g_A^2}{4F_0^2}\right)\frac{m_N m_\pi}{4\pi}\left[-\frac{3}{4}\left(\frac{m_\pi}{p}\right)^2+\left(\frac{m_\pi}{2p}+\frac{3}{8}\left(\frac{m_\pi}{p}\right)^3\right)\arctan\left(\frac{2p}{m_\pi}\right)\right]\mathcal{A}^v_{LO}\,. \tag{4.48}$$

At N^{2}LO diagrams of Fig.4.13 with one (or two) potential pion exchange in the nucleon external legs give the following contribution

$$\mathcal{A}^{mix,I}_{N^2LO} = \sqrt{2}\left(\frac{g_A^2}{4F_0^2}\right)^2\left(\frac{m_N m_\pi}{4\pi}\right)^2\left[\mathcal{Z}\left(\frac{p}{m_\pi}\right)-i\frac{3p}{2m_\pi}\mathcal{Y}\left(\frac{p}{m_\pi}\right)\right.$$
$$\left.-i\left(\frac{p}{m_\pi}+\frac{m_\pi}{2p}\ln\left(1-i\frac{2p}{m_\pi}\right)\right)\mathcal{X}\left(\frac{p}{m_\pi}\right)\right]\mathcal{A}^v_{LO}\,. \tag{4.49}$$

The $\mathcal{X}$, $\mathcal{Y}$, $\mathcal{Z}$ functions where defined in [85] and we write them here for completeness

$$\mathcal{X}(\alpha) = -\frac{3}{4\alpha^2}-\frac{3i}{4\alpha}+\frac{i\alpha}{2}+i\left(\frac{1}{2\alpha}+\frac{3}{8\alpha^3}\right)\ln(1-2i\alpha)\,, \tag{4.50}$$

$$\begin{aligned}\mathcal{Y}(\alpha) &= -\frac{2}{5}+\frac{3}{10\alpha^2}+\left(\frac{3}{8\alpha^5}+\frac{5}{4\alpha^3}-\frac{2\alpha}{5}\right)\tan^{-1}(\alpha)-\left(\frac{3}{8\alpha^5}+\frac{5}{4\alpha^3}\right)\tan^{-1}(2\alpha) \\ &+\frac{(15-4\alpha^2)}{80\alpha^6}\ln(1+\alpha^2)-\frac{(3+16\alpha^2+16\alpha^4)}{32\alpha^7}\mathrm{Im}\left[Li_2\left(\frac{2\alpha^2+i\alpha}{1+4\alpha^2}\right)+Li_2(-2\alpha^2-i\alpha)\right] \\ &+i\left[\frac{3}{8\alpha^3}+\frac{1}{2\alpha}-\frac{\alpha}{2}-\frac{(3+10\alpha^2)}{16\alpha^5}\ln(1+4\alpha^2)+\frac{(3+16\alpha^2+16\alpha^4)}{128\alpha^7}\ln^2(1+4\alpha^2)\right],\end{aligned} \tag{4.51}$$

$$\begin{aligned}\mathcal{Z}(\alpha) &= -\frac{7}{40}+\frac{9i}{16\alpha^3}+\frac{21}{40\alpha^2}+\frac{3i}{40\alpha}-\frac{3i\alpha}{5}+\frac{29\alpha^2}{200}+\left(\frac{3\alpha^2}{5}-\frac{9}{16\alpha^4}-\frac{15}{8\alpha^2}\right)\ln 2 \\ &+\frac{3\,(16\alpha^7-50\alpha^3-4i\alpha^2-15\alpha+15i)}{80\alpha^5}\ln(1-i\alpha) \\ &+\frac{(-9\,i+27\,\alpha-24\,i\,\alpha^2+78\,\alpha^3-16\,\alpha^5)}{32\alpha^5}\ln(1-2i\alpha) \\ &-\frac{(9+48\alpha^2+48\alpha^4)}{64\alpha^6}\left[\frac{3}{2}\ln^2(1-2i\alpha)+2\mathrm{Li}_2(-1+2i\alpha)+\mathrm{Li}_2\left(\frac{1+2i\alpha}{-1+2i\alpha}\right)+\frac{\pi^2}{4}\right].\end{aligned} \tag{4.52}$$

The derivative vertex of (4.15) proportional to B'_v contributes to the mixing amplitude through the first diagram of Fig.4.14

$$\mathcal{A}^{mix,II}_{N^2LO} = i\sqrt{2}p^2\frac{B'_v}{A_v}\mathcal{A}^v_{LO}. \tag{4.53}$$

The last contribution to the ${}^3S_1$–${}^3D_1$ mixing amplitude comes from the first diagram of Fig4.15a

$$\begin{aligned}\mathcal{A}^{mix,III}_{N^2LO} =&\sqrt{2}\left(\frac{g_A^2}{4F_0^2}\right)\frac{m_N m_\pi}{4\pi}\left(\frac{-E+\delta_{m_v}}{4A_v^2}\right)\left[-\frac{3}{4}\left(\frac{m_\pi}{p}\right)^2+\left(\frac{3}{8}\left(\frac{m_\pi}{p}\right)^3+\frac{m_\pi}{2p}\right)\arctan\left(\frac{2p}{m_\pi}\right)\right.\\ &\left.+i\left\{-\frac{3m_\pi}{4p}+\frac{p}{2m_\pi}+\left(\frac{m_\pi}{4p}+\frac{3}{16}\left(\frac{m_\pi}{p}\right)^3\right)\ln\left(1+\frac{4p^2}{m_\pi^2}\right)\right\}\right](\mathcal{A}^v_{LO})^2\,.\end{aligned} \tag{4.54}$$

The ${}^3D_1$ amplitude starts at NLO with the contribution coming from the one pion exchange diagram

$$\mathcal{A}^{{}^3D_1}_{NLO} = \left(\frac{g_A^2}{4F_0^2}\right)\left[-\frac{1}{2}-\frac{3}{4}\left(\frac{m_\pi}{p}\right)^2+\left(\frac{3}{16}\left(\frac{m_\pi}{p}\right)^4+\frac{1}{2}\left(\frac{m_\pi}{p}\right)^2\right)\ln\left(1+\frac{4p^2}{m_\pi^2}\right)\right]. \tag{4.55}$$

At N^{2}LO there are two contributions from Fig.4.13 from the two diagrams in which all external nucleon legs have a potential pion exchange. The correspond-

ing amplitudes are

$$\begin{aligned}\mathcal{A}^{^3D_1,I}_{N^2LO} = &\left(\frac{g_A^2}{4F_0^2}\right)^2\left(\frac{m_N m_\pi}{4\pi}\right)\frac{3}{2}\left(-\frac{2}{7}+\frac{54}{35}\left(\frac{m_\pi}{p}\right)^4-\frac{19}{70}\left(\frac{m_\pi}{p}\right)^2\right.\\
&+\left(\frac{9}{8}\left(\frac{m_\pi}{p}\right)^5+\frac{7}{4}\left(\frac{m_\pi}{p}\right)^3+\frac{4m_\pi}{5p}-\frac{2p}{7m_\pi}\right)\arctan\left(\frac{p}{m_\pi}\right)\\
&-\left(\frac{9}{8}\left(\frac{m_\pi}{p}\right)^5+\frac{7}{4}\left(\frac{m_\pi}{p}\right)^3\right)\arctan\left(\frac{2p}{m_\pi}\right)-\left(\frac{549}{560}\left(\frac{m_\pi}{p}\right)^6+\frac{3}{4}\left(\frac{m_\pi}{p}\right)^4\right)\ln\left(1+\frac{p^2}{m_\pi^2}\right)\\
&-\left(\frac{9}{32}\left(\frac{m_\pi}{p}\right)^7+\left(\frac{m_\pi}{p}\right)^5+\left(\frac{m_\pi}{p}\right)^3\right)\mathrm{Im}\left[\mathrm{Li}_2\left(\frac{-im_\pi p-2p^2}{m_\pi^2}\right)+\mathrm{Li}_2\left(\frac{im_\pi p+2p^2}{m_\pi^2+4p^2}\right)\right]\\
&+i\left\{\frac{9}{8}\left(\frac{m_\pi}{p}\right)^3-\frac{m}{2p}+\frac{p}{2m}-\left(\frac{9}{16}\left(\frac{m_\pi}{p}\right)^5+\frac{7}{8}\left(\frac{m_\pi}{p}\right)^3\right)\ln\left(1+\frac{4p^2}{m_\pi^2}\right)\right.\\
&\left.\left.+\left(\frac{9}{128}\left(\frac{m_\pi}{p}\right)^7+\frac{1}{4}\left(\frac{m_\pi}{p}\right)^5+\frac{1}{4}\left(\frac{m_\pi}{p}\right)^3\right)\ln^2\left(1+\frac{4p^2}{m^2}\right)\right\}\right),\end{aligned} \tag{4.56}$$

$$\begin{aligned}\mathcal{A}^{^3D_1,II}_{N^2LO} = 2\left(\frac{g_A^2}{4F_0^2}\right)^2\left(\frac{m_N m_\pi}{4\pi}\right)^2&\left[-\frac{3}{4}\left(\frac{m_\pi}{p}\right)^2+\left(\frac{m_\pi}{2p}+\frac{3}{8}\left(\frac{m_\pi}{p}\right)^3\right)\arctan\left(\frac{2p}{m_\pi}\right)\right.\\
&\left.+i\left\{-\frac{3m_\pi}{4p}+\frac{p}{2m_\pi}+\left(\frac{m_\pi}{4p}+\frac{3}{16}\left(\frac{m_\pi}{p}\right)^3\right)\ln\left(1+\frac{4p^2}{m_\pi^2}\right)\right\}\right]^2\mathcal{A}^v_{LO}\,.\end{aligned} \tag{4.57}$$

4.7 The pionless nucleon–nucleon effective field theory

For $p \lesssim \frac{m_\pi^2}{\Lambda_\chi}$ the calculation must be organized in a different way. This is very much facilitated if we integrate out nucleon three momenta of the order of m_π first, which leads to the so called pionless nucleon–nucleon effective field theory (/NNEFT) [67, 86, 82]. This effective field theory has been successfully used in numerous processes at very low energy (see [83] for a recent review). The Lagrangian of the $N_B = 1$ sector of this theory remains the same as in pNNEFT (4.19) (the relativistic correction (4.44) becomes negligible). For the $N_B = 2$ sector the only formal difference from pNNEFT is that the non–local potentials (4.20) become local and can be organized in powers of p^2/m_π^2. The pion exchange potential in (4.37) becomes $O(p^2/m_\pi^2\Lambda_\chi^2)$ and hence beyond N^{3}LO in this region.

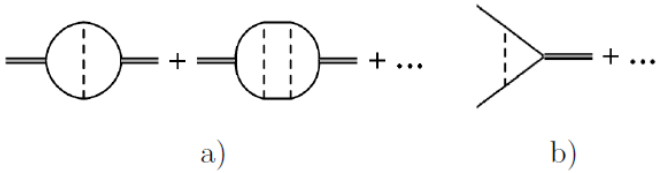

Figure 4.17: Contributions to the matching between pNNEFT and $\not\pi$NNEFT. a) Leading and NLO contributions to the residual mass. b) NLO correction to the dibaryon–nucleon vertex low energy constant. Dashed lines represent the one pion exchange potential.

The derivative dibaryon–nucleon vertices in (4.23) also become beyond this order. The remaining terms in the Lagrangian are the same as those in pNNEFT, namely (4.21) and (4.22), with the parameters redefined as follows. Self energies in Fig.4.17a can be expanded giving contributions to the dibaryon residual mass as well as time derivative terms. The latter can be reabsorbed by field redefinitions of the dibaryon fields. The dibaryon–nucleon vertex gets contributions from the diagrams in Fig.4.17b, redefining the A_i. Recall that the one pion exchange potentials in Fig.4.17 corresponds to potential pions with $\vec{q} \sim m_\pi$ and not to potential pions with $\vec{q} \sim \sqrt{m_\pi m_N}$ like the ones considered in section 4.4.

The contributions to the residual mass from the first diagram in Fig.4.17a is of order $\mathcal{O}\left(m_\pi^2/\Lambda_\chi\right)$. This diagram contains a divergence proportional to the quark mass which is renormalized by the counterterm of the same order proportional to the quark mass from (4.12).

$$\begin{aligned}
\delta_{m_v}^{LO} &= \delta'_{m_v} + 2\frac{v_1}{B_0}m_\pi^2 - 8c_1 m_\pi^2 - A_v^2 \frac{g_A^2}{2F_0^2}\left(\frac{m_\pi m_N}{4\pi}\right)^2 \ln\left(\frac{m_\pi^2}{\mu^2}\right), \\
\delta_{m_s}^{LO} &= \delta'_{m_s} + 2\frac{s_1+s_2}{B_0}m_\pi^2 - 8c_1 m_\pi^2 - A_s^2 \frac{g_A^2}{2F_0^2}\left(\frac{m_\pi m_N}{4\pi}\right)^2 \ln\left(\frac{m_\pi^2}{\mu^2}\right).
\end{aligned} \tag{4.58}$$

The second diagram in Fig.4.17a is NLO, $\mathcal{O}\left(m_\pi^3/\Lambda_\chi\right)$

$$\begin{aligned}\delta_{m_v}^{NLO} &= -\frac{3g_A^2}{32\pi F_0^2}m_\pi^3 + \left(\frac{g_A^2}{4F_0^2}\right)\frac{m_\pi^3}{8\pi}\frac{A_v^2}{A_s^2} + c_{sv}\left(\frac{g_A}{2F_0^2}\right)\frac{m_\pi^3}{8\pi}\frac{A_v}{A_s} \\ &\quad + A_v^2\left(\frac{g_A^2}{2F_0^2}\right)^2\left(\frac{m_\pi m_N}{4\pi}\right)^3\frac{5}{2}\left(6+13\ln(2)\right), \\ \delta_{m_s}^{NLO} &= -\frac{3g_A^2}{32\pi F_0^2}m_\pi^3 + \left(\frac{g_A^2}{4F_0^2}\right)\frac{m_\pi^3}{8\pi}\frac{A_s^2}{A_v^2} + c_{sv}\left(\frac{g_A}{2F_0^2}\right)\frac{m_\pi^3}{8\pi}\frac{A_s}{A_v} \\ &\quad + A_s^2\left(\frac{g_A^2}{2F_0^2}\right)^2\left(\frac{m_\pi m_N}{4\pi}\right)^3 2\ln(2)\,.\end{aligned} \tag{4.59}$$

The dibaryon–nucleon vertex up to NLO get only one new contribution from the first diagram in Fig.4.17b. Defining $A_{i,NLO}^2 = A_i^2\Delta_{NLO}$, $i = s, v$,

$$\Delta_{NLO} = \frac{g_A^2}{4F_0^2}\frac{m_\pi m_N}{4\pi}\,. \tag{4.60}$$

Note that the parametric suppression of an extra pion exchange in the diagrams of Fig.4.17 is $m_\pi m_N/\Lambda_\chi^2$ whereas the one in the diagrams in Fig.4.4 and 4.5 is $m_\pi^{1/2}m_N^{3/2}/\Lambda_\chi^2$. Hence the resummation of diagrams in Fig.4.17 is less important

There are also higher order self–energy diagrams for the dibaryon fields not shown in paper which contribute to the residual dibaryon masses at N^{2}LO, like the ones involving three potential pion exchanges. In the study of the scattering lengths of section 4.9 we will work up to NLO precision, and these contributions will not be needed. This is, in principle, not the case for the nucleon–nucleon scattering amplitudes up to N^{2}LO. In this case, however, the sum of all the contributions to the residual mass act as only one free parameter regardless. A similar argumentation can be made for the dibaryon–nucleon vertices. When we compare the nucleon–nucleon scattering amplitudes with experimental data in section 4.8 we will chose to reshufle all matching contributions to the dibaryon–nucleon vertices to the residual mass through field redefinitions of the dibaryon fields. This way the couplings constants A_i will remain the same as in pNNEFT while all the new dependences are carried by the residual masses.

Since the dibaryon residual masses are no longer small, but of the same order, when compared to p, residual masses have to be kept in the dibaryon propagators. Hence we will use (4.16) rather than (4.18) as the dibaryon propagator. The

LO amplitude for the pionless effective field theory is obtained from the diagram in Fig.4.11 using the new dibaryon propagator

$$\mathcal{A}^{j,\not\pi}_{LO} = \frac{-4A_j^2}{\delta_{m_j} + i\frac{A_j^2 m_N p}{\pi}} \qquad j = s, v. \tag{4.61}$$

Note that the LO amplitude is of order $O(1/m_\pi^2)$ instead of $O(1/m_\pi\Lambda_\chi)$ as in pNNEFT, however since contributions to the S matrix are proportional to the momentum the final size of the LO contributions to the observables (as well as the NLO and N^{2}LO ones) remains the same as in the high energy region. Note also that both scale invariance and Wigner symmetry are lost in the low energy region.

The form of the amplitude remains the same at NLO (only A_i and δ_{m_i} get redefined). At N^{2}LO (i.e. $O(1/\Lambda_\chi^2)$) a contribution corresponding to Fig.4.12b arises

$$\mathcal{A}^{i,\not\pi}_{N^2LO} = -\left(\frac{E}{4A_i^2}\right)(\mathcal{A}^{i,\not\pi}_{LO})^2 \qquad i = s, v. \tag{4.62}$$

The form of the N^{2}LO expression turns out to be valid also up to N^{3}LO (i.e. $O(m_\pi/\Lambda_\chi^3)$, again only A_i and δ_{m_i} get redefined) The sum of diagrams in Fig.4.14. is no longer zero but the momentum dependence of the vertex involved makes them beyond N^{3}LO.

No contributions to $\mathcal{A}^{mix,\not\pi}$ or to $\mathcal{A}^{^3D_1,\not\pi}$ appear up to N^{2}LO (the first diagram of Fig.4.15.a contributes to $\mathcal{A}^{mix,\not\pi}$ at N^{3}LO; this amplitude matches a straightforward expansion for $p \ll m_\pi$ of the pNNEFT mixing amplitude).

4.8 Comparison of the phase shifts with experimental data

4.8.1 The $^1S_0$ channel

In this section we compare our results for the $^1S_0$ channel with its corresponding phase shift data. In order to compute the phase shift the amplitude has been introduced in $\exp(2i\delta) = 1 + ipm_N\mathcal{A}/2\pi$. After expanding both sides in powers of $(m_\pi/\Lambda_\chi)^n$ the expressions for δ^{LO}, δ^{NLO} and, δ^{N^2LO} are obtained.

We will not display the results for δ^{LO}. At this order our approach does not uniquely determine the phase shift in the high energy region. This can be

	A_s^{NLO}	$A_s^{N^2LO}$	$\delta_{m_s}^{NLO}$	$\delta_{m_s}^{N^2LO}$	$\delta_{m_s}^{NLO,\not\pi}$	$\delta_{m_s}^{N^2LO,\not\pi}$
NLO	0.0291		−1.40		−3.90	
N^{2}LO	0.0361	0.0277	−13.7	−17.4	2.10	−1.89

Table 4.1: Fit values of the parameters for the ${}^1S_0$ channel. The units of dibaryon nucleon–vertices A_i are MeV$^{-1/2}$, the residual masses δ_{m_i}, MeV.

easily seen if the expression for the phase shift is written in terms of the real and imaginary parts of the amplitude

$$\delta = \arctan\left(\frac{\mathrm{Im}\mathcal{A}}{\mathrm{Re}\mathcal{A}}\right). \tag{4.63}$$

Since our LO amplitude (4.38) has no real part, then $\delta = \pm\pi/2$. Continuity with the low energy expression selects the plus sign.

A_s and δ_{m_s} receive corrections in the matching from NNEFT to pNNEFT, both at NLO and N^{2}LO. If the whole expressions for A_s and δ_{m_s} were to be used in the N^{2}LO amplitude, higher order terms would be introduced. Therefore we will differentiate between A_s^{NLO} and $A_s^{N^2LO}$ as well as between $\delta_{m_s}^{NLO}$ and $\delta_{m_s}^{N^2LO}$, which we will consider as independent parameters. Recall that the expression for the phase shift in the low energy region shares the same A_s as in the high energy one, but has an independent δ_{m_s}, which we will label $\delta_{m_s}^{\not\pi}$. Because of this shared parameter (A_s) we have made a common fit of the low and high energy region phase shift at each order. The low energy region phase shift (calculated in $\not\pi$NNEFT) has been fitted to data in the 0-3MeV range and the high energy region phase shift (calculated in pNNEFT) to data in the 3-50MeV. Results for the ${}^1S_0$ channel parameters are summarized in Table 4.1.

The phase shifts are plotted in Fig.4.18 (NLO) and Fig.4.19 (N^{2}LO) versus center–of–mass energy. The low energy region and the high energy region phase shifts have been plotted in the 0-4MeV and 1-50MeV range respectively.

4.8.2 The ${}^3S_1$–${}^3D_1$ channel

In this section we analyze ${}^3S_1$–${}^3D_1$ channel. We compare the ${}^3S_1$ and ${}^3D_1$ phase shifts to data as well as the mixing angle. The usual expression for the S-matrix

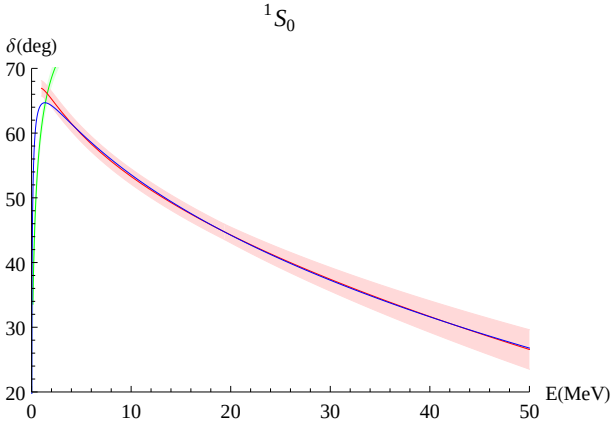

Figure 4.18: Plot of the NLO expression for the $^1S_0$ phase shift versus center–of–mass energy. The blue line shows the Nijmegen data for the $^1S_0$ phase shift, while the red and green line correspond to the high energy and low energy expressions respectively. The fitting procedure is explained in the text. Error bands correspond to $\pm(\frac{m_\pi}{m_N})^2$ for $p \leq m_\pi$ and to $\pm(\frac{p}{m_N})^2$ for $p > m_\pi$.

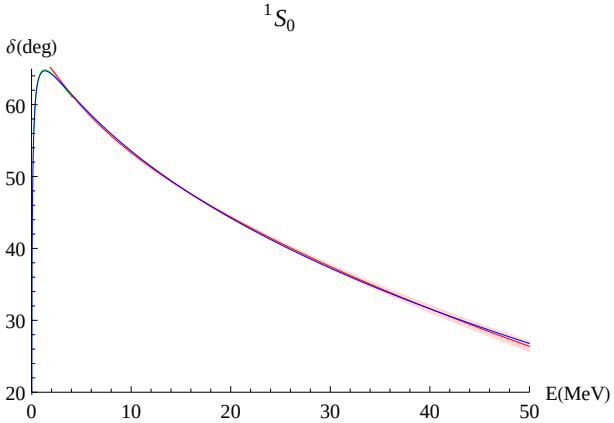

Figure 4.19: Plot of the N^{2}LO expression for the $^1S_0$ phase shift versus center–of–mass energy. As in the previous figure the blue line shows the Nijmegen data for the $^1S_0$ phase shift. The red line corresponds to the high energy expression and the green one to the low energy one (which totally overlaps the data). Error bands correspond to $\pm(\frac{m_\pi}{m_N})^3$ for $p \leq m_\pi$ and to $\pm(\frac{p}{m_N})^3$ for $p > m_\pi$.

	A_v^{NLO}	$A_v^{N^2LO}$	$\delta_{m_v}^{NLO}$	$\delta_{m_v}^{N^2LO}$	$\delta_{m_v}^{NLO,\not\pi}$	$\delta_{m_v}^{N^2LO,\not\pi}$	B'_v/A_v
NLO	0.0305		12.14		8.30		
N^{2}LO	0.0431	0.0429	−9.29	−13.3	−23.0	19.9	$-1.78\cdot10^{-5}$

Table 4.2: Fit values of the parameters for the ${}^3S_1-{}^3D_1$ channel, excluding the N^{2}LO ${}^3S_1$ phase shift in the high energy region. The units of dibaryon nucleon–vertices A_i are MeV$^{-1/2}$, the residual masses δ_{m_i}, MeV, and of B'_v/A_v, MeV^{-2}.

in this channel

$$S = 1+i\frac{pm_N}{2\pi}\begin{pmatrix} \mathcal{A}^v & \mathcal{A}^{mix} \\ \mathcal{A}^{mix} & \mathcal{A}^{^3D_1} \end{pmatrix} = \begin{pmatrix} e^{2i\delta^{(^3S_1)}}\cos(2\epsilon) & ie^{i\delta^{(^3S_1)}+i\delta^{(^3D_1)}}\sin(2\epsilon) \\ ie^{i\delta^{(^3S_1)}+i\delta^{(^3D_1)}}\sin(2\epsilon) & e^{2i\delta^{(^3D_1)}}\cos(2\epsilon) \end{pmatrix}. \tag{4.64}$$

To obtain the phase shift expression at each order we expand both sides in powers $(m_\pi/\Lambda_\chi)^n$, as we did in the previous section, and solve the resulting system to obtain $\delta^{v,LO}$, $\delta^{v,NLO}$ and, δ^{v,N^2LO}; $\delta^{^3D_1,NLO}$ and, $\delta^{^3D_1,N^2LO}$; ϵ^{NLO} and ϵ^{N^2LO}. There is no ϵ^{LO} or $\delta^{^3D_1,LO}$ due to the fact that $\mathcal{A}^{mix}$ and $\mathcal{A}^{^3D_1}$ start at NLO.

The fitting procedure for the NLO result is analogous to the one used for the ${}^1S_0$ channel. For the N^{2}LO one, several changes had to be introduced. A common fit to the low energy phase shift and to the mixing angle has been made, whereas the high energy phase shift has been left out and fitted independently. This is because all attempts to fit the high energy phase shift together with the other two expressions failed. The N^{2}LO pNNEFT phase shift fit delivers a value for $A_v^{N^2LO}$ (Table 4.3) which is far away from the expected natural size. We think this is the reason why we were unable to perform a successful common fit: whereas the mixing angle and the low energy phase shift favor natural size parameters, the high energy phase shift does not. This is a clear sign that our approach fails to converge in the ${}^3S_1$–${}^3D_1$ channel, we will comment on it further in the next section. Note that the parameter B'_v/A_v only appears in the N^{2}LO the mixing angle. ϵ^{NLO}, $\delta^{^3D_1,NLO}$ and, $\delta^{^3D_1,N^2LO}$ do not contain free parameters.

The ${}^3S_1$ phase shifts are plotted in Fig.4.20(NLO) and Fig.4.21(N^{2}LO), the mixing angle in Fig.4.22 and the ${}^3D_1$ phase shift in Fig.4.23. All ${}^3S_1$–${}^3D_1$ channel plots are versus center–of–mass energy. The low energy region and high energy region phase shifts have been plotted in the 0-4MeV and 1-50MeV range respectively, the mixing angle and the ${}^3D_1$ phase shift have been plotted in the 0-50MeV range. Results for the ${}^3S_1$–${}^3D_1$ channel parameters are summarized in Table 4.2 and Table 4.3.

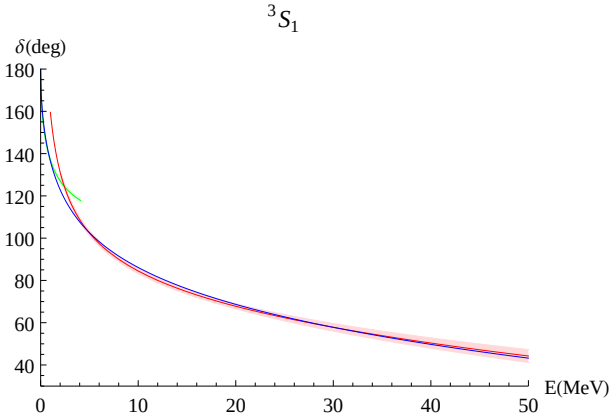

Figure 4.20: Plot of the NLO expression for the $^3S_1$ phase shift versus center–of–mass energy. The blue line shows the Nijmegen data for the $^3S_1$ phase shift, the red line corresponds to the high energy region expression and the green to the low energy region one. The fitting procedure is explained in the text. Error bands correspond to $\pm(\frac{m_\pi}{m_N})^2$ for $p \leq m_\pi$ and to $\pm(\frac{p}{m_N})^2$ for $p > m_\pi$.

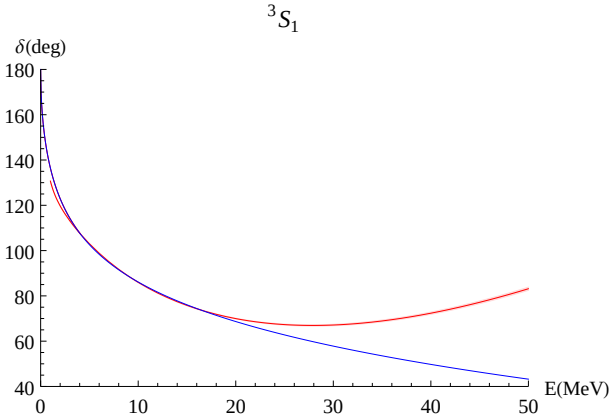

Figure 4.21: Plot of the N^{2}LO expression for the $^3S_1$ phase shift versus center–of–mass energy. The blue curve is the Nijmegen data for the $^3S_1$ phase shift, while red line corresponds to the high energy region expression. The curve for the low energy expression totally overlaps with data. The fitting procedure is explained in the text. Error bands correspond to $\pm(\frac{m_\pi}{m_N})^3$ for $p \leq m_\pi$ and to $\pm(\frac{p}{m_N})^3$ for $p > m_\pi$.

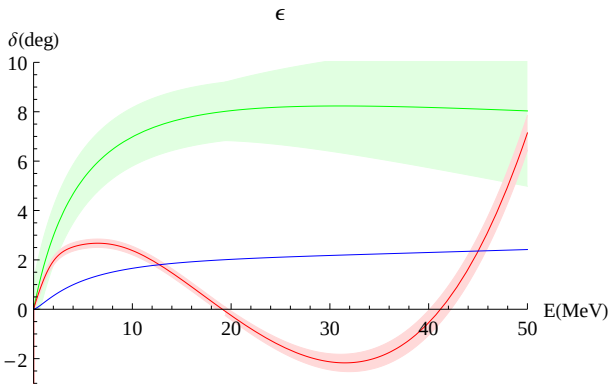

Figure 4.22: Plot of the mixing angle versus center–of–mass energy. The blue line shows the Nijmegen data, the green and red lines the NLO and N^{2}LO expression respectively. The NLO expression has no free parameters. The free parameters of the N^{2}LO expression have been fitted as explained in the text. The light green (light red) error bands correspond to $\pm(\frac{m_\pi}{m_N})^{2(3)}$ for $p \leq m_\pi$ and to $\pm(\frac{p}{m_N})^{2(3)}$ for $p > m_\pi$.

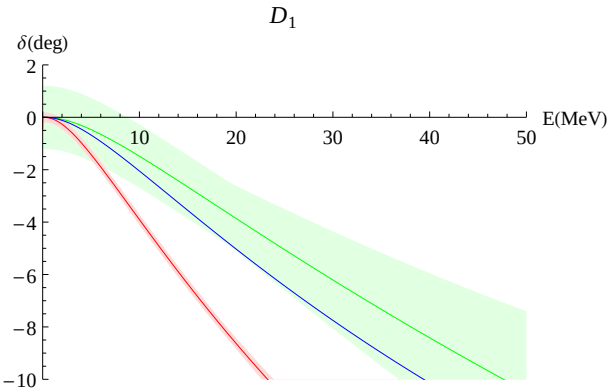

Figure 4.23: Plot of the ${}^3D_1$ phase shift versus center–of–mass energy. The blue line shows the Nijmegen data, the green and red lines the NLO and N^{2}LO expression respectively. Neither the NLO or the N^{2}LO expression have free parameters. The light green (light red) error bands correspond to $\pm(\frac{m_\pi}{m_N})^{2(3)}$ for $p \leq m_\pi$ and to $\pm(\frac{p}{m_N})^{2(3)}$ for $p > m_\pi$.

A_v^{NLO}	$A_v^{N^2LO}$	$\delta_{m_v}^{NLO}$	$\delta_{m_v}^{N^2LO}$
0.0206	0.00996	35.3	3.04

Table 4.3: Fit values of the parameters delivered by the N^{2}LO $^3S_1$ phase shift in the high energy region. The units of dibaryon nucleon–vertices A_i are MeV$^{-1/2}$, the residual masses δ_{m_i}, MeV, and of B'_v/A_v, MeV^{-2}.

	ζ_1	ζ_2	ζ_3
$^1S_0$	$\frac{\pi\delta'_{m_s}}{m_N A_s^2}$	$\frac{2\pi((s_1+s_2)/B_0-8c_1)}{m_N A_s^2}$	$\frac{g_A^2}{32m_N F_0^2}\left(\frac{1}{A_v^2}+\frac{2c_{sv}}{g_A A_s A_v}-\frac{3}{A_s^2}\right)-\frac{g_A^2}{8F_0^2}\frac{(s_1+s_2)/B_0-8c_1}{A_s^2}+\left(\frac{g_A^2 m_N}{2F_0^2}\right)^2\frac{\log(2)}{128\pi^2}$
$^3S_1$	$\frac{\pi\delta'_{m_v}}{m_N A_v^2}$	$\frac{2\pi(v_1/B_0-8c_1)}{m_N A_s^2}$	$\frac{g_A^2}{32m_N F_0^2}\left(\frac{1}{A_s^2}+\frac{2c_{sv}}{g_A A_s A_v}-\frac{3}{A_v^2}\right)-\frac{g_A^2}{8F_0^2}\frac{(v_1/B_0-8c_1)}{A_v^2}+5\left(\frac{g_A^2 m_N}{2F_0^2}\right)^2\frac{6+13\log(2)}{256\pi^2}$

Table 4.4: Independent free parameters in terms of the effective theory low energy constants.

4.9 Comparison of the scattering lengths with lattice data

In section 4.7 we have computed the matching for the dibaryon residual mass and dibaryon–nucleon vertices up to NLO. With these ingredients we can write the expression for the scattering lengths up to order $\mathcal{O}\left(m_\pi^3/\Lambda_\chi\right)$

$$a_i^{-1} = \frac{\pi\delta_{m_i}^{LO}}{m_N A_i^2}\left(1-\Delta_{NLO}\right)+\frac{\pi\delta_{m_i}^{NLO}}{m_N A_i^2} \quad , i = s(^1S_0)\,, v(^3S_1)\,. \tag{4.65}$$

The expressions for the scattering lengths can be rewritten to collect all the parameters into three independent ones

$$\begin{aligned} a_i^{-1} =& \zeta_{i1}\left(1-\frac{g_A^2 m_N}{16\pi F_0^2}m_\pi\right)+\left[\zeta_{i2}-\frac{g_A^2 m_N}{32\pi F_0^2}\ln\left(\frac{m_\pi^2}{\mu^2}\right)\right]m_\pi^2+\zeta_{i3}m_\pi^3 \\ &+\frac{1}{2}\left(\frac{g_A^2 m_N}{16\pi F_0^2}\right)^2 m_\pi^3\ln\left(\frac{m_\pi^2}{\mu^2}\right) \quad , \quad i = s(^1S_0)\,, v(^3S_1)\,, \end{aligned} \tag{4.66}$$

the expression obtained is quite simple and emphasizes the m_π dependence. The relation of the ζ parameters to the low energy constants of the EFT can be found in Table 4.4. The expected sizes of these parameter are, $\zeta_{i1} \sim \mathcal{O}\left(m_\pi^2/\Lambda_\chi\right)$, $\zeta_{i2} \sim \mathcal{O}\left(1/\Lambda_\chi\right)$ and $\zeta_{i3} \sim \mathcal{O}\left(1/\Lambda_\chi^2\right)$.

The first lattice QCD calculation of the nucleon–nucleon scattering lengths was performed by Fukugita *et al* [107, 108] in the quenched approximation with

$m_\pi(MeV)$	$a^{\,^1S_0}(fm)$	$a^{\,^3S_1}(fm)$
353.7	0.63 ± 0.50	0.63 ± 0.74
492.5	0.65 ± 0.18	0.41 ± 0.28
593	0.0 ± 0.5	-0.2 ± 1.3
390	$0.118^{+0.109}_{-0.126}$	$0.052^{+0.18}_{-0.24}$

Table 4.5: Lattice data point used to fit the scattering lengths. The first three data points are from [110] and the fourth one from [111].

Wilson quark action. More recent studies using the quenched approximation have been carried out by Aoki *et al* [109]. The NPLQCD collaboration has performed unquenched calculations in mixed–action (domain wall–staggered) [110] and anisotropic clover-quark action [111]. We fitted the lattice data of the NPLQCD collaboration (see Table.4.5). Unfortunately all data points are above or close to $350MeV$, a scale beyond which it is not clear that Chiral extrapolations for the nucleon–nucleon system are still valid. Thus the obtained results have to be taken with caution. We forced the expressions for the scattering lengths to reproduce the experimental values at the physical pion mass, $a^{\,^1S_0} = -23.7$ fm, $a^{\,^3S_1} = 5.38$ fm. This allows to solve one parameter as a function of the remaining ones, we chose to solve ζ_{i1}. The remaining parameters have been obtained by minimizing an augmented chi–square distribution [112] for each scattering length. The augmented chi–square distribution is defined as the sum of the chi-square function with a set of priors for every one of the free parameters to be fitted,

$$\chi^2_{aug} = \chi^2_{a^i} + \chi^2_{prior}\,,$$
$$\chi^2_{a^i} = \frac{1}{n}\sum_{j=1}^{n}\frac{\left(a^i(m_{\pi,j}) - a^i_j\right)^2}{\delta^2_{a^i_j}}\,,\ \chi^2_{prior} = \frac{1}{N}\sum_{k=1}^{N}\frac{\left(\log\|x_k\| - \log\|\bar{x}_k\|\right)^2}{\log^2 R_k}\,,\ i = {}^1S_0, {}^3S_1\,, \tag{4.67}$$

where a^i_j and $\delta_{a^i_j}$ stand for the value of scattering length and its uncertainity at the pion mass $m_{\pi,j}$ respectively. n is the total number of lattice data points. Furthermore, x_k refers to the free parameters, N being their total number. The free parameters are, ζ_{i2} at LO, and ζ_{i2} and ζ_{i3} at NLO. The prior is a Gaussian weight distribution centered at $\|\bar{x}_k\|$ with and standard deviaton R_k. The values of $\|\bar{x}_k\|$ and R_k are obtained from naive dimensional analysis. For instance, if the parameter x_k is of order $\mathcal{O}(1)$, we would expect it to be in the range $0.1 <$

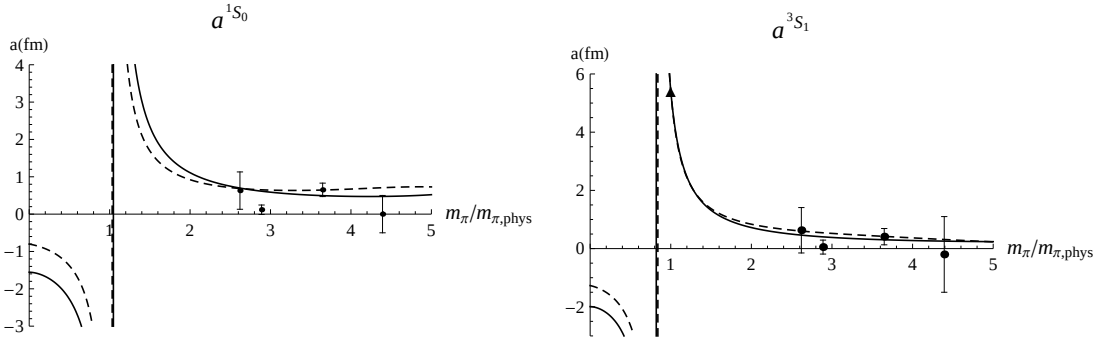

Figure 4.24: Plot of $a^{1S_0}(a^{3S_1})$ in the left(right) hand side. The solid and dashed lines correspond to the LO and NLO respectively. The triangular dot in the a^{3S_1} figure corresponds the physical value of the scattering length, in the a^{1S_0} figure the physical point is out of scale.

$\|x_k\| < 10$, which translates to setting $\log(\|\bar{x}_k\|) = 0$ and $\log(R_k) = 1$ for the kth parameter. We have taken logarithms in the prior functions to achieve equal weights for the subranges $0.1 < \|x_k\| < 1$ and $1 < \|x_k\| < 10$. For ζ_{i2} priors are set to $\bar{\zeta}_{i2} = \frac{1}{\Lambda_\chi}$ and $\log(R_{\zeta_{i2}}) = 1$, and for ζ_{i3} to $\bar{\zeta}_{i3} = \frac{1}{\Lambda_\chi^2}$ and $\log(R_{\zeta_{i3}}) = 1$. The plots corresponding to the fits of the LO and NLO expressions of the scattering lengths as a function of the quark mass are displayed in Fig.4.24. The chi-squared per degree of freedom is defined as

$$\chi^2_{a^i,d.o.f} = \frac{1}{n-1-N}\sum_{j=1}^{n}\frac{\left(a^i(m_{\pi,j}) - a^i_j\right)^2}{\delta^2_{a^i_j}} \quad , \quad i = {}^1S_0, {}^3S_1\,. \tag{4.68}$$

The values obtained for the parameters and the chi-squared per degree of freedom are collected in Table 4.6 and Table 4.7. The values obtained for ζ_{s1} and ζ_{i3}, $i = s, v$ at NLO are on the limit of what we would consider natural size. This could indicate that significant cancellations occur at the physical pion mass in order to produce the observed values of the scattering lengths. Note that the fine tunning increases with the precision of the expression used.

The m_q–dependence of the scattering lengths has been studied previously in [104, 113] using numerical solutions to the Lippmann–Schwinger equation with potentials obtained from Weinberg's power counting, and in [105, 99] in the framework of BBSvK counting. All these papers were written before the first unquenched lattice results appeared and hence do not use lattice data to fit

LO	$\chi^2_{d.o.f}$	$\zeta_1(MeV)$	$\zeta_2(MeV^{-1})$
${}^1S_0$	3.74	-126	$0.67 \cdot 10^{-3}$
${}^3S_1$	0.91	-98	$1.59 \cdot 10^{-3}$

Table 4.6: LO scattering lengths fit parameters.

NLO	$\chi^2_{d.o.f}$	$\zeta_1(MeV)$	$\zeta_2(MeV^{-1})$	$\zeta_3(MeV^{-2})$
${}^1S_0$	2.4	-246	$4.56 \cdot 10^{-3}$	$9.21 \cdot 10^{-6}$
${}^3S_1$	0.4	-155	$3.83 \cdot 10^{-3}$	$10.1 \cdot 10^{-6}$

Table 4.7: NLO scattering lengths fit parameters.

their unknown free parameters. In both approaches the behavior of the scattering length was studied for a suitable range of the unknown parameters. Special attention was devoted to the extrapolations to the Chiral limit. A more recent study can be found in [114] using the power counting of [100] and lattice data of the NPLQCD collaboration. In the ${}^1S_0$ channel our results in the Chiral limit indicate that the scattering length remains negative, thus the system is unbounded, coinciding with the predictions of mentioned previous works, albeit our value seems slightly smaller. In the ${}^3S_1$ channel our extrapolation of the scattering length to the Chiral limit shows that it evolves from positive values at the physical pion mass to negative values, hence going from a bounded nucleon–nucleon system to an unbounded one. This is opposite to the results in [104, 113], and to those in [105, 99], for most of the parameter space, in which the scattering length remains positive in the whole range from the Chiral limit to the physical pion mass. Nevertheless, in [105, 99] a behavior similar to the one we have obtained is observed in certain regions of the parameter space. In [114], the only one of the pevious works on the m_q–dependence of the scattering lengths that has used lattice data, the ${}^3S_1$ channel goes to negative values in the Chiral limit, and overall presents a very similar results to ours.

4.10 Conclusions

We have constructed a Chiral effective field theory for the nucleon–nucleon system which contains dibaryon fields as fundamental degrees of freedom. The large scattering lengths in the ${}^1S_0$ and the ${}^3S_1$ channels force the dibaryon residual masses to be much smaller than the pion mass. We organize the calculation in a series of effective theories, which are obtained by sequentially integrating

out higher energy and momentum scales. We first integrate out energy scales of the order of the pion mass. This leads to an effective theory with dibaryon and nucleon fields, pNNEFT. The latter interact through non–local potentials.

We have showed that in the matching calculation of the residual mass certain classes of diagrams involving potential pion exchanges in loops with radiation pions can be summed up in the ${}^3S_1$ channel. This is important because each of these exchanges introduces a parametric suppression of only $\mathrm{O}(\sqrt{m_\pi/m_N})$ that numerically turns out to be $\mathrm{O}(1)$. The resummation is possible because after radiating a pion a nucleon–nucleon system in the ${}^3S_1$ channel changes into the ${}^1S_0$ channel, and in this channel the one pion exchange potential at high momentum transfer becomes a contact interaction. We showed that by performing dibaryon local field redefinitions we can get rid of the contact interaction, and hence the contribution of all diagrams involving these potential pion exchanges must be zero. We checked this cancellation by explicitly computing the diagrams and adding them up. Unfortunately, in the ${}^1S_0$ channel it has not been possible for us to compute the contribution of an arbitrary number of potential pions in a loop with a radiation pion. This is because after radiating a pion a nucleon–nucleon system in the ${}^1S_0$ channel changes into the ${}^3S_1$ channel, and in this channel the one pion exchange potential at high momentum transfer does not reduce to a contact interaction anymore. However, similar arguments still apply to the diagrams with only one potential pion, which should then add up to zero. This is in contradiction with the results of [32, 84], and we have pointed out a possible source of the discrepancy in section 4.4.2. It is very likely that in the ${}^1S_0$ channel the perturbative series breaks down as in the ${}^3S_1$ channel, which means that it is possible that our expressions for $a^{{}^1S_0}$ are missing large contributions, and hence, are unreliable.

For three momenta much smaller than the pion mass, it is convenient to further integrate out three momenta of the order of pion mass, which leads to the $\not\pi$NNEFT. In this theory non–local potentials can be expanded in powers of $\frac{p^2}{m_\pi^2}$ and become local. Self energies can be expanded giving contributions to the dibaryon residual mass as well as time derivative terms. The latter can be reabsorbed by field redefinitions of the dibaryon fields. We have computed the matching between $\not\pi$NNEFT and pNNEFT of the dibaryon residual masses, and the dibaryon–nucleon coupling A_i up to NLO.

We have calculated the nucleon–nucleon scattering amplitudes for energies smaller than the pion mass in the ${}^1S_0$ and the ${}^3S_1 - {}^3D_1$ channels at N^{2}LO. For three momenta of the order of the pion mass, the scattering amplitudes are calcu-

lated in pNNEFT, for momenta of the order $\mathcal{O}\left(m_\pi^2/m_n\right)$ in $\not\pi$NNEFT. By splitting the calculation in this way we can take advantage of the modern techniques of the threshold expansions and dimensional regularization so that all integrals only depend on a single scale [74, 95, 65]. There is no need to introduce a PDS scheme [76]. The technical complexity of the N^{2}LO calculation is similar to the one in the KSW scheme [84], but our final expressions are simpler.

The numerical results for the phase shifts and mixing angle are also similar to the ones obtained in the KSW approach. Hence a good description of the ${}^1S_0$ channel is obtained, but for the ${}^3S_1 - {}^3D_1$ channel our results also fail to describe data. The ${}^3S_1$ phase shift shows a good agreement with data up to center of mass energies of $50MeV$ at NLO, but at N^{2}LO the range of the agreement is reduced, up to $20MeV$. only, even when the high energy region of this channel is fitted independently, as in the plot of Fig.4.21. The mixing angle poorly agrees with data, but shows a marginal improvement from NLO to N^{2}LO. The N^{2}LO mixing angle plot is significantly different from the one shown in [84], this is a consequence of making a common fit of the ${}^3S_1$ phase shift in the low energy region and the mixing angle. For a different fitting approach with plot closer to [84] see [33]. Comparison with data for the ${}^3D_1$ phase shift it is never good. Particularly worrying is the fact that for the ${}^3S_1$ and the ${}^3D_1$ phase shift the N^{2}LO calculation compares worse to data than the NLO one. The reasons of this failure can be traced back to the iteration of the OPE potential , the first diagram in Fig.4.13, which gives a very large contribution [84]. This may be interpreted as an indication that pion exchanges must be iterated at all orders, as originally proposed by Weinberg [22]. However, the removal of the cut-off in this approach appears to require an infinite number of counterterms, one for each partial wave [96, 97, 98] (see also [99]). A very recent proposal, which keeps the essentials of KSW counting, consist in introducing a Pauli-Villars regularization for the pion exchanges and staying at the regularized level [100]. This seems to produce slightly better results, but it is unclear at the moment that, staying at regularized level, this approach is superior to Weinberg's one [83] (see [101, 102] for very recent efforts on the renormalization of Weinberg's approach).

We have given Chiral extrapolation formulas for $1/a^{{}^1S_0}$ and $1/a^{{}^3S_1}$ up to corrections of order $\mathcal{O}\left(m_\pi^3/\Lambda_\chi^2\right)$ depending on three independent free parameters. In section 4.9 we carried out a fit of these expressions to lattice data from the NPLQCD collaboration [110, 111]. The results in Fig.4.24, Table 4.6 and Table 4.7 show that our expressions for $a^{{}^3S_1}$ are much more compatible with lattice data than those for $a^{{}^1S_0}$, which could indicate that the missing, potentially large,

contributions to $a^{^1S_0}$ previously mentioned do exist. Using this results to extrapolate the scattering lengths in the Chiral limit we obtain that $a^{^1S_0}$ keeps is negative sign, while $a^{^3S_1}$ changes from positive to negative. However, at this stage, lattice data sets available are rather small, with relatively large pion masses, and often computed using different approaches, making it difficult hold any strong statement at this respect.

CHAPTER

5

CHIRAL PERTURBATION THEORY WITH A LIGHT SCALAR FIELD

5.1 Introduction

Chiral Perturbation Theory (χPT), see Chapter 2, has become a standard tool for the phenomenological description of QCD processes involving pseudo–Goldstone bosons at low–energy. Scattering amplitudes can be systematically calculated within this framework to a given order in $p^2 \sim m_\pi^2$ over Λ_χ^2 . However, when pion scattering amplitudes are calculated in the isoscalar channel, a bad convergence is observed, even at reasonably low–momenta. This has led some authors to resum certain classes of diagrams, using a number of unitarization techniques (see, for instance, [116, 117, 118, 119, 120]). Most of these approaches improve considerably the description of data with respect to standard χPT, and indicate that a scalar isospin zero resonance at relatively low–mass, the sigma, exist. In fact the mass and width of the sigma resonance are nowadays claimed to be known very accurately $m_\sigma = 441^{+16}_{-8}\,\mathrm{MeV}\,, \Gamma/2 = 272^{+9}_{-12.5}\,\mathrm{MeV}$ [121, 122] (see also [123]).

Under the $SU(3)$ perspective one may find surprising that the effective theory contains kaons but not other states with similar masses, but different quantum numbers, that can be equally excited in a collision at intermediate stages. The relatively low–mass of the sigma resonance, with respect to the Chiral cutoff, Λ_χ, and its proximity to the value of the kaon mass suggests that it may be convenient to introduce it as an explicit degree of freedom in an extension of χPT. It is in fact an old observation by Weinberg [124], that the explicit inclusion of resonances in a Lagrangian generically improves perturbation theory.

We implement this observation in this chapter, in a Chiral effective theory

framework that involves a dynamical singlet field together with the lowest pseudo–Goldstone bosons. We write down the most general $SU(2)$ Chiral Lagrangian including an isospin zero scalar field at order p^4 and calculate a number of observables at this order. We show that for a large scalar mass, the effect of the scalar reduces to just redefinitions of the low–energy constants, hence explicitly demonstrating that our approach is compatible with standard χPT. However if we count the mass of the scalar as order p^2, namely of the same size as the pion mass, the non-analytic pieces of our amplitudes differ from those of χPT. Furthermore, the quark mass dependence of the observables is also different. We compare this effective theory, which we call χPT_S, versus standard χPT against lattice data on m_π and F_π [125] and show that at the current precision the lattice data is unable to tell apart χPT from χPT_S.

The present chapter is based in the work presented in Refs.[35, 36]

5.2 Lagrangian and power counting

Our aim is to construct an effective field theory containing pions and a singlet scalar field as a degrees of freedom, that holds for processes involving only low–energy pions as the asymptotic states

$$p \sim m_\pi (\sim 140\,\text{MeV}) \lesssim m_S (\sim 440\,\text{MeV}) \ll \Lambda_\chi. \tag{5.1}$$

The structure of the effective Lagrangian will be independent of the underlying mechanism of spontaneous Chiral symmetry breaking. It consists of an infinite tower of Chiral invariant monomials combining pions and a singlet scalar field with the generic appearance

$$\mathcal{L}^{\text{eff}} = \sum_{(k,l,r)} \mathcal{L}_{(k,l,r)}\,, \tag{5.2}$$

where $\mathcal{L}_{(k,l,r)}$ contains k powers of derivatives, l powers of the scalar or pseudoscalar sources and finally r powers of the singlet field.

$$\mathcal{L}_{(k,l,r)} \sim \Lambda_\chi^4 \left(\frac{p}{\Lambda_\chi}\right)^{k+r} \left(\frac{m_\text{q}}{\Lambda_\chi}\right)^{l}, \tag{5.3}$$

being p a typical meson momentum. One possible manner to relate these scales is to assume that $p^2 \sim m_\pi^2 \sim m_\text{q}\Lambda_\chi$, like in standard χPT. Hence, in the Chiral

counting $\mathcal{L}_{(k,l,r)}$ is of order p^{k+r+2l}. Notice that terms with $k+r+l<4$ correspond to relevant operators and, hence, their dimensionful constant may be tuned to a scale smaller than the natural one Λ_χ, as it happens in standard χPT ($F_\pi \ll \Lambda_\chi$).

The Lagrangian involving pions and scalar fields transforming as a singlet under $SU(2)_R \times SU(2)_L$, respecting Chiral symmetry, P and C invariance, has been presented in the linear approximation in [126, 127] and up to quadratic terms in [128]. For the time being, we will collect only the relevant terms necessary for our purposes. The leading order (LO) consist in the standard Goldstone boson Chiral Lagrangian, that we do not discuss further, a scalar Goldstone boson interaction term, and the singlet field self-interaction.

5.2.1 Leading Lagrangian

Consider first the part of $\mathcal{L}^{\text{eff}}$ containing only the singlet scalar field. In the absence of any symmetry hint we are forced to write the most general polynomial functional

$$\mathcal{L}^S = \frac{1}{2}\partial_\mu S \partial^\mu S - \frac{1}{2}\mathring{m}_S^2 SS - \lambda_1 S - \frac{\lambda_3}{3!}S^3 - \frac{\lambda_4}{4!}S^4 + \cdots \tag{5.4}$$

where the dots indicate terms suppressed by powers of $1/\Lambda_\chi$. Suppose that we deal with the Chiral limit. At LO λ_1 must be set to zero in order to avoid mixing of S with the vacuum, and at higher orders it must be adjusted for the same purpose. The mass and the coupling constants above are functions of the small scale $\mathring{m}_S$ and the large scale Λ_χ, ($\mathring{m}_S^2 \ll \Lambda_\chi$). Their natural values would be $\lambda_3 \sim \mathcal{O}(\Lambda_\chi)$ and $\lambda_4 \sim \mathcal{O}(1)$. In that case, the scalar sector above becomes strongly coupled. However, strongly coupled scalar theories in four dimensions are believed to be trivial [132, 133]. Their exact correlation functions factorize according to Wick's theorem and consequently they behave as if the theory were non-interacting. A practical way of taking this fact into account is just setting $\lambda_3 = \lambda_4 = 0$, which we will do in the following. When the interactions of the scalar with the pseudo-Goldstone bosons are taken into account, small ($\mathring{m}_S^2/\Lambda_\chi^2$ suppressed) but non-vanishing values of λ_3 and λ_4 are required to ensure perturbative renormalization of the whole $\mathcal{L}^{\text{eff}}$.

The purely pseudo–Goldstone sector is given by the usual χPT LO lagrangian of Eq.(2.43). The pion–scalar Lagrangian is contructed with the building blocks

of Chapter 2 for the pions and powers of the scalar field

$$\begin{aligned}\mathcal{L}^{(2)} = & \left(\frac{F_0^2}{4} + F_0 c_{1d} S + c_{2d} S^2 + \cdots\right) \mathrm{Tr}\left[D_\mu U D^\mu U^\dagger\right] \\ & + \left(\frac{F_0^2}{4} + F_0 c_{1m} S + c_{2m} S^2 + \cdots\right) \mathrm{Tr}\left[\chi^\dagger U + \chi U^\dagger\right] \end{aligned} \tag{5.5}$$

where the ellipsis stand for higher order terms involving more powers of the singlet field (or derivatives on them), which are suppressed by powers of $1/\Lambda_\chi$.

At this point a small digression is in order; notice the peculiarity of (5.5) with respect to the usual Chiral expansion. At this order, both expansions can be cast in the form,

$$\mathcal{L} \sim \sum_k b_k(\Lambda_\chi, S)\mathbb{O}^{(k)} \tag{5.6}$$

$\mathbb{O}^{(k)}$ being an operator of order k including only the pseudo-Goldstone bosons and $b_k(\Lambda_\chi, S)$ its corresponding "Wilson coefficient", that can depend on the singlet field if one considers the theory with the scalar field inclusion. While in the standard theory the power counting is given entirely by the operator, i.e. $b_k(\Lambda_\chi) \sim \mathcal{O}(\Lambda_\chi^{4-k})$, in the extended version one also has to take into account that the Wilson coefficients themselves have a power expansion in S/Λ_χ. At higher orders operators containing the derivatives of the scalar field must also be included.

Before closing this section we would like to remark that even if we have kept for F_0 and B_0 the same names as in χPT, they are now parameters of a different theory and, hence, their values are expected to differ from those in χPT.

5.2.2 Comparison with the linear-σ model

Hitherto we have included in a dynamical fashion a scalar particle interacting with pseudo-Goldstone bosons. One may wonder if there is any relation between the effective theory just introduced and the old linear sigma model [134] (see [135] for a review), which we discuss next. The starting point for the construction of the linear-σ model is an $O(4)$ invariant action. The global $O(4)$ symmetry is spontaneously broken down to $O(3)$ because the scalar field develops a non-zero vacuum expectation value v.

The Lagrangian reads

$$\mathcal{L}_\sigma = \frac{1}{2}\left(\partial_\mu\sigma\partial^\mu\sigma + \partial_\mu\vec{\varphi}\partial^\mu\vec{\varphi}\right) - \frac{\lambda}{4}\left(\sigma^2 + \vec{\varphi}^2 - v^2\right)^2 , \tag{5.7}$$

where $\vec{\varphi}$ is an isotriplet pseudoscalar field, usually identified with the pion, and σ is an isosinglet scalar field that, after the shift $\sigma \to \sigma + v$ is usually identified with the sigma resonance. We do not display the part of the model containing nucleons because it has no relevance for our discussion. Since $O(4) \cong SU(2) \times SU(2)$ for group elements close to the identity, the model transforms correctly under the $SU(2)_R \times SU(2)_L$ Chiral symmetry of two-flavor QCD with massless quarks. To see this explicitly we make the change $\Sigma = \sigma \mathbf{1} - i\vec{\tau}\cdot\vec{\varphi}$, being $\vec{\tau}$ the Pauli matrices. Then (5.7) can be written as

$$\mathcal{L}_\sigma = \frac{1}{4}\mathrm{Tr}\left[\partial_\mu \Sigma \partial^\mu \Sigma^\dagger\right] - \frac{\lambda}{16}\left(\mathrm{Tr}\left[\Sigma^\dagger \Sigma\right] - 2v^2\right)^2 , \tag{5.8}$$

that explicitly exhibits the desired symmetry (2.13), if we transform $\Sigma \overset{G}{\to} g_R\, \Sigma\, g_L^{-1}$ [115]. The traditional identification of the $\vec{\varphi}$ fields with the pions and the σ field (after the shift) with the sigma resonance, which is fine concerning the transformations under the unbroken subgroup $O(3) \cong SU(2)$, becomes problematic if one wishes to implement the non-linear $SU(2)_R \times SU(2)_L$ symmetry that the model retains after the shift $\sigma \to \sigma + v$ is performed. In order to make the non-linear $SU(2)_R \times SU(2)_L$ symmetry manifest in the Lagrangian above and keep the transformations of the Goldstone bosons in the standard way [17, 16], as we have done in the previous section, it is convenient to perform a polar decomposition of Σ, $\Sigma = (v + S)U$, with U being a unitary matrix collecting the phases, to be identified with the U appearing in (2.17), and S a real scalar field, to be identified with our singlet field above. We remark that S must not be mistaken by the σ field in the original variables of the linear sigma model. The symmetry transformations of the fields S and U are the same as in (2.13). This change of variables leads to

$$\mathcal{L}_\sigma = \left(\frac{v^2}{4} + \frac{v}{2}S + \frac{1}{4}S^2\right)\mathrm{Tr}\left[D_\mu U D^\mu U^\dagger\right] + \frac{1}{2}\partial_\mu S \partial^\mu S - \lambda v^2\left(S^2 + \frac{S^3}{v} + \frac{S^4}{4v^2}\right) . \tag{5.9}$$

The terms with covariant derivatives above have the very same functional form as the terms with derivatives of (5.5), with the identifications $v = F_0$, $c_{1d} = 1/2$ and $c_{2d} = 1/4$. However, the terms with no derivatives, the potential, are set to zero (or, at higher orders, to small values uncorrelated to the rest of the parameters) in $\chi\mathrm{PT}_S$, except for the mass term, for which $\mathring{m}_S^2 = 2\lambda v^2$. This is because the underlying mechanism of Chiral symmetry breaking is assumed to take place at the scale Λ_χ, and hence it must not be described in the effective theory.

Since pions are not massless in nature, a small explicit breaking of the $O(4)$

symmetry had to be introduced. This was traditionally done by adding a term $\delta\mathcal{L}_\sigma = H\sigma$. In terms of the new variables this term reads:

$$\delta\mathcal{L}_\sigma = H\sigma = \frac{H}{4}\mathrm{Tr}\left[\Sigma + \Sigma^\dagger\right] = \frac{H}{4}(v+S)\mathrm{Tr}\left[U + U^\dagger\right]. \tag{5.10}$$

Hence, it has exactly the same functional form as the terms with no derivatives in (5.5), once χ is set to $2B_0\hat{m}\mathbf{1}$, with the identifications $H = 2F_0B_0\hat{m}$, $c_{1m} = 1/4$ and $c_{2m} = 0$.

In summary, the Lagrangian of $\chi\mathrm{PT}_S$ at LO differs from the one of the linear sigma model *only* in two respects: (i) the self-interactions of the scalar field S are set to zero (or, at higher orders, to small values uncorrelated to the rest of the parameters), and (ii) it has four additional free parameters controlling the interaction of the scalar field S with the pions: c_{1d}, c_{2d}, c_{1m}, c_{2m}.

5.2.3 Chiral symmetry constraints

To envisage the effects of explicit Chiral symmetry breaking on the dynamics of the singlet field we set U to the vacuum configuration ($U = \mathbf{1}$). The terms proportional to the quark masses in (5.5) induce new terms in the Lagrangian of S, that can be reshuffled into the coefficients of (5.4). For the first two terms one finds explicitly

$$\lambda_1 \to \lambda_1 - 8F_0c_{1m}B_0\hat{m}\,, \quad \mathring{m}_S^2 \to m_S^2 = \mathring{m}_S^2 - 16c_{2m}B_0\hat{m}\,. \tag{5.11}$$

As a consequence the singlet field is brought out of its minimum in the Chiral limit by terms proportional to $\hat{m}$. Hence, the direct consequence of the inclusion of non-vanishing quark masses results in a new contribution to the singlet-vacuum mixing. The new scalar field describing the first excitation with respect to the vacuum may be obtained by carrying out the following shift:

$$S \to S + F_0S_0 \quad \text{with} \quad S_0 = 8c_{1m}\frac{B_0\hat{m}}{m_S^2} - \frac{\lambda_1}{m_S^2F_0}\,. \tag{5.12}$$

After this shift, and upon separating the vacuum contribution, the original Lagrangian (5.5) keeps essentially the same form,

$$\begin{aligned}\mathcal{L}^{(2)} = &\left(\frac{F_0^2}{4} r_{0d} + F_0 r_{1d} S + r_{2d} S^2 + \cdots\right) \mathrm{Tr}\left[D_\mu U D^\mu U^\dagger\right] + \\ &\left(\frac{F_0^2}{4} r_{0m} + F_0 r_{1m} S + r_{2m} S^2 + \cdots\right) \left(\mathrm{Tr}\left[\chi^\dagger U + \chi U^\dagger\right] - \mathrm{Tr}\left[\chi^\dagger + \chi\right]\right) ,\end{aligned} \tag{5.13}$$

provided we redefine the low–energy constants as,

$$\begin{aligned} r_{0d} &= 1 + 4c_{1d} S_0 + 4c_{2d} S_0^2 + \dots , & r_{0m} &= 1 + 4c_{1m} S_0 + 4c_{2m} S_0^2 + \dots , \\ r_{1d} &= c_{1d} + 2c_{2d} S_0 + \dots , & r_{1m} &= c_{1m} + 2c_{2m} S_0 + \dots , \\ r_{2d} &= c_{2d} + \dots , & r_{2m} &= c_{2m} + \dots . \end{aligned} \tag{5.14}$$

In the previous expression all the terms explicitly depicted are $\mathcal{O}(1)$ quantities and ellipsis stand for subleading contributions, $c_{nx} S_0^{(n-1)} \sim (F_0/\Lambda_\chi)^{n-2}$, for $n > 2$ ($x = d, m$).

There is a subtle point that must be addressed before going on: for generic values of the low-energy constants the shift (5.12) breaks Chiral symmetry. This is most apparent if we lift the scalar and pseudoscalar sources from its vacuum values to arbitrary ones. Namely, if the original scalar field in (5.4) is a singlet under Chiral symmetry, the scalar field after the shift (5.12) is not. This is so for any value of the parameters, except for those that fulfill

$$\lambda_1 = \frac{c_{1m} \mathring{m}_S^2 F_0}{2c_{2m}} . \tag{5.15}$$

If we choose λ_1 as above, the shift becomes independent of the quark masses ($S_0 = -c_{1m}/2c_{2m}$), and hence the scalar field after the shift is still a scalar under Chiral symmetry, as it should. Moreover, for this choice, $r_{1m} = 0$, and r_{0m} and r_{0d} can be set to 1 by a redefinition of B_0 and F_0 respectively. The net result is equivalent to choosing $\lambda_1 = c_{1m} = 0$ in (5.4) and (5.5). This has in fact a simple interpretation. If we impose to our original scalar field to be a singlet under Chiral symmetry for any value of the external sources and not to mix with the vacuum, then the only solution at tree level is $\lambda_1 = c_{1m} = 0$. We shall adopt this option from now on. At higher orders these two parameters must be tuned so that no mixing with the vacuum occurs at any given order. Note finally that the value $c_{1m} = 0$ is incompatible with the linear sigma model one $c_{1m} = 1/4$.

5.2.4 Next-to-leading Lagrangian

In computing loop graphs, we will encounter ultraviolet divergences. These will be regularized within the same dimensional regularization scheme as used in [13], and the elimination of the divergences proceeds through suitable counter-terms. Like in [13] we will deal with contributions up to including terms of order p^4. Since the singlet fields will only enter in internal propagators, the counter-term Lagrangian we need only involves pions, and hence it has the same functional form as the one in χPT. The coefficients, however, receive extra contributions due to the appearance of the c_{ix} ($i = 1, 2$, $x = d, m$) bare parameters. In addition, unlike standard χPT, now F_0 and B_0 need to be renormalized. In order to take this into account we chose to include explicitly the corresponding counter-terms below. Using the $SU_L(2) \times SU_R(2)$ formalism [52], rather than the $O(4)$ one, [13], we have

$$\begin{aligned}\mathcal{L}^{(4)} =& \frac{1}{4}\ell_1 \mathrm{Tr}\left[D_\mu U D^\mu U^\dagger\right]^2 + \frac{1}{4}\ell_2 \mathrm{Tr}\left[D_\nu U D^\mu U^\dagger\right]\mathrm{Tr}\left[D^\nu U D_\mu U^\dagger\right] \\ &+ \frac{1}{16}\ell_3 \mathrm{Tr}\left[\chi^\dagger U + \chi U^\dagger\right]^2 + \frac{1}{4}\ell_4 \mathrm{Tr}\left[D^\mu U^\dagger D_\mu \chi + D^\mu \chi^\dagger D_\mu U\right] \\ &+ Z_1 \mathring{m}_S^2 \mathrm{Tr}\left[\chi^\dagger U + \chi U^\dagger\right] + Z_2 \mathring{m}_S^2 \mathrm{Tr}\left[D_\mu U D^\mu U^\dagger\right] \\ &+ f_{2p}\,\Box S \,\Box S + d_{2m}\partial_\mu S \partial^\mu S \mathrm{Tr}\left[\chi^\dagger U + \chi U^\dagger\right] + b_{2m} S^2 \mathrm{Tr}\left[\chi^\dagger U + \chi U^\dagger\right]^2 \\ &+ a_{2m} S^2 \mathrm{Tr}\left[\chi^\dagger \chi\right] + e_{2m} S^2 \Re[\det(\chi)] \ldots .\end{aligned} \tag{5.16}$$

In order to avoid confusion with the values that the low–energy constants take in χPT and $\chi\mathrm{PT}_S$, we shall denote the former l_i, $i = 1, \ldots, 4$ and the latter ℓ_i, $i = 1, \ldots, 4$. The relations between l_i, l_i^r and $\bar{l}_i$, $i = 1, \ldots, 4$ that appear in the paper are the standard ones in χPT [13]. In this work ℓ_1 and ℓ_2 will not be necessary for renormalization. For the observables that we will consider, the pole at $d = 4$ is removed by the following two kinds of renormalization constants which occur in the Lagrangian $\mathcal{L}^{(4)}$

$$\begin{aligned}&\ell_i := \ell_i^r + \gamma_i \lambda\,, \ (i = 3, 4) \quad Z_j := Z_j^r + \Gamma_j \lambda\,, \\ &f_{2p} := f_{2p}^r + \Gamma_f \lambda\,, \quad d_{jm} := d_{jm}^r + \Delta_j \lambda\,, \ (j = 1\,, 2)\,,\end{aligned} \tag{5.17}$$

$$\text{with} \quad \lambda = \frac{1}{16\pi^2}\left(\frac{1}{d-4} - \frac{1}{2}[\ln 4\pi + \Gamma'(1) + 1]\right),$$

where combination $d_{1m} \equiv 32 b_{2m} + 2 a_{2m} + e_{2m}$ is indistinguishable in the observables that we will consider, and is renormalized as a whole. The first kind of

(a) (b) (c) (d)

Figure 5.1: Self energy diagrams. Solid lines denote the scalar and the dotted ones pions. Diagram (a) corresponds to NLO counterterms.

renormalization constants, γ_i, are a simple redefinition of the divergent part in the standard monomials of χPT

$$\gamma_3 = -\frac{1}{2} + 32c_{2m}\left(c_{2m} - c_{2d}\right) - 8c_{1d}^2\left(1 - 4c_{2m}\right) , \quad \gamma_4 = 2 + 4c_{1d}^2\left(1 - 8c_{2m}\right) + 32c_{2d}c_{2m} . \tag{5.18}$$

While the second, absent in χPT, are entirely due to the interaction of pions with the singlet field. The first two sources are proportional to B_0 and other to F_0 respectively

$$\begin{aligned} &\Gamma_1 = -2\left(c_{1d}^2 - c_{2d} + c_{2m}\right) , \Gamma_2 = c_{1d}^2 - c_{2d} , \\ &\Gamma_f = \frac{12c_{1d}^2}{F_0^2} , \ \Delta_1 = \frac{24}{F_0^2}\left(c_{2m} - c_{2d} + 6c_{1d}^2\right) , \ \Delta_2 = -\frac{9c_{1d}^2}{F_0^2} . \end{aligned} \tag{5.19}$$

Recall that, like F_0 and B_0, ℓ_3^r and ℓ_4^r are now parameters of a theory different form χPT and, hence, their values are expected to differ from the ones in the latter. Note also that our approach differs of that in [126] in the respect that pions and the singlet field are both dynamical in the same energy range and thus both will be allowed to run inside loops. In that respect, any estimate of the low–energy constants by matching the observables derived from χPT_S with those obtained from a Lagrangian of resonance exchange as in [126] should keep the singlet field S in the latter as a dynamical low–energy degree of freedom. Loop effects of scalar resonances coupled to pseudo-Goldstone bosons have been studied in [128, 129, 130, 131]

5.3 The axial-vector two-point function

We are now in the position to perform a complete NLO analysis of the pion mass and decay constant including the radiative correction due to the singlet field

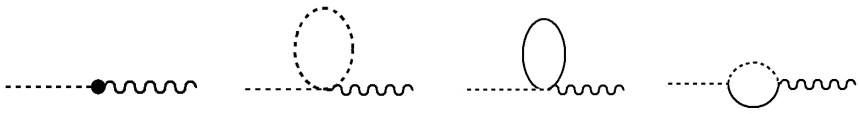

(a) (b) (c) (d)

Figure 5.2: Diagrams contributing to the decay constant. Solid lines denote the scalar and the dotted ones pions. Diagram (a) corresponds to NLO counterterms.

and obtain the first modification to the standard analysis. In order to calculate them we focus in the sequel in the axial-vector two-point Green function. The first quantity will be defined through the position of the pole in the two-point function while the second one can be obtained directly from its residue.

At the Born level the expressions for the pion mass and decay constant do not differ from those of the standard χPT theory while at NLO corrections are slightly more cumbersome. The diagrams contributing at $\mathcal{O}(p^4)$ to $m^2_{\rm PS}$ and $F_{\rm PS}$ are represented in Fig.5.1 and in Fig.5.2 respectively. In both figures the diagram (a) is the usual couterterm contribution, and the diagram (b) the usual tadpole contribution, already encounter in the standard theory. Diagrams (c) and (d) are new and appear because of the singlet field.

We cast the expressions for the mass and decay constant as

$$\begin{aligned} m^2_{\rm PS} =& 2B_0\hat{m} + U_m + P_m + \mathcal{O}(p^6)\,, \\ F_{\rm PS} =& F_0\left(1 + U_F + P_F + \mathcal{O}(p^6)\right)\,. \end{aligned} \tag{5.20}$$

They contain contributions related to the unitarity cut (U_m, U_F) in the s-channel, Fig.5.1d, and a polynomial term in s ($= m^2_\pi$) which includes logarithms (P_m, P_F). We have, for the mass

$$\begin{aligned} U_m =& -\frac{4c^2_{1d}}{F_0^2}\bar{J}(m^2_\pi, m^2_S; m^2_\pi)\left(m^2_S - 2m^2_\pi\right)^2\,, \\ P_m =& \frac{4m^4_\pi}{F_0^2}\left(\frac{\mu_S - \mu_\pi}{\Delta_{\pi S}}\right)\left(c^2_{1d}m^2_S - 4c_{2m}\Gamma_1\Delta_{\pi S}\right) + \frac{m^4_\pi}{16\pi^2F_0^2}\bar{\ell}_3\gamma_3 + \frac{m^2_\pi \mathring{m}^2_S}{8\pi^2F_0^2}\bar{Z}_1\Gamma_1\,. \end{aligned} \tag{5.21}$$

and for the decay constant

$$
\begin{aligned}
U_F =& \frac{2c_{1d}^2}{F_0^2 m_\pi^2}\bar{J}(m_\pi^2, m_S^2; m_\pi^2)\left(\frac{2m_\pi^2 - m_S^2}{4m_\pi^2 - m_S^2}\right)\left(14m_\pi^4 - 15m_\pi^2 m_S^2 + 3m_S^4\right) , \\
P_F =& \frac{c_{1d}^2}{8\pi^2 F_0^2}\frac{\left(m_S^2 - 2m_\pi^2\right)^2}{4m_\pi^2 - m_S^2} + \frac{4m_\pi^2}{F_0^2}\left(\frac{\mu_\pi - \mu_S}{\Delta_{\pi S}}\right)\left(\frac{c_{1d}^2\left(m_S^2 - 2m_\pi^2\right)^2}{\left(4m_\pi^2 - m_S^2\right)} + 4c_{2m}\Gamma_2\Delta_{\pi S}\right) \\
&+ \frac{m_\pi^2}{32\pi^2 F_0^2}\gamma_4\bar{\ell}_4 + \frac{\mathring{m}_S^2}{8\pi^2 F_0^2}\bar{Z}_2\Gamma_2 .
\end{aligned}
\tag{5.22}
$$

The functions $\bar{J}$ and μ_a ($a = \pi, S$) are displayed in the Appendix E. In addition we have used the scale independent quantities $\bar{\ell}_i$ and $\bar{Z}_j$, that are defined as follows:

$$
\ell_i^r = \frac{\gamma_i}{32\pi^2}\left[\bar{\ell}_i + \ln\left(\frac{m_\pi^2}{\Lambda^2}\right)\right] (i = 3, 4) , \quad Z_j^r = \frac{\Gamma_j}{32\pi^2}\left[\bar{Z}_j + \ln\left(\frac{m_S^2}{\Lambda^2}\right)\right] (j = 1, 2) , \tag{5.23}
$$

where $\bar{\ell}_i$ constants are in χPT_S the equivalent of the $\bar{l}_i$ in χPT, and Λ is the renormalization scale.

Both quantities in (5.20) have the following virtues that constitute non-trivial tests on their correctness:

1. Despite their appearance, they are finite in the Chiral limit, $\hat{m} \to 0$. More explicitly, in this limit the pion mass vanishes, as it should, while the decay constant reads,

$$
F_{\text{PS}} = F_0\left(1 + \frac{\mathring{m}_S^2}{8F_0^2\pi^2}\left[\bar{Z}_2\Gamma_2 + \frac{1}{2}c_{1d}^2\right]\right) . \tag{5.24}
$$

2. Setting $c_{ix} \to 0$ ($x = m, d$) in (5.20) they reduce to their standard χPT values

$$
m_{\text{PS}\,\chi\text{PT}}^2 = 2B_0\hat{m}\left(1 - \frac{1}{16\pi^2 F_0^2}B_0\hat{m}\bar{l}_3\right) , \quad F_{PS\,\chi\text{PT}} = F_0\left(1 + \frac{1}{8\pi^2 F_0^2}B_0\hat{m}\bar{l}_4\right) . \tag{5.25}
$$

To conclude this section we integrate out the singlet field. In the infrared limit, $m_\pi^2 \sim p^2 \ll \mathring{m}_S^2$, χPT_S has to reduce to χPT, where the only dynamical degrees of freedom are the pions [13]. In oder to do so we keep $\mathring{m}_S^2$ fixed and expand the above observables around $m_\pi \sim 0$. At NLO order in this expansion

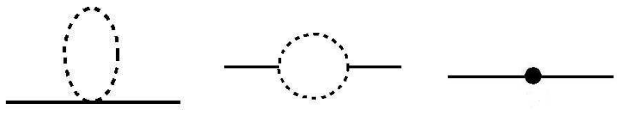

Figure 5.3: Diagrams contributing to the scalar field self–energy. Solid lines denote the scalar and the dotted ones pions.

we indeed recover (5.25) after the identification

$$\begin{aligned}\bar{l}_3 &= -2\bar{\ell}_3\gamma_3 - 32\Gamma_1 \log\left(\frac{m_\pi^2}{\mathring{m}_S^2}\right) c_{2m} - \frac{4}{3}c_{1d}^2\left(1+12c_{2m}\right)\\ \bar{l}_4 &= \frac{1}{2}\bar{\ell}_4\gamma_4 - 16\Gamma_2 \log\left(\frac{m_\pi^2}{\mathring{m}_S^2}\right) c_{2m} + c_{1d}^2\left[1-8c_{2m}+2\log\left(\frac{m_\pi^2}{\mathring{m}_S^2}\right)\right]\end{aligned} \tag{5.26}$$

5.4 Sigma mass and decay width

We can compute the scalar self–energy to one loop, and identify its pole as the mass of the sigma resonance at NLO. The diagrams contributing to the scalar self energy are shown in Fig.5.3. The sigma mass at NLO reads

$$\begin{aligned}m_{S,\,\mathrm{NLO}}^2 =& m_S^2 - \frac{3c_{1d}^2 m_S^4 \bar{f}_{2p}}{8\pi^2 F_0^2} - \frac{3m_\pi^4 \bar{d}_{1m}}{4\pi^2 F_0^2}\left(c_{2m}-c_{2d}+6c_{1d}^2\right) + \frac{9c_{1d}^2 m_S^2 m_\pi^2 \bar{d}_{2m}}{4\pi^2 F_0^2}\\ &- \frac{6c_{1d}^2}{F_0^2}\bar{J}(m_\pi^2, m_\pi^2; m_S^2)\left(m_S^2-2m_\pi^2\right)^2 ,\end{aligned} \tag{5.27}$$

where we have defined the scale independent quantities

$$f_{2p}^r = \frac{\Gamma_f}{32\pi^2}\left[\bar{f}_{2p} + \ln\left(\frac{m_\pi^2}{\Lambda^2}\right)\right], \quad d_{im}^r = \frac{\Delta_i}{32\pi^2}\left[\bar{d}_{im} + \ln\left(\frac{m_\pi^2}{\Lambda^2}\right)\right], \ (i=1,2), \tag{5.28}$$

where Λ is the renormalization scale.

In χPT$_S$ it is possible to compute the sigma decay width, a calculation that is not possible within standard χPT, unless it is supplemented by some unitarization technique. The LO expression for the sigma decay width reads:

$$\frac{\Gamma}{2} = \frac{3c_{1d}^2}{8\pi F_0^2 m_S}\sqrt{1-\frac{4m_\pi^2}{m_S^2}}\left(m_S^2-2m_\pi^2\right)^2 . \tag{5.29}$$

The behavior of the sigma pole as a function of the quark mass has been studied in [136, 137]. Our main difference with these articles is that we only have one polein s, in the positive complex half–plane, whereas in [136, 137] there is a pole in each of complex half–planes. This is due to the use of the power counting and perturbation theory in order to find the pole in our approach. In [136] the pole is shown to reach the real axis below π–π threshold, while from Eq.(5.29) our theory predicts that the pole reaches the real axis just on threshold. In Fig.2 from [136] value of the square of the sigma mass was shown to branch, such behavior is a consequence of the two poles in the sigma mass, and is not reproduced in our expressions because we always have a single pole.

5.5 Pion-pion scattering lengths

(a) (b)

Figure 5.4: Diagrams contributing to the scattering lengths. Solid lines denote the scalar and the dotted ones pions.

Let us next consider the $\pi - \pi$ scattering lengths. The expressions for these quantities will be different from those computed using χPT already at LO due to the presence of new diagrams with a scalar particle in the intermediate states. The diagrams contributing to the scattering amplitudes are depicted in Fig.5.4, and the explicit expressions for the scattering lengths at LO are given by

$$\begin{aligned} a_0^0 = &\quad \frac{m_\pi^2}{\pi F_0^2}\left(\frac{7}{32} - \frac{3}{2}\frac{m_\pi^2}{4m_\pi^2 - m_S^2}c_{1d}^2 + \frac{m_\pi^2}{m_S^2}c_{1d}^2\right), \\ a_0^2 = &\quad -\frac{m_\pi^2}{\pi F_0^2}\left(\frac{1}{16} - \frac{m_\pi^2}{m_S^2}c_{1d}^2\right). \end{aligned} \tag{5.30}$$

By using the physical quantities for $F_{\rm PS}\,, m_{\rm PS}$ and taking specific values for the mass and width of the sigma resonance from [121]

$$F_\pi = 92.419\,\text{MeV}\,, \quad \text{m}_{\pi,\text{ph}} = 139.57\,\text{MeV}\,, \quad \text{m}_{\text{S, CCL}} = 441.2\,\text{MeV}\,, \quad \Gamma_{\text{CCL}}/2 = 272\,, \tag{5.31}$$

we obtain from (5.29)

$$c_{1d}^2 = 0.457\,. \tag{5.32}$$

Now, inputing all this information into (5.30) we can compute the values of the scattering lengths. The results, displayed in Table 5.1, show that, for a_0^0, χPT_S overshoots the experimental value by roughly the same amount than LO χPT undershoots it, whereas for a_0^2 χPT_S is roughly a factor of three off the experimental value, namely much worse than LO χPT, which provides a number pretty close to it already at LO. The mismatch in a_0^2 may be understood as follows. In the decoupling limit ($\mathring{m}_S^2 \gg m_\pi^2, p^2$) this contribution gives

$$\text{Fig.5.4 b} = -\frac{1}{2}c_{1d}^2 F_0^2 \langle D_\mu U D^\mu U^\dagger\rangle \frac{1}{-\Box - m_S^2}\langle D_\mu U D^\mu U^\dagger\rangle \to c_{1d}^2 \frac{F_0^2}{2\mathring{m}_S^2}\langle D_\mu U D^\mu U^\dagger\rangle^2\,, \tag{5.33}$$

i.e. it reduces to a contact–term which is proportional to l_1 in χPT. By direct identification one finds the value of the χPT constant in terms of the χPT_S parameters

$$\bar{l}_1^{\text{LO}} = 192\pi^2 \frac{F_0^2 c_{1d}^2}{\mathring{m}_S^2}\,. \tag{5.34}$$

Note that the usual 4π suppression factors coming from loop integrals are absent in the tree level calculation above. It is easy to check that the last operator in (5.33) reproduces the scattering lengths (5.30) in the decoupling limit

$$a_0^0 = \frac{m_\pi^2}{\pi F_0^2}\left(\frac{7}{32} + \frac{5}{2}\frac{m_\pi^2}{\mathring{m}_S^2}c_{1d}^2\right), \quad a_0^2 = -\frac{m_\pi^2}{\pi F_0^2}\left(\frac{1}{16} - \frac{m_\pi^2}{\mathring{m}_S^2}c_{1d}^2\right). \tag{5.35}$$

Using (5.31) leads to $\bar{l}_1^{\text{LO}} \sim 38$, roughly 100 times bigger and with opposite sign than the standard NLO value for this quantity in χPT, $\bar{l}_1 \sim -1.8$, [138]. This indicates that a large negative value is expected for ℓ_1, and, consequently, that NLO contributions are going to be large, at least the ones related to the ℓ_1 operator.

5.6 Matching with lattice data: the pion mass and decay constant

The expressions for the pion mass and decay constant (5.20) depend on several low–energy constants not constrained by Chiral symmetry, $\ell_3^r, \ell_4^r, c_{1d}, c_{2y}$ ($y = d, m$) in addition to the quark masses and the bare parameters F_0, B_0, $\mathring{m}_S^2$. At this point, and for fitting purposes, the finite part of the counterterms $Z_{1,2}^r$ can

	a_0^0	a_0^2
Exp.(stat)(syst)	$0.2210(47)(40)$	$-0.0429(44)(28)$
Beyond NLO χPT	0.220 ± 0.005	-0.0444 ± 0.0010
χPT, LO	0.159	−0.0454
χPT, NLO	0.228	−0.0405
χPT$_S$, LO	0.275	−0.0121
χPT$_S$, LO+ℓ_1	0.210	−0.0296
Linear sigma model	0.696	−0.0404

Table 5.1: Values obtained for the scattering lengths from χPT, χPT$_S$ and the linear sigma model (bottom panel). LO expressions are fixed by the pion mass and decay constant for χPT, plus the sigma resonance mass for the linear sigma model, plus the sigma resonance width for χPT$_S$. NLO χPT values are obtained by fitting $\bar{l}_1 + 2\bar{l}_2$ and $\bar{l}_3$ to the lattice data of ref. [139]. LO+ℓ_1 χPT$_S$ is obtained by fitting ℓ_1 and c_{2m} to the same lattice data. In the central panel we show theoretical results that go beyond NLO χ PT from Ref.[138]. In the upper panel we show the values of the scattering lengths extracted from experimental data [140].

be absorbed into F_0, B_0. Then, we have eight independent parameters at our disposal at NLO.

Lattice QCD offers a new arena for determining the low–energy constants. Unlike physical experiments, lattice calculations use different unphysical quark masses, providing for each point what can be considered as an uncorrelated *experimental* datum with Gaussian errors. We will use the lattice data based on maximally $n_f = 2$ twisted fermions to fit the low–energy constants [125]. More precisely the data ensembles labeled as A1– A4, B1– B6, C1– C4, D1 and D2 in the Appendix C of that reference. Both finite volume effects and discretization errors are small in the data sets we use, and will be ignored in the following. We will also use in our analysis a single lattice scale $r_0 = 0.446\,\mathrm{fm}$ for all data sets as a simplification, which is justified because its value varies very little from one data set to another.

Given the limited quantity and quality of the available data, the number of free parameters is too large to expect a brute force best fit to provide sensible values for all of them. We have rather used a general three–fold strategy:

1. We identified $F_{\rm PS}$ (5.20) with its physical value at the physical pion mass (5.31). This allows to write F_0 as a function of the remaining parameters. This determination is done perturbatively.

We have used the same procedure to fix the bare scalar mass through (5.11): one imposes to the tree level scalar mass to take its physical value (5.20).

2. The c_{1d} parameter appears in our expressions always squared, hence we will use c_{1d}^2 as the free parameter. As we have seen its value can be extracted through the sigma decay width, (5.32).

3. For each point in the c_{2x} ($x = d, m$) parameter-space we fitted the lattice data minimizing an augmented chi-square distribution that includes both observables in (5.20) [112]. The augmented chi-square distribution is defined as the sum of the chi-square functions for each observable together with a set of priors for every one of the free parameters to be fitted

$$\chi^2_{aug} = \chi^2_{m^2_{PS}} + \chi^2_{F_{\rm PS}} + \chi^2_{prior}\,,$$
$$\chi^2_g = \frac{1}{n}\sum_i^n \frac{\left(g(\hat{m}_i) - g_i\right)^2}{\delta^2_{g_i}} \quad , \quad \chi^2_{prior} = \frac{1}{N}\sum_i^N \frac{\left(\log x_i - \log\|\bar{x}_i\|\right)^2}{\log^2 R_i}\,, \tag{5.36}$$

where g stands either for m_{PS} or F_{PS} and g_i for the corresponding lattice data at the quark mass $\hat{m}_i$. Furthermore, x_i refer to the fitted parameters N being their total number. At NLO $N = 3$ and $x_i = \{B_0/(2600\,\mathrm{MeV})\,, \ell^r_3\,, \ell^r_4\}$. The prior is a Gaussian weight distribution centered at $\|\bar{x}_i\|$ with and standard deviaton R_i. The prior information on the low–energy constants is obtained from naive dimensional analysis. For instance, if the parameter x_k is of order $\mathcal{O}(1)$, we expect it to be in the range $0.1 < \|x_k\| < 10$, which translates to setting $\log(\|\bar{x}_k\|) = 0$ and $\log(R_k) = 1$ for the kth parameter. We have taken logarithms in the prior functions to achieve equal weights for the subranges $0.1 < \|x_k\| < 1$ and $1 < \|x_k\| < 10$.

Within the previous outlined procedure we have fitted the expressions for the observables $m^2_{\rm PS}$ and $F_{\rm PS}$, (5.20), to the full range of available quark masses m_q, the $\overline{MS}$ running mass at the scale $\mu = 2$GeV. Throughout this section we have used $\Lambda = 770\,\mathrm{MeV}$ as the renormalization scale value. The chi-square per degree of freedom, $\chi^2_{d.o.f}$ is

$$\chi^2_{d.o.f} = \frac{n\chi^2_{m^2_{PS}} + n\chi^2_{F_{PS}}}{2n - 1 - N'}\,, \tag{5.37}$$

where N' is the number of free parameters, including the fitted and scanned ones. Thus for the NLO fit $N' = 5$.

5.6.1 χPT results

Before we move ahead with the $\chi\mathrm{PT}_S$ case, and for comparison purposes, we present the outputs we obtain for χPT. From the previous steps in the fitting procedure we only make use of the first to fix the physical point of F_{PS} and the third to introduce the priors to the corresponding parameters.

Born approximation

In this case the bare parameter F_0 is fixed by the physical decay constant $F_0 = 92.419\,\mathrm{MeV}$ and only B_0 is a free parameter, obtaining

$$B_0 = 2250.4\,\mathrm{MeV}\,, \tag{5.38}$$

with $\chi^2_{d.o.f} = \frac{1560}{30}$.

Next-to-leading results

For χPT the NLO expressions in (5.20) have three free parameters, B_0, l_3^r, and l_4^r while F_0 has been fixed perturbatively at the physical point. The fitting procedure leads to

$$B_0 = 2499(10)\,\mathrm{MeV}\,, \quad l_3^r = 0.91(6)\times 10^{-3}\,, \quad l_4^r = 7.13(5)\times 10^{-3}\,. \tag{5.39}$$

Using these values on the constraints imposed in the fist step of the fitting procedure we obtain F_0

$$F_0 = 86.36(1)\,\mathrm{MeV}\,, \tag{5.40}$$

with the final value $\chi^2_{d.o.f} = \frac{16.9}{28}$.

The results, together with the lattice data, are plotted in dashed lines in Fig.5.6. The adjustment for the pion mass to the lattice points is quite remarkable, with only a small deviation for large values of the quark masses. The pion decay constant fit also reaches a good agreement with the lattice data.

The results for the low–energy constants, (5.39), are compatible with standard values in the literature

$$\begin{array}{llll} [13] & \bar{l}_3 = 2.9 \pm 2.4\,, & [138] & \bar{l}_4 = 4.4 \pm 0.2\,. \\ \text{eq (5.39)} & \bar{l}_3 = 3.99 \pm 0.04\,, & & \bar{l}_4 = 4.54 \pm 0.01\,. \end{array} \tag{5.41}$$

These estimates are in reasonable agreement with those obtained by resonance

saturation [126]

$$\bar{l}_3 = 2.9 \pm 2.4\,, \quad \bar{l}_4 = 4.3 \pm 0.9\,. \tag{5.42}$$

The determination of the uncertainties in this section has been performed as follows. We assume each data point corresponds to Gaussian distribution with expected value and variance defined by the data point value and uncertainty respectively, then we generate random data sets according to these distributions and perform a fit for each one. The final parameters are obtained from the average of the results of these fits, while the uncertainty is obtained from the variance. Comparing our results with those from Table 5.1 in [125] we observe that F_0, $\bar{l}_4$ and B_0 values are within one sigma while $\bar{l}_3$ is within two sigmas. Note that our uncertainty analysis does not include systematic uncertainties because we have used only one set of data ensembles and we do not include finite size corrections. Statistical uncertainties in our fit are significantly smaller than those of [125]. This is because we have taken r_0 as a fix value rather than as an additional free parameter. If we estimate the uncertainty of r_0 as the one given in [125] and we extrapolate the effect to our results we obtain uncertainties in the same range as in [125]. Furthermore, since $m_{\rm PS}^2$ depends quadratically on r_0 while $F_{\rm PS}$ only linearly, our F_0 and $\bar{l}_4$ should be in better agreement with those of [125] than our B_0 and $\bar{l}_3$, as it is the case.

The estimation of uncertainties above is not directly applicable to the following section because for the fit to χ PT$_S$ expressions some of the parameters will be obtained by scanning a suitable range. In any case, we are not interested at this point in an accurate determination of the χPT$_S$ parameters but rather in finding out if parameter sets of this theory exists which are both compatible with lattice data and with physical observables.

5.6.2 χPT$_S$ results

The LO χPT$_S$ expressions are identical to those of standard χPT, therefore the same analysis as in the previous section applies. At NLO appear four extra free parameters to fit $c_{2d}\,, c_{2m}\,, \ell_3^r$ and ℓ_4^r and the non-analytical dependence on the light quark masses is greatly augmented (5.20).

The relative large number of free parameters appearing NLO means there is no unique solution for the best fit. Indeed, if we look at the contour level plot of the $\chi^2_{d.o.f}$ corresponding to the (c_{2d}, c_{2m}) region scanned, shown in Fig.5.5, we can see regions of parameter sets with $\chi^2_{d.o.f}$ smaller than one. Thus any parameter set on those regions has to be considered a valid solution. Keeping

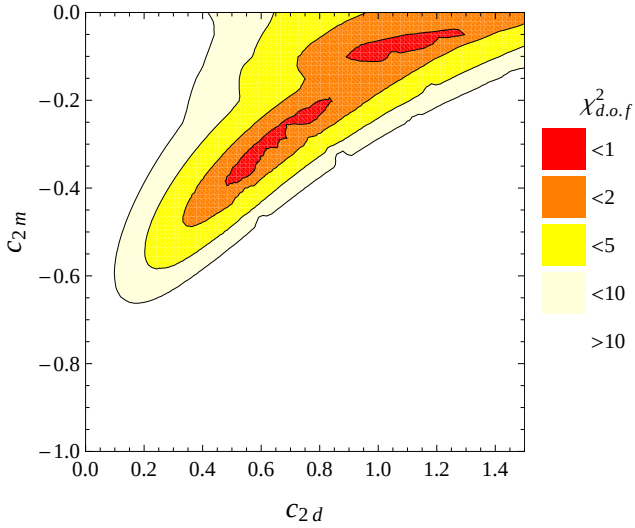

Figure 5.5: $\chi^2_{d.o.f}$ swept over a (c_{2d}, c_{2m}) grid corresponding to fits to NLO order expressions. The fits are forced to reproduce the pion decay constant, the mass of the sigma resonance and its width at the physical point.

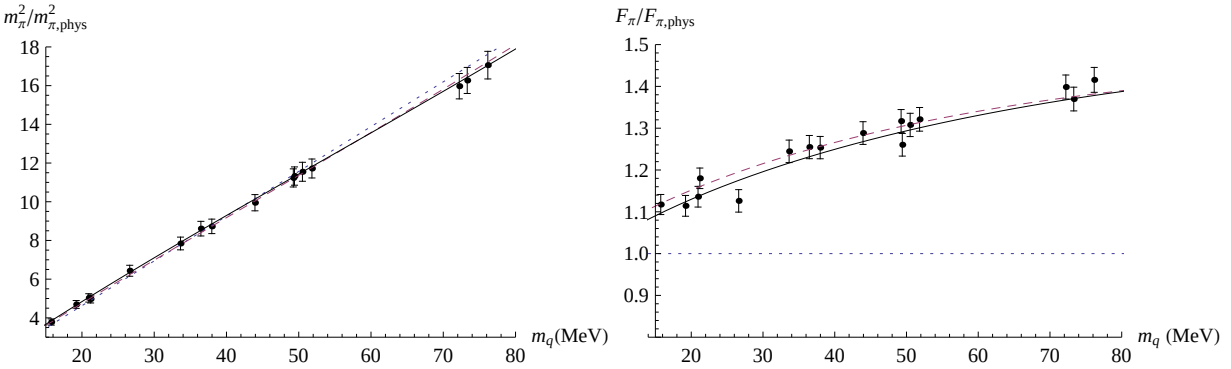

Figure 5.6: The best fits of the LO (dotted line), NLO χPT (dashed line) and χPT_S (solid line) expressions. Note that the LO expression is the same for χPT and χPT_S.

this in mind, the following are the results for the best fit obtained, which have been used for Fig.5.6,

$$\begin{aligned} &B_0 = 1680.5\,\text{MeV}\,, \quad c_{2d} = 1.21\,, \quad c_{2m} = -0.083\,, \\ &\ell_3^r = -1.12\times 10^{-3}\,, \quad \ell_4^r = 6.94\times 10^{-3}\,. \end{aligned} \tag{5.43}$$

Using these in (5.11) and (5.20) we obtain the values of the remaining parameters

$$F_0 = 101.2\,\text{MeV}\,, \quad \mathring{m}_S = 426\,\text{MeV}\,. \tag{5.44}$$

with

$$\chi^2_{d.o.f} = \frac{16.7}{26}\,. \tag{5.45}$$

Scalar resonance contribution to χPT low–energy constants

It is instructive to show how the low–energy constants ℓ_3^r and ℓ_4^r of χPT_S above compare with the standard low–energy constants of χPT. This is done through the matching formula (5.26). We obtain that the corresponding values of $\bar{l}_3$ and $\bar{l}_4$ read:

$$\bar{l}_3 = 3.40\,, \quad \bar{l}_4 = 5.16\,, \tag{5.46}$$

thus, $\bar{l}_3$ and $\bar{l}_4$ are somewhat higher than the values in (5.41). From (5.26) we can easily find out the fraction of $\bar{l}_3$ and $\bar{l}_4$ that is exclusively due to the light scalar field by setting ℓ_3^r and ℓ_4^r to zero. It amounts to a 43% for $\bar{l}_3$ (with opposite sign) and to a 20% for $\bar{l}_4$. This suggest that the impact of the singlet field in both $\bar{l}_3$ and $\bar{l}_4$ is quite substantial. Note that the contributions of the scalar field to these low–energy constants comes entirely through loops, and hence have nothing to do with the tree-level contributions obtained in [126].

Quark mass determination

The last application we have explored is the determination of the light quark masses, and the comparison with the results obtained from χPT and lattice QCD. Given a set of parameters the expressions for m^2_{PS} (5.20) and (5.25), become a function of $\hat{m}$. Setting m^2_{PS} to the value of the physical mass of the pion we can solve the equation to obtain the value of $\hat{m}$ at the physical point. The results obtained for $\hat{m}$ for the best χPT_S and χPT fits are displayed in Table 5.2. The

	$\hat{m}$ (MeV)
Latt.(stat)(syst)	3.469(47)(48)
Beyond NLO χPT	3.54(19)(17)
χPT, LO fit	4.32
χPT, NLO fit	4.39
χPT$_S$, NLO fit	3.26

Table 5.2: The values obtained light quark masses from our fits (bottom panel), at LO χPT and χPT$_S$ are identical. In the central panel we show theoretical results that go beyond NLO χPT from ref. [125]. In the upper panel we show the values from lattice QCD at the physical point [103].

expressions used for light quark masses match the order at which the fit has been performed, at NLO the equation has been solved perturbatively.

5.7 Matching with lattice data: S-wave scattering lengths

The available lattice results for the S-wave scattering lengths use relatively large pion masses, which makes Chiral extrapolations less reliable. In fact, until recently only calculations of a_0^2 were available [141, 142, 143, 144, 145, 146, 147], and the only existing calculation of both a_0^2 and a_0^0 neglects the disconnected contributions to the latter [139]. Nevertheless we shall use lattice data of the last reference in order to get a feeling on how χPT$_S$ performs with respect to the S-wave scattering lengths.

As we discussed in section 5.5, the S-wave scattering lengths of χPT$_S$ at LO are fixed once we input the mass and the width of the sigma resonance in addition to the pion mass and decay constant. Their evolution with the light quark masses is given by that of the pion mass and the low–energy constants c_{2m}. By making a combined fit to a_0^2 and a_0^0 we obtain the red lines in Fig.5.7. We observed that for a_0^0 χPT$_S$ provides a better description of data than LO χPT (black lines), but for a_0^2 a much worse one. As argued in section 5.5, large NLO corrections due to ℓ_1 are expected. We may estimated them by just adding its contribution to LO expression. If we fit ℓ_1, we obtain the dashed lines in Fig.5.7, and the following numbers.

$$a_0^0 = 0.210 \quad , \quad a_0^2 = -0.0296 \quad , \quad \bar{\ell}_1 \equiv 96\pi^2 \ell_1 = -16.9\,. \tag{5.47}$$

Note that we get a large negative number for $\bar{\ell}_1$, consistent with the expectations.

We see that the description of both scattering lengths improves considerably, the quality of a_0^0 being comparable to that of NLO χPT (black dashed lines). The plots of NLO χPT in Fig.5.7 are obtained by fitting $l_1^r + l_2^r$ and l_3^r. The values delivered by the fit are

$$\bar{l}_1 + 2\bar{l}_2 = 1.4 \quad , \quad \bar{l}_3 = -9.3\,, \tag{5.48}$$

which differ quite a lot from the standard values in χPT at one loop, for instance, $\bar{l}_1 + 2\bar{l}_2 \sim 9.0$ is given in [138] and $\bar{l}_3 \sim 2.9$ in [13]. In fact if $\bar{l}_3$ is fixed to the last value rather than fitted a very bad description of a_0^0 is obtained, whereas the one of a_0^2 remains quite good.

The results above encourage us to attempt an extraction of the sigma resonance parameters from the lattice data. We obtain from the fit (to both a_0^2 and a_0^0)

$$c_{2m} = -0.228 \quad , \quad \bar{\ell}_1 = -10.9 \quad , \quad c_{1d}^2 = 0.304 \quad , \quad \mathring{m}_S = 483\text{MeV}\,, \tag{5.49}$$

which produce the following numbers for the sigma decay width and the S-wave scattering lengths

$$m_S = 486\text{MeV} \quad , \quad \frac{\Gamma}{2} = 236\text{MeV} \quad , \quad a_0^0 = 0.177 \quad , \quad a_0^2 = -0.0361\,. \tag{5.50}$$

The numbers above are quite reasonable for a LO approximation augmented by ℓ_1, even more if one takes into account that the lattice data is at relatively large pion masses. It shows that our approach may eventually allow for a precise extraction of the sigma resonance parameters from lattice QCD. Note in particular that the value of c_{2m} is compatible with the region of low $\chi^2_{d.o.f.}$ of Fig.5.5 and that $\bar{\ell}_1$ remains with a large negative value.

5.8 Discussion and Conclusions

We have considered the possibility that the spectrum of QCD in the Chiral limit contains an isosinglet scalar with a mass much lower than the typical hadronic scale Λ_χ, and have constructed the corresponding effective theory that includes it together with the standard pseudo-Goldstone bosons, χPT_S. This effective theory has the same degrees of freedom as the linear sigma model, but differs from it in two important points. First of all, it is conceptually different because

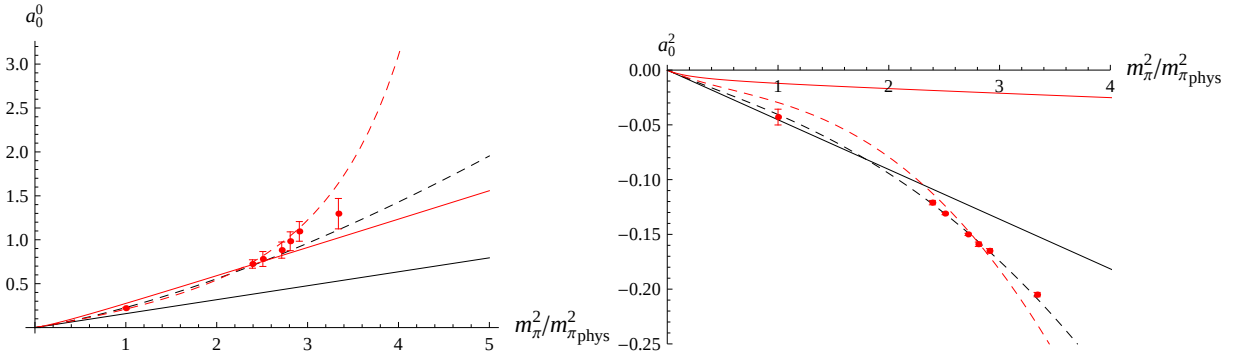

Figure 5.7: The best fits of the LO χPT (black solid line), NLO χPT (black dashed line), LO $\chi\mathrm{PT}_S$ (red solid line) and LO $\chi\mathrm{PT}_S$ augmented by the operator proportional to ℓ_1 (red dashed line). Red dots are lattice data from [139].

the mechanism of spontaneous symmetry breaking is assumed to occur at the scale Λ_χ, and hence it is not described within the effective theory. Second, there is a power counting and hence the LO Lagrangian can be augmented at the desired order by adding power suppressed operators. The LO Lagrangian has initially four free parameters more than the linear sigma model, and hence enjoys a larger flexibility to describe data. As explained in the section 5.2.3, one of these parameters (c_{1m}) must be set to zero for consistency, whereas in the linear sigma model it takes a non–zero value. If we force the LO fits of the pion mass and decay constant to go through the linear sigma model values we obtain a $\chi^2_{d.o.f} \sim 135$, namely worse than in LO $\chi\mathrm{PT}_S$ (which coincides with LO χPT). Inputing the sigma mass, the linear sigma model delivers a relatively low value for the decay width ($\Gamma/2 = 188$), a very large value for the isospin zero scattering length ($a_0^0 = 0.696$) but a pretty reasonable one for the isospin two one ($a_0^2 = -0.0404$), see Table 5.1. We have also computed the scalar mass at NLO.

At tree level $\chi\mathrm{PT}_S$ gives definite predictions for S-wave scattering lengths if the mass and decay width of the sigma resonance are used as an input, which are shown in Table 5.1. Neither the value of the isospin zero one (a_0^0) nor the one of the isospin two (a_0^2) are close to the experimental numbers. Although the value of a_0^0 is slightly closer to it than the one obtained in tree-level χPT, the value of a_0^2 is much further away. As argued in section 5.5, this is due to the fact that sizable NLO corrections due to a large value of ℓ_1 are expected. If we simulate them by letting ℓ_1 be a free parameter, the combined fits to the lattice data of

ref. [139] to a_0^0 and a_0^2 become rather good, see Fig.5.7. Note that, although NLO χPT produces a better description of a_0^0 and a_0^2 if $l_1^r + 2l_2^r$ and l_3^r are fitted to data, the values delivered by the fits of those LECS are incompatible with the ones currently used in χPT. We have also shown how the combined fits to the S-wave scattering lengths may be used to extract the resonance parameters of the sigma from Chiral extrapolations of lattice QCD data.

Loop corrections in χPT_S have been explored in the calculation of F_π and m_π at NLO. The dynamical scalar field introduces new non-analyticities in the quark mass dependence of these observables, and requires a renormalization of B_0 and F_0, which are absent in χPT. The fits to the lattice data of Ref.[125] for these observables at NLO in χPT_S are of similar quality as those at NLO in χPT. However, when the value of the average light quark masses is extracted from the fit, χPT_S produces numbers that are closer to those of direct lattice extractions than χPT does, see Table 5.2.

We have restricted ourselves to the flavor $SU(2)$ case, the extension to flavor $SU(3)$ is straightforward. In fact because flavor is conserved at any vertex, the contribution to observables with pions involving scalar fields in internal lines are identical and independent of the group, at the order we have calculated. Furthermore, because we will have more parameters at our disposal and $m_S \approx m_K \approx m_\eta$ we expect that the tension between the different contributions to higher Chiral orders [148] is alleviated.

Let us also mention that Lagrangians identical to the first line of (5.5) are currently being used in the context of composite Higgs models [149]. In that context, χPT_S would correspond to an effective theory at the electroweak scale under the assumption that the spontaneous symmetry breaking mechanism takes place at a much higher scale. Small explicit breaking of custodial symmetry at that scale may be taken into account by terms similar to those in the second line of (5.5).

In summary, we have shown how to consistently introduce a light isosinglet scalar particle in a Chiral effective field theory framework, χPT_S. This has consequences concerning the dependence of physical observables on the light quark masses, which have been shown to be compatible with current lattice data. We have also shown that our formalism has the potential to extract the mass and width of the sigma resonance from lattice QCD data. Finally, it would be interesting to explore the consequences of χPT_S in the Chiral approach to nuclear forces [22] (see [83] for a recent reviews), since the exchange of a scalar particle is known to be an important ingredient of the nuclear force in one-boson exchange models [150].

CHAPTER

6

CONCLUSIONS AND OUTLOOK

The first three chapters of this thesis have been devoted to the theoretical background. We presented the novel work of this thesis in chapters 4 and 5. In chapter 4 we have constructed a Chiral effective field theory for the nucleon–nucleon system which contains dibaryon fields as fundamental degrees of freedom. The large scattering lengths in the ${}^1S_0$ and the ${}^3S_1$ channels force the dibaryon residual masses to be much smaller than the pion mass. We organized the calculation in a series of effective theories, which are obtained by sequentially integrating out higher energy and momentum scales. We first integrate out energy scales of the order of the pion mass. This leads to an effective theory with dibaryon and nucleon fields, pNNEFT. For three momenta much smaller than the pion mass, it is convenient to further integrate out three momenta of the order of pion mass, which leads to the $\not\pi$NNEFT.

We have calculated the nucleon–nucleon scattering amplitudes for energies smaller than the pion mass in the ${}^1S_0$ and the ${}^3S_1$–${}^3D_1$ channels at N^{2}LO. For three momenta of the order of the pion mass, the scattering amplitudes are calculated in pNNEFT, for momenta of the order $\mathcal{O}\left(m_\pi^2/m_n\right)$ in $\not\pi$NNEFT. The numerical results for the phase shifts and mixing angle are also similar to the ones obtained in the KSW approach. A good description of the ${}^1S_0$ channel is obtained, but for the ${}^3S_1$–${}^3D_1$ channel our results also fail to describe data. The reasons of this failure can be traced back to the iteration of the one potential pion exchange potential. This may be interpreted as an indication that pion exchanges must be iterated at all orders, as originally proposed by Weinberg [22]. Weinberg's proposal however could not naturally accommodate the size of the scattering lengths and had renormalization problems.

We have calculated the matching of the dibaryon residual masses and dibaryon–nucleon couplings up to NLO. We have showed that, certain class of diagrams

that contribute to the residual mass, involving n potential pion exchanges in loops with radiation a pion, have to be summed in the ${}^3S_1$ channel. In the ${}^3S_1$ channel the diagrams can be calculated for any n and the resummation can be carried out. However in the ${}^1S_0$ channel the resummation is not possible, but it is very likely that loop contributions are still large. Using the results for the matching for residual masses and dibaryon–nucleon coupling for $\not\pi$NNEFT we have given Chiral extrapolation formulas for $1/a^{{}^1S_0}$ and $1/a^{{}^3S_1}$ up to corrections of order $\mathcal{O}\left(m_\pi^3/\Lambda_\chi^2\right)$ depending on three independent free parameters. We have fitted these expressions to lattice data and compared the results to previous studies of the quark mass dependence of the scattering lengths.

The nucleon–nucleon effective field theory with dibaryon fields presented in this thesis has simple counting rules and is renormalizable. Since no counterterm has to be enhanced like in the KSW approach [76], naive dimensional analysis is sufficient to assess the size of the effective field theory low–energy constants, keeping the perturbative expansion under control. The small dibaryon residual masses allow to naturally accommodate the extra scale introduced by the large scattering lengths in the S–wave channels. The bad convergence in the ${}^3S_1$ channel is due to the large contribution of the two potential pion exchanges diagram, which indicates that these contributions should be better resummed. Until it is known how to do such a resummation in a consistent way, the full description of the nuclear interactions from QCD through effective field theories is still open. We believe that once a strategy for such resummation is devised NNEFT with dibaryon fields provides natural formalism for the description of nuclear interactions.

In chapter 5 we have considered the possibility that the spectrum of QCD in the Chiral limit contains an isosinglet scalar with a mass much lower than the typical hadronic scale Λ_χ, and have constructed the corresponding effective theory that includes it together with the standard pseudo-Goldstone bosons, χPT_S. In the purely scalar sector of the theory we argued that the scalar self interactions can be ignored. Demanding that the scalar does not mix with the vacuum together with Chiral symmetry imposes that two of the low–energy constants should be taken as zero.

The linear sigma model has the same degrees of freedom as χPT_S. Nevertheless, we pointed out that there are two crucial differences. The spontaneous symmetry breaking mechanism in the linear sigma model is contained in it, this results in constraints on the couplings. On the other hand, in χPT_S the spontaneous symmetry breaking is supposed to happen at an unknown high energy

scale, which leaves the low–energy couplings free. As a consequence χPT$_S$ has more freedom to describe lattice data. The second important difference is that χPT$_S$ is an effective field theory, and as such, there is consistent way to improve the precision of the calculations.

We have presented the calculation of F_π and m_π at NLO. The dynamical scalar field introduces new non-analyticities in the quark mass dependence of these observables, and requires a renormalization of B_0 and F_0, which are absent in χPT. We have used lattice data from Ref.[125] to fit the low–energy constants. The $\chi^2_{d.o.f}$ delivered by the χPT$_S$ fits are similar to χPT ones indicating that lattice data does not favor any of the theories over the other. However, when the value of the average light quark masses is extracted from the fit, χPT$_S$ produces numbers that are closer to those of direct lattice extractions than χPT does, see Table 5.2.

The χPT$_S$ expressions for the S-wave pion–pion scattering lengths differ from those of χPT already at leading order. Furthermore χPT$_S$ allows for the calculation of the sigma decay width. Using the input of the sigma mass and decay width values from Ref.[121] we obtain the value of the only free parameter that appears on the pion–pion scattering lengths expressions, and with it we calculate the numerical values of the scattering lengths. Neither the value of the a_0^0 nor the one of a_0^2 are close to the experimental numbers. Although the value of a_0^0 is slightly closer to it than the one obtained in tree-level χPT, the value of a_0^2 is much further away. We argue, using the decoupling limit, that this is due to the sizable NLO corrections because of the large value of ℓ_1. We also show a different approach in which we fit the scattering length expressions with all parameters free to lattice data and use the results to provide predictions for the sigma mass and decay width.

Future work in χPT$_S$ should be aimed to the calculation of the pion–pion scattering lengths at NLO to determine whether χPT$_S$ improves on χPT on the description of a_0^0 while not spoiling a_0^2. It would be interesting to include χPT$_S$ in the study of the nuclear forces in the context of Chiral effective field theories, since the exchange of a scalar particle is known to be an important ingredient of the nuclear force in one-boson exchange models [150]. Finally, the χPT$_S$ Lagrangian is identical to the ones used in composite Higgs models [149] which opens a new field of applications of the formalism developed in this thesis.

APPENDIX

A

BRIEF INTRODUCTION TO LATTICE QCD

Lattice field theory provides a mathematically well–defined framework for a formulation of non–perturbative QCD [27]. The idea is to replace the four–dimensional Minkowski space–time continuum with a discrete lattice in a four–dimensional Euclidean space. In quantum field theory, information is obtained from correlation functions, which have a functional integral representation. Lattice field theory introduces an ultraviolet cutoff at the outset and gives a non–perturbative definition of the functional integral [28, 29, 30]. For any lattice spacing a, the maximum momentum which can arise on the lattice is $p_{max} \sim \pi/a$, which goes to infinity as $a \to \infty$. The fermion fields $\psi(x)$ and $\bar{\psi}(x)$ live on lattice sites x. Gauge fields live on links through the variables

$$U_\mu(x) = \mathcal{P} \exp \int_0^a ds A_\mu \left(x + se_\mu\right) , \tag{A.1}$$

where $\mathcal{P}$ denotes the path ordering, $A_\mu = A_\mu^a \lambda^a/2$, with A_μ^a the gluon fields and $\lambda^a/2$ the generators of the $SU(3)$ color gauge group, e_μ is the unit vector in the μ direction. In lattice QCD the correlation functions are expressed as

$$\langle \mathcal{O}_1, \ldots \mathcal{O}_n \rangle = \frac{1}{Z} \int \prod_{x,\mu} dU_\mu(x) \prod_x d\psi(x) d\bar{\psi}(x) \mathcal{O}_1, \ldots \mathcal{O}_n e^{-S_{QCD}} , \tag{A.2}$$

where

$$Z = \int \prod_{x,\mu} dU_\mu(x) \prod_x d\psi(x) d\bar{\psi}(x) e^{-S_{QCD}} , \tag{A.3}$$

and S_{QCD} is the lattice QCD action. With quarks on sites and gluons on links, it is possible to devise lattice actions that respect gauge symmetry. When the limit in which the lattice spacng is taken to zero

The fermionic nature of the quark fields means that they anticommute. This is accounted for by describing the quark fields using Grassmann variables. We call the continum limit when the lattice spacing is taken to zero. In the continum limit we have to specify how the bare couplings behave. The correct continum limit is obtained when the physical quantities are kept fixed.

$$S_q = \sum_{\alpha\beta} \bar{\psi}_\alpha M_{\alpha\beta} \psi_\beta \tag{A.4}$$

where α and β collectively label discrete space–time, spin and internal quantum numbers. The matrix $M_{\alpha\beta}$ is a discretized version of the Dirac operator $\not{D} + m$, where m is the quark mass matrix. $M_{\alpha\beta}$ depends on the gauge field $U(x)$. Since the quark action is a quadratic form, the integral can be carried out exactly

$$\int \prod_{\alpha\beta} d\bar{\psi}_\alpha \psi_\beta e^{-\bar{\psi} M \psi} = \det M \tag{A.5}$$

With the quarks integrated analytically, the gluons can be numerically integrated with a Monte Carlo method. The weighting factor in the path integrals in Euclidean space-time is now $e^{-S_g(U)} \det M$, where S_g is the pure lattice gauge action. On a computer with finite memory, one must introduce a finite space–time volume, providing an infrared cutoff. The Monte Carlo method of integration consists to generate an ensemble of random variables according to Boltzmann weighting and the integrals involved in Eq.A.2 are approximated by averages on the simulated ensemble. Apart from systematic effects due to non–zero lattice spacing and finite volume, lattice QCD simulations produce results that are exact on the given lattice, up to statistical errors.

APPENDIX

B

PAULI AND GELL–MANN MATRICES

B.1 Pauli Matrices

The generators of the $SU(2)$ group are $t_i = \sigma_i/2$, $(i = 1, 2, 3)$, where σ_i are the Pauli matrices. We will use σ to denote Pauli matrices with spin indices and τ to denote isospin indices. The σ are

$$\sigma_1 = \begin{pmatrix} 0 & 1 \\ 1 & 0 \end{pmatrix}, \sigma_2 = \begin{pmatrix} 0 & -i \\ i & 0 \end{pmatrix}, \sigma_3 = \begin{pmatrix} 1 & 0 \\ 0 & 1 \end{pmatrix}. \tag{B.1}$$

The main properties of σ_i are as follows

$$\begin{aligned} &\sigma_i^\dagger = \sigma_i\,,\ \mathrm{Tr}\,\sigma_i = 0\,,\ \mathrm{det}\sigma_i = -1 \\ &\sigma_i\sigma_k = \delta_{ik} + i\epsilon_{ijk}\sigma_j \end{aligned} \tag{B.2}$$

Using the last property of (B.2) one can derive the following useful relations

$$\begin{aligned} &\sigma_i^2 = \mathbf{1}\,,\ [\sigma_i, \sigma_k] = 2i\epsilon_{ikj}\sigma_j\,,\ \{\sigma_i, \sigma_k\} = 2\delta_{ik}\,, \\ &\sigma_i\sigma_k\sigma_l = i\epsilon_{ikl}\mathbf{1} + \delta_{ik}\sigma_l - \delta_{il}\sigma_k + \delta_{kl}\sigma_i\,, \\ &\mathrm{Tr}\,\sigma_i\sigma_k = 2\delta_{ik}\,,\ \mathrm{Tr}\,\sigma_i\sigma_k\sigma_l = 2i\epsilon_{ikl}\,, \\ &\mathrm{Tr}\,\sigma_i\sigma_k\sigma_l\sigma_m = 2\left(\delta_{ik}\delta_{lm} + \delta_{im}\delta_{kl} - \delta_{il}\delta_{km}\right) \end{aligned} \tag{B.3}$$

B.2 Gell–Mann Matrices

The generators of the $SU(3)$ group are $T_i = \lambda_i/2$, $(i = 1, \ldots, 8)$, where λ_i are the Gell–Mann matrices. The λ_i are defined as

$$\begin{aligned}
\lambda_1 &= \begin{pmatrix} 0 & 1 & 0 \\ 1 & 0 & 0 \\ 0 & 0 & 0 \end{pmatrix}, \lambda_2 = \begin{pmatrix} 0 & -i & 0 \\ i & 0 & 0 \\ 0 & 0 & 0 \end{pmatrix}, \lambda_3 = \begin{pmatrix} 1 & 0 & 0 \\ 0 & -1 & 0 \\ 0 & 0 & 0 \end{pmatrix}, \\
\lambda_4 &= \begin{pmatrix} 0 & 0 & 1 \\ 0 & 0 & 0 \\ 1 & 0 & 0 \end{pmatrix}, \lambda_5 = \begin{pmatrix} 0 & 0 & -i \\ 0 & 0 & 0 \\ i & 0 & 0 \end{pmatrix}, \lambda_6 = \begin{pmatrix} 0 & 0 & 0 \\ 0 & 0 & 1 \\ 0 & 1 & 0 \end{pmatrix}, \\
\lambda_7 &= \begin{pmatrix} 0 & 0 & 0 \\ 0 & 0 & -i \\ 0 & i & 0 \end{pmatrix}, \lambda_7 = \frac{1}{\sqrt{3}} \begin{pmatrix} 1 & 0 & 0 \\ 0 & 1 & 0 \\ 0 & 0 & -2 \end{pmatrix}.
\end{aligned} \tag{B.4}$$

The main properties are more conveniently given by in terms of the generators

$$\begin{aligned}
&T^a T^b = \frac{1}{6}\delta^{ab} + \frac{1}{2}\left(d^{abk} + i f^{abk}\right) T^k, \\
&T_i^\dagger = T_i, \det T_i = 0, (i = 1, \ldots, 7), \det T_8 = -\frac{1}{12\sqrt{3}}, \\
&\left[T^a, T^b\right] = i f^{abc} T^c, \left\{T^a, T^b\right\} = \frac{1}{3}\delta^{ab} + d^{abc} T^c,
\end{aligned} \tag{B.5}$$

where d^{abc} $\left(f^{abc}\right)$ is the totally symmetric (anti–symmetric) group structure constants. The non zero elements of f^{abc} and d^{abc} are

$$\begin{aligned}
&f_{123} = 1, f_{147} = -f_{156} = f_{246} = f_{257} = f_{345} = -f_{367} = \frac{1}{2}, f_{458} = f_{678} = \frac{\sqrt{3}}{2}, \\
&d_{146} = d_{157} = -d_{247} = d_{256} = d_{344} = d_{355} = -d_{366} = -d_{377} = \frac{1}{2}, \\
&d_{118} = d_{228} = d_{338} = -d_{888} = \frac{1}{\sqrt{3}}, d_{448} = d_{588} = d_{668} = d_{778} = -\frac{1}{2\sqrt{3}}.
\end{aligned} \tag{B.6}$$

The traces of any string of T^a matrices can be evaluated recursively using the first relation in (B.5)

$$\mathrm{Tr}\, T^a = 0, \mathrm{Tr}\, T^a T^b = \frac{1}{2}\delta^{ab}, \mathrm{Tr}\, T^a T^b T^c = \frac{1}{4}\left(d^{abc} + i f^{abc}\right). \tag{B.7}$$

The structure constants fulfill the following Jacobi identities

$$\begin{aligned} f_{abk}f_{kcl} + f_{bck}f_{kal} + f_{cak}f_{kbl} &= 0\,, \\ d_{abk}f_{kcl} + d_{bck}f_{kal} + d_{cak}f_{kbl} &= 0\,. \end{aligned} \tag{B.8}$$

APPENDIX

C

LOOP INTEGRALS FOR NNEFT

In this appendix we present the specific results for the loop integrals used in chapter 4. We used dimensional regularization and $\overline{MS}$ subtraction scheme.

NNEFT to pNNEFT matching integrals

The results of the contributions for the matching between NNEFT and pNNEFT in section 4.4 are presented in terms of $B(\beta_1, \beta_2)$, which is defined as

$$B(\beta_1, \beta_2) = (\mu^2)^{d-4} \int \frac{d^{d-1}q}{(4\pi)^{d-1}} \frac{\vec{q}^2}{(\vec{q}^2 + m_\pi^2)^{\beta_1}} \frac{1}{(\vec{q}^2 + m_\pi^2 - \alpha^4)^{\beta_2}} \,. \tag{C.1}$$

Using relation (4.32) one can always decompose the integral into terms with $\beta_1 > 0$ and $\beta_2 > 0$. The result for $B(\beta_1, \beta_2)$ with both arguments positive is

$$B(\beta_1, \beta_2) = (\mu^2)^{d-4} \frac{d-1}{2(4\pi)^{(d-1)/2}} \frac{\Gamma\left(\beta_1 + \beta_2 + \frac{d+1}{2}\right)}{\Gamma(\beta_1)\,\Gamma(\beta_2)} \mathcal{K} \,. \tag{C.2}$$

where μ is the renormalization scale, and $\mathcal{K}$ is the Feynman parameter integral

$$\int_0^1 dx\, (1-x)^{\beta_1 - 1}\, x^{\beta_2 - 1} \left(m_\pi^2 - x\alpha^4\right)^{\frac{d+1}{2} - \beta_1 - \beta_2} \,. \tag{C.3}$$

In the case $m_\pi > \alpha^2$, K is

$$\begin{aligned} \mathcal{K} = \left(m_\pi^2\right)^{\frac{d+1}{2} - \beta_1 - \beta_2} \pi \csc(\pi\beta_2) \frac{\Gamma(\beta_1)}{\Gamma(\beta_1 + \beta_2)\,\Gamma(1 - \beta_2)} \\ \times {}_2\tilde{F}_1\left[\beta_2, -\frac{d+1}{2} + \beta_1 + \beta_2, \beta_1 + \beta_2; \frac{\alpha^4}{m_\pi^2}\right], \end{aligned} \tag{C.4}$$

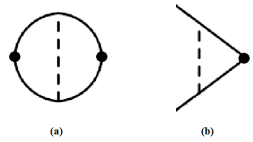

Figure C.1: Integrals with one potential pion. The black dots indicate the insertion of a vertex, but non of the vertex factors are included in the results of the integrals.

and for $m_\pi < \alpha^2$

$$\begin{aligned}\mathcal{K} =& e^{i\pi\left(\frac{d+1}{2}-\beta_1-\beta_2\right)}\alpha^{4\left(\frac{d+1}{2}-\beta_1-\beta_2\right)}\frac{\Gamma\left(\frac{d+1}{2}-\beta_1\right)\Gamma\left(\beta_1\right)}{\Gamma\left(\frac{d+1}{2}\right)}\,{}_2F_1\left[\frac{d+1}{2},\beta_1+\beta_2-\frac{d+1}{2},\beta_1-\frac{d-1}{2};\frac{m_\pi^2}{\alpha^4}\right]\\ &+\pi m_\pi^{d+1-2\beta_1}\alpha^{-4(2\beta_1+\beta_2)}\left[e^{i\pi\left(\frac{d+1}{2}-\beta_1-\beta_2\right)}\sec\left(\pi\left(\frac{d}{2}-\beta_1\right)\right)-e^{2i\pi\left(\frac{d+1}{2}-\beta_1-\beta_2\right)}\csc\left(\pi\beta_2\right)\right]\\ &\times\frac{\Gamma\left(\frac{d+3}{2}-\beta_1-\beta_2\right)}{\Gamma\left(\frac{d+3}{2}-\beta_1\right)\Gamma\left(1-\beta_2\right)}\,{}_2F_1\left[1-\beta_1,\beta_2,\frac{d+3}{2}-\beta_1;\frac{m_\pi^2}{\alpha^4}\right],\end{aligned} \tag{C.5}$$

Integrals with one potential pion

In Fig.C.1 are the integrals involving only one potential pion exchange. The following expressions are valid for ${}^1S_0$ and ${}^3S_1$ channels.

$$\begin{aligned}I_a^{1\pi} =& -i\frac{g_A^2}{4F_0^2}\frac{m_N p}{4\pi}\left[1-\frac{m_\pi^2}{2p^2}ln\left(1-\frac{2ip}{m_\pi}\right)\right],\\ I_b^{1\pi} =& i\frac{g_A^2}{4F_0^2}\left(\frac{m_N p}{4\pi}\right)^2\left[-1-\frac{m_\pi^2}{2p^2}\ln\left(\frac{\mu^2}{m_\pi^2}\right)+\ln\left(1-\frac{2ip}{m_\pi}\right)\right],\end{aligned} \tag{C.6}$$

where p is the magnitude of the external three–momenta, and μ is the renormalization scale. For the ${}^3S_1$–${}^3D_1$ mixing only Fig.C.1.b has a non vanishing projection, the integral can be extracted from (4.48).

Integrals with two potetial pions

In Fig.C.2 are the integrals involving only two potential pion exchange. In this case the projections to the channels ${}^1S_0$, ${}^3S_1$ are different. For the ${}^1S_0$ channel the results are as follows

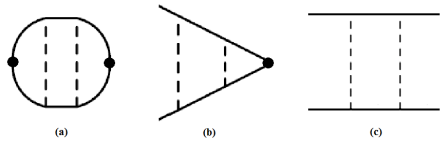

Figure C.2: Integrals with two potential pion. The black dots indicate the insertion of a vertex, but non of the vertex factors are included in the results of the integrals.

$$
\begin{aligned}
I^{2\pi}_{a,s} &= -\left(\frac{g_A^2}{4F_0^2}\right)^2 \left(\frac{m_N p}{4\pi}\right)^3 \left[1 + \frac{m_\pi^2}{p^2}\left(\ln\left(\frac{\mu^2}{m_\pi^2}\right) - 3 + 2\ln 2 - 2\ln\left(1 - \frac{2ip}{m_\pi}\right)\right)\right. \\
&\quad \left. -\frac{m_\pi^4}{p^4}\left(\mathrm{Li}_2\left(\frac{m_\pi}{-m_\pi + 2ip}\right) + \frac{\pi^2}{12}\right)\right] \\
I^{2\pi}_{b,s} &= -\left(\frac{g_A^2}{4F_0^2}\right)^2 \left(\frac{m_N p}{4\pi}\right)^2 \left[\frac{p^2}{m_\pi^2} + \frac{m_\pi^2}{2p^2}\left(\ln\left(\frac{\mu^2}{m_\pi^2}\right) - 3 + 2\ln 2\right) - \frac{3m_\pi^2}{2p^2}\ln\left(1 - \frac{2ip}{m_\pi}\right)\right. \\
&\quad \left. \frac{m_\pi^4}{4p^4}\left(\frac{3}{2}\ln^2\left(1 - \frac{2ip}{m_\pi}\right) + 2\mathrm{Li}_2\left(\frac{-m_\pi + 2ip}{m_\pi}\right) + \mathrm{Li}_2\left(\frac{m_\pi + 2ip}{-m_\pi + 2ip}\right) + \frac{\pi^2}{4}\right)\right] \\
I^{2\pi}_{c,s} &= -\left(\frac{g_A^2}{4F_0^2}\right)^2 \frac{m_N p}{4\pi}\left[-1 + \frac{m_\pi^2}{p^2}\ln\left(1 - \frac{2ip}{m_\pi}\right) + \frac{m_\pi^4}{p^4}\left(-\frac{1}{4}\ln\left(1 + \frac{4p^2}{m_\pi^2}\right)\right.\right. \\
&\quad \left.\left. i\mathrm{Im}\left[\mathrm{Li}_2\left(\frac{2p^2 - ipm_\pi}{m_\pi^2 + 4p^2}\right) + \mathrm{Li}_2\left(\frac{-2p^2 + ipm_\pi}{m_\pi^2}\right)\right]\right)\right]
\end{aligned}
\tag{C.7}
$$

In the $^3S_1$ channel

$$
\begin{aligned}
I^{2\pi}_{a,v} =& 3\left(\frac{g_A^2}{4F_0^2}\right)^2\left(\frac{m_N p}{4\pi}\right)^3\left[-\frac{7im_\pi^3}{3p^3}+\frac{5m_\pi^2}{3p^2}-\frac{4im_\pi}{p}+\frac{1}{2}-\frac{9m_\pi^4}{8p^4}+\frac{im_\pi^5}{p^5}\right.\\
&+\frac{3m_\pi^6}{8p^6}+\left(\frac{3im_\pi^7}{4p^7}-\frac{3m_\pi^6}{4p^6}+\frac{im_\pi^5}{p^5}-\frac{m_\pi^4}{2p^4}\right)\ln 2-2\left(1+\frac{m_\pi^2}{p^2}\right)\ln\left(\frac{\mu^2}{m_\pi^2}\right)\\
&-\left(\frac{3im_\pi^7}{4p^7}-\frac{3m_\pi^6}{4p^6}+\frac{im_\pi^5}{p^5}-\frac{m_\pi^4}{2p^4}\right)\ln\left(1-\frac{2ip}{m_\pi}\right)+\left(\frac{m_\pi^4}{p^4}+\frac{m_\pi^6}{p^6}+\frac{3m_\pi^8}{8p^8}\right)\\
&\left.\times\left[\mathrm{Li}_2\left(\frac{m_\pi}{-m_\pi+2ip}\right)+\frac{\pi^2}{12}\right]+\left(\frac{3im_\pi^7}{4p^7}-\frac{3m_\pi^6}{4p^6}+\frac{im_\pi^5}{p^5}-\frac{m_\pi^4}{2p^4}+4\frac{m_\pi^2}{p^2}+4\right)\ln\left(1-\frac{ip}{m_\pi}\right)\right],\\
I^{2\pi}_{b,v} =& \frac{3}{2}\left(\frac{g_A^2}{4F_0^2}\right)^2\left(\frac{m_N p}{4\pi}\right)^2\left[\frac{13m_\pi^2}{6p^2}-\frac{4im_\pi}{p}-\frac{3m_\pi^4}{2p^4}-\frac{3im_\pi^3}{2p^3}+\frac{3im_\pi^5}{4p^5}-\left(\frac{3m_\pi^6}{4p^6}+\frac{m_\pi^4}{2p^4}\right)\ln 2\right.\\
&+\left(\frac{3im_\pi^7}{4p^7}-\frac{3m_\pi^6}{4p^6}+\frac{im_\pi^5}{p^5}-\frac{m_\pi^4}{2p^4}+\frac{4m_\pi^2}{p^2}+4\right)\ln\left(1-\frac{ip}{m_\pi}\right)-2\left(1+\frac{m_\pi^2}{p^2}\right)\ln\left(\frac{\mu^2}{m_\pi^2}\right)\\
&-\left(\frac{3m_\pi^8}{16p^8}+\frac{m_\pi^6}{2p^6}+\frac{m_\pi^4}{2p^4}\right)\left[\frac{3}{2}\ln^2\left(1-\frac{2ip}{m_\pi}\right)+2\mathrm{Li}_2\left(-1+\frac{2ip}{m_\pi}\right)+\mathrm{Li}_2\left(\frac{m_\pi+2ip}{-m_\pi+2ip}\right)+\frac{\pi^2}{4}\right]\\
&\left.+\left(-\frac{3im_\pi^7}{8p^7}+\frac{9m_\pi^6}{8p^6}-\frac{im_\pi^5}{2p^5}+\frac{3m_\pi^4}{4p^2}\right)\ln\left(1-\frac{2ip}{m_\pi}\right)\right],\\
I^{2\pi}_{c,v} =& \left(\frac{g_A^2}{4F_0^2}\right)^2\left(\frac{m_N p}{4\pi}\right)\left[-\frac{2m_\pi}{p}-\frac{m_\pi^3}{2p^3}+\frac{3im_\pi^4}{8p^4}-\frac{im_\pi^2}{2p^2}+\frac{i}{2}-i\left(\frac{3m_\pi^6}{16p^6}+\frac{m_\pi^4}{8p^4}\right)\ln\left(1+\frac{4p^2}{m_\pi^2}\right)\right.\\
&+\left(\frac{3m_\pi^6}{8p^6}+\frac{m_\pi^4}{4p^4}-\frac{2m_\pi^2}{p^2}-2\right)\arctan\left(\frac{p}{m_\pi}\right)-\left(\frac{3m_\pi^6}{8p^6}+\frac{m_\pi^4}{4p^4}\right)\arctan\left(\frac{2p}{m_\pi}\right)\\
&+\left(\frac{3m_\pi^7}{16p^7}+\frac{m_\pi^5}{4p^5}\right)\ln\left(1+\frac{p^2}{m_\pi^2}\right)+i\left(\frac{3m_\pi^8}{128p^8}+\frac{m_\pi^6}{16p^6}\frac{m_\pi^4}{16p^4}\right)\ln^2\left(1+\frac{4p^2}{m_\pi^2}\right)\\
&\left.\left.-\left(\frac{3m_\pi^8}{32p^8}+\frac{m_\pi^6}{4p^6}+\frac{m_\pi^4}{4p^4}\right)\mathrm{Im}\left[\mathrm{Li}_2\left(\frac{2p^2+ipm_\pi}{m_\pi^2}\right)+\mathrm{Li}_2\left(\frac{-2p^2-ipm_\pi}{m_\pi^2}\right)\right]\right].
\end{aligned}
\tag{C.8}
$$

For the ${}^3S_1$–${}^3D_1$ mixing only Fig.C.2.c has a non vanishing projection, the integral can be extracted from (4.49).

APPENDIX

D

THE COMPLETE NLO LAGRANGIAN IN THE $N_B = 2$ SECTOR

We list here all the operators of the NLO Lagrangian in the $N_B = 2$, many of which do not contribute to our calculations. We use for organization purposes the standard chiral counting, namely $\partial_0 \sim \partial_i = \mathcal{O}(p)$ and the quark mass matrix $\mathcal{M} = \mathcal{O}(p^2)$

The dibaryon Lagrangian

The full list of operators in $\mathcal{L}_D^{(2)}$ of (4.12) follows

$$
\begin{aligned}
&Tr[D_s(u\mathcal{M}^\dagger u + u^\dagger \mathcal{M} u^\dagger)D_s^\dagger] \quad , \quad Tr[D_s^\dagger(u\mathcal{M}^\dagger u + u^\dagger \mathcal{M} u^\dagger)D_s] \quad , \\
&Tr[D_s^\dagger D_s u_0 u_0] \, , \, Tr[D_s^\dagger D_s u_i u_i] \, , \, Tr[D_s D_s^\dagger u_i u_i] \, , \, Tr[D_s^\dagger u_0 D_s u_0] \, , \, Tr[D_s^\dagger u_i D_s u_i] \\
&\vec{D}_v^\dagger \cdot \vec{D}_v Tr[u^\dagger \mathcal{M} u^\dagger + u\mathcal{M}^\dagger u] \quad , \quad \vec{D}_v^\dagger \cdot \vec{D}_v Tr[u_0 u_0] \quad , \quad \vec{D}_v^\dagger \cdot \vec{D}_v Tr[u_i u_i] \\
&(D_v^{i\dagger} D_v^j + D_v^i D_v^{j\dagger}) Tr[u_i u_j] \quad , \quad Tr[D_s^\dagger \vec{u} \times \vec{u}] \vec{D}_v + \text{h.c.} \\
&\vec{\partial} \vec{D}_v^\dagger Tr[u_0 D_s] + \text{h.c.} \quad , \quad \vec{D}_v^\dagger Tr[u_0 \vec{d} D_s] + \text{h.c.} \\
&Tr[\vec{d} D_s^\dagger \vec{d} D_s] \quad , \quad \left(\vec{\partial} \vec{D}_v^\dagger\right)\left(\vec{\partial} \vec{D}_v\right) \quad , \quad \vec{D}_v^\dagger \vec{\partial}^2 \vec{D}_v
\end{aligned}
\tag{D.1}
$$

In Ref. [31] terms mixing the scalar and vector dibaryon as well as terms with space derivatives on the dibaryon field were not displayed[1].

[1] The two additional terms that were displayed in [31] turn out to be redundant.

The dibaryon-nucleon vertex

The full list of operators in $\mathcal{L}^{(2)}_{DN}$ of (4.15) follows (hermitian conjugates are omited)

$$
\begin{aligned}
&(N^\dagger\sigma^2\tau^a\tau^2\vec{D}^2N^*)D_{s,a} \quad , \quad (N^\dagger\tau^2\vec{\sigma}\sigma^2\vec{D}^2N^*)\cdot\vec{D}_v \quad , \quad (D_iN^\dagger\tau^2\sigma^i\sigma^2D_jN^*)D_v^j \\
&(N^\dagger\sigma^2D_s\tau^2N^*)\left(Tr(u_0u_0) \quad , \quad Tr(u_iu_i) \quad , \quad Tr(u\mathcal{M}^\dagger u + u^\dagger\mathcal{M}u^\dagger)\right) \\
&N^\dagger\left(u_0D_su_0\ ,\ u_iD_su_i\ ,\ D_su\mathcal{M}^\dagger u\ ,\ D_su^\dagger\mathcal{M}u^\dagger\ ,\ u^\dagger\mathcal{M}u^\dagger D_s\ ,\ u\mathcal{M}^\dagger uD_s\right)\tau^2\sigma^2N^* \\
&N^\dagger\sigma^i\left(\delta^{ij}u\mathcal{M}^\dagger u\ ,\ \delta^{ij}u^\dagger\mathcal{M}u^\dagger\ ,\ \epsilon^{ijk}u_k\ ,\ u_iu_j\ ,\ \epsilon^{ijk}D^ku_0\ ,\ \epsilon^{ijk}u_0D_k\right)\tau^2\sigma^2N^*D_v^j \\
&N^\dagger\tau^2\sigma^i\sigma^2N^*\left(\delta^{ij}Tr(u_0u_0)\ ,\ \delta^{ij}Tr(u_ku_k)\ ,\ \delta^{ij}Tr(u\mathcal{M}^\dagger u + u^\dagger\mathcal{M}u^\dagger)\ ,\ Tr(u_iu_j)\right)D_v^j \\
&N^\dagger\sigma^i\left(u^iD_s \quad , \quad D_su^i \quad , \quad \epsilon^{ijk}u_ju_kD_s \quad , \quad \epsilon^{ijk}u_jD_su_k \quad , \quad \epsilon^{ijk}D_su_ju_k\right)\tau^2\sigma^2N^* \\
&N^\dagger\left(u^i \quad , \quad \epsilon^{ijk}u_ju_k \quad , \quad u_0D^i \quad , \quad D^iu_0\right)\tau^2\sigma^2N^*D_v^i
\end{aligned}
\tag{D.2}
$$

APPENDIX

E

LOOP INTEGRALS FOR χPT$_S$

Through the calculations in chapter 5 we have used the following set of integrals

$$A[m_a^2] = \frac{\Lambda^{4-d}}{i}\int \frac{d^dk}{(2\pi)^d}\frac{1}{k^2-m_a^2} = m_a^2\left(-2\lambda+\mu_a\right). \tag{E.1}$$

$$B[m_a^2,m_b^2;p^2] = \frac{\Lambda^{4-d}}{i}\int \frac{d^dk}{(2\pi)^d}\frac{1}{k^2-m_a^2}\frac{1}{(k-p)^2-m_b^2} = -2\lambda+\frac{m_a^2\mu_a-m_b^2\mu_b}{\Delta_{ab}}+\bar{J}[m_a^2,m_b^2;p^2]. \tag{E.2}$$

Which finite parts are given in terms of

$$\mu_a = -\frac{1}{16\pi^2}\log\left(\frac{m_a^2}{\Lambda^2}\right), \tag{E.3}$$

$$\bar{J}(m_a^2,m_b^2;p^2) = \frac{1}{32\pi^2}\left[2+\left(-\frac{\Delta}{p^2}+\frac{\Sigma}{\Delta}\right)\log\left(\frac{m_a^2}{m_b^2}\right)-\frac{\nu}{p^2}\log\left(\frac{\left(p^2+\nu\right)^2-\Delta^2}{\left(p^2-\nu\right)^2-\Delta^2}\right)\right], \tag{E.4}$$

with $\Delta = \Delta_{ab} = m_a^2-m_b^2$, $\Sigma = m_a^2+m_b^2$, and $\nu^2 = \left(p^2-(m_a-m_b)^2\right)\left(p^2-(m_a+m_b)^2\right)$.
As a last comment, we have used $\overline{\text{MS}}$ subtraction scheme

$$\lambda = \frac{1}{16\pi^2}\left(\frac{1}{d-4}-\frac{1}{2}\left[-\gamma_E+\ln(4\pi)+1\right]\right). \tag{E.5}$$

BIBLIOGRAPHY

[1] A. V. Manohar, In *Schladming 1996, Perturbative and nonperturbative aspects of quantum field theory* 311-362 [hep-ph/9606222]. v

[2] S. Scherer and M. R. Schindler, hep-ph/0505265. v

[3] S. Scherer, Adv. Nucl. Phys. **27** (2003) 277 [hep-ph/0210398]. v

[4] R. Machleidt and D. R. Entem, Phys. Rept. **503** (2011) 1 [arXiv:1105.2919 [nucl-th]]. v

[5] E. Epelbaum, arXiv:1001.3229 [nucl-th]. v

[6] D. J. Gross and F. Wilczek, Phys. Rev. Lett. **30** (1973) 1343. xv, xxi, 1, 3

[7] S. Weinberg, Phys. Rev. Lett. **31** (1973) 494. xv, xxi, 1

[8] H. Fritzsch, M. Gell-Mann and H. Leutwyler, Phys. Lett. B **47**, 365 (1973). xv, xxi, 1, 4

[9] D. J. Gross and F. Wilczek, Phys. Rev. D **8** (1973) 3633. xv, xxi, 3

[10] H. D. Politzer, Phys. Rev. Lett. **30**, 1346 (1973). xv, xxi, 3

[11] M. Gell-Mann, Phys. Lett. **8** (1964) 214. xv, xxi, 3

[12] S. Weinberg, Physica A **96** (1979) 327. xv, xxi, 13, 20, 22

[13] J. Gasser and H. Leutwyler, Annals Phys. **158**, 142 (1984). xvi, xxii, 21, 25, 86, 89, 95, 100

[14] J. Gasser and H. Leutwyler, Nucl. Phys. B **250**, 465 (1985). xvi, xxii, 21, 25

[15] J. Gasser and H. Leutwyler, Phys. Rept. **87** (1982) 77. xvi, xxii

[16] C. G. . Callan, S. R. Coleman, J. Wess and B. Zumino, Phys. Rev. **177**, 2247 (1969). xvi, xxii, 14, 15, 27, 28, 83

[17] S. R. Coleman, J. Wess and B. Zumino, Phys. Rev. **177**, 2239 (1969). xvi, xxii, 14, 15, 27, 28, 83

[18] S. Weinberg, Phys. Rev. **166**, 1568 (1968). xvi, xxii, 14, 27

[19] E. E. Jenkins and A. V. Manohar, Phys. Lett. B **255** (1991) 558. xvi, xxii, 30

[20] E. E. Jenkins and A. V. Manohar, Phys. Lett. B **259**, 353 (1991). xvi, xxii, 30

[21] T. Becher and H. Leutwyler, Eur. Phys. J. C **9**, 643 (1999) [arXiv:hep-ph/9901384]. xvi, xxii, 30

[22] S. Weinberg, Phys. Lett. B **251**, 288 (1990). xvi, xviii, xxii, 34, 35, 38, 76, 102, 103

[23] S. Weinberg, Nucl. Phys. B **363**, 3 (1991). xvi, xxii, 34, 35, 38

[24] S. Weinberg, Phys. Rev. **130** (1963) 776. xvii, xxiii

[25] S. Weinberg, Phys. Rev. **131** (1963) 440. xvii, xxiii

[26] S. Weinberg, Phys. Rev. **137**, B672 (1965). xvii, xxiii

[27] K. G. Wilson, Phys. Rev. D **10**, 2445 (1974). xvii, xxiii, 107

[28] H. J. Rothe, World Sci. Lect. Notes Phys. **43**, 1 (1992). 107

[29] I. Montvay and G. Munster, *Cambridge, UK: Univ. Pr. (1994) 491 p. (Cambridge monographs on mathematical physics)* 107

[30] J. Smit, Cambridge Lect. Notes Phys. **15**, 1 (2002). 107

[31] J. Soto and J. Tarrus, Phys. Rev. C **78** (2008) 024003 [arXiv:0712.3404 [nucl-th]]. xxiv, 44, 117

[32] J. Soto and J. Tarrus, Phys. Rev. C **81** (2010) 014005 [arXiv:0906.1194 [nucl-th]]. xxiv, 44, 49, 54, 75

[33] J. Tarrus, PoS E **FT09** (2009) 026 arXiv:0910.0502 [nucl-th]. xxiv, 44, 76

[34] J. Soto and J. Tarrus, Phys. Rev. C **85** (2012) 044001 arXiv:1112.4426 [nucl-th]. xxiv, 44

[35] J. Tarrus, AIP Conf. Proc. **1343** (2011) 268. xxiv, 80

[36] J. Soto, P. Talavera and J. Tarrus, arXiv:1110.6156 [hep-ph]. xxiv, 80

[37] C. N. Yang and R. L. Mills, Phys. Rev. **96** (1954) 191. 1

[38] K. Nakamura *et al.* [Particle Data Group], J. Phys. G **37** (2010) 075021. 2

[39] W. A. Bardeen, A. J. Buras, D. W. Duke and T. Muta, Phys. Rev. D **18**, 3998 (1978). 3

[40] G. 't Hooft and M. J. G. Veltman, Nucl. Phys. B **44**, 189 (1972). 3

[41] S. L. Adler, Phys. Rev. **177** (1969) 2426. 5

[42] S. L. Adler and W. A. Bardeen, Phys. Rev. **182** (1969) 1517. 5

[43] W. A. Bardeen, Phys. Rev. **184**, 1848 (1969). 5

[44] J. Goldstone, Nuovo Cim. **19**, 154 (1961). 7

[45] Y. Nambu, Phys. Rev. **117**, 648 (1960). 7

[46] Y. Nambu and G. Jona-Lasinio, Phys. Rev. **122**, 345 (1961). 7

[47] J. Goldstone, A. Salam and S. Weinberg, Phys. Rev. **127**, 965 (1962). 7

[48] R. F. Dashen, Phys. Rev. D **3**, 1879 (1971). 11

[49] S. Weinberg, Phys. Rev. Lett. **29**, 1698 (1972). 12

[50] A. Manohar and H. Georgi, Nucl. Phys. B **234**, 189 (1984). 20

[51] H. Leutwyler, Annals Phys. **235**, 165 (1994) [arXiv:hep-ph/9311274]. 22

[52] M. Knecht and R. Urech, Nucl. Phys. B **519**, 329 (1998) [arXiv:hep-ph/9709348]. 25, 86

[53] A. Krause, Helv. Phys. Acta **63** (1990) 3. 29

[54] J. Gasser, M. E. Sainio and A. Svarc, Nucl. Phys. B **307**, 779 (1988). 29

[55] J. Gegelia, G. Japaridze and X. Q. Wang, J. Phys. G G **29** (2003) 2303 [hep-ph/9910260]. 30

[56] T. Fuchs, J. Gegelia, G. Japaridze and S. Scherer, Phys. Rev. D **68** (2003) 056005 [hep-ph/0302117]. 30

[57] H. Georgi, Phys. Lett. B **240**, 447 (1990). 30

[58] L. L. Foldy and S. A. Wouthuysen, Phys. Rev. **78**, 29 (1950). 30

[59] V. Pascalutsa, Hadronic J. Suppl. **16** (2001) 1. 31

[60] N. Fettes, U. G. Meissner, M. Mojzis and S. Steininger, Annals Phys. **283** (2000) 273 [Erratum-ibid. **288** (2001) 249] [arXiv:hep-ph/0001308]. 32, 33

[61] J. M. M. Hall and V. Pascalutsa, arXiv:1203.0724 [hep-ph]. 32

[62] M. E. Luke and A. V. Manohar, Phys. Lett. B **286** (1992) 348 [arXiv:hep-ph/9205228]. 32

[63] L. Girlanda, S. Pastore, R. Schiavilla and M. Viviani, Phys. Rev. C **81**, 034005 (2010) [arXiv:1001.3676 [nucl-th]]. 34

[64] B. A. Kniehl, A. A. Penin, V. A. Smirnov and M. Steinhauser, Nucl. Phys. B **635** (2002) 357 [hep-ph/0203166]. 36

[65] A. Pineda and J. Soto, Phys. Rev. D **59** (1999) 016005 [hep-ph/9805424]. 36, 54, 76

[66] A. V. Manohar and I. W. Stewart, Phys. Rev. D **76** (2007) 074002 [hep-ph/0605001]. 36

[67] D. B. Kaplan, M. J. Savage and M. B. Wise, Nucl. Phys. B **478**, 629 (1996) [arXiv:nucl-th/9605002]. 38, 62

[68] E. Epelbaum, W. Gloeckle and U. G. Meissner, Nucl. Phys. A **637** (1998) 107 [arXiv:nucl-th/9801064]. 38

[69] E. Epelbaum, W. Gloeckle and U. G. Meissner, Nucl. Phys. A **671** (2000) 295 [arXiv:nucl-th/9910064]. 38

[70] N. Kaiser, Phys. Rev. C **62**, 024001 (2000) [arXiv:nucl-th/9912054]. 38

[71] N. Kaiser, Phys. Rev. C **61** (2000) 014003 [arXiv:nucl-th/9910044]. 38

[72] N. Kaiser, Phys. Rev. C **64** (2001) 057001 [arXiv:nucl-th/0107064]. 38

[73] N. Kaiser, Phys. Rev. C **65** (2002) 017001 [arXiv:nucl-th/0109071]. 38

[74] M. Beneke and V. A. Smirnov, Nucl. Phys. B **522** (1998) 321 [hep-ph/9711391]. 38, 76

[75] M. E. Luke and A. V. Manohar, Phys. Rev. D **55**, 4129 (1997) [arXiv:hep-ph/9610534]. 42

[76] D. B. Kaplan, M. J. Savage and M. B. Wise, Phys. Lett. B **424** (1998) 390 [arXiv:nucl-th/9801034]. xvii, xviii, xix, xxiii, 42, 43, 76, 104

[77] D. B. Kaplan, M. J. Savage and M. B. Wise, Nucl. Phys. B **534**, 329 (1998) [arXiv:nucl-th/9802075].

[78] D. B. Kaplan, Nucl. Phys. B **494**, 471 (1997) [arXiv:nucl-th/9610052]. 42

[79] P. F. Bedaque and U. van Kolck, Phys. Lett. B **428**, 221 (1998) [arXiv:nucl-th/9710073]. 44

[80] P. F. Bedaque and H. W. Griesshammer, Nucl. Phys. A **671**, 357 (2000) [arXiv:nucl-th/9907077]. 44, 45

[81] H. W. Hammer, D. R. Phillips and L. Platter, Eur. Phys. J. A **32**, 335 (2007) [arXiv:0704.3726 [nucl-th]]. 44, 45

[82] S. R. Beane and M. J. Savage, Nucl. Phys. A **694**, 511 (2001) [arXiv:nucl-th/0011067]. 44

[83] E. Epelbaum, H. W. Hammer and U. G. Meissner, arXiv:0811.1338 [nucl-th]. 44, 45, 62

[84] S. Fleming, T. Mehen and I. W. Stewart, Nucl. Phys. A **677**, 313 (2000). 62, 76, 102

[85] S. Fleming, T. Mehen and I. W. Stewart, Phys. Rev. C **61**, 044005 (2000). 54, 75, 76

[86] U. van Kolck, Nucl. Phys. A **645**, 273 (1999). 43, 60

[87] T. Mehen, I. W. Stewart and M. B. Wise, Phys. Rev. Lett. **83**, 931 (1999). 47, 62

[88] S. i. Ando and C. H. Hyun, Phys. Rev. C **72**, 014008 (2005). 47, 49, 53

[89] S. i. Ando and K. Kubodera, Phys. Lett. B **633**, 253 (2006). 47

[90] S. Ando, R. H. Cyburt, S. W. Hong and C. H. Hyun, Phys. Rev. C **74**, 025809 (2006). 47

[91] D. Eiras and J. Soto, Eur. Phys. J. A **17**, 89 (2003). 47

[92] A. Pineda and J. Soto, Nucl. Phys. Proc. Suppl. **64**, 428 (1998). 48, 51

[93] J. Mondejar and J. Soto, Eur. Phys. J. A **32**, 77 (2007). 48

[94] V. Bernard, N. Kaiser and U. G. Meissner, Z. Phys. C **60**, 111 (1993). 48, 49

[95] A. V. Manohar, Phys. Rev. D **56**, 230 (1997). 54

[96] M. Pavon Valderrama and E. Ruiz Arriola, Phys. Rev. C **72**, 054002 (2005). 76

[97] A. Nogga, R. G. E. Timmermans and U. van Kolck, Phys. Rev. C **72**, 054006 (2005). 51, 76

[98] M. Pavon Valderrama and E. Ruiz Arriola, Phys. Rev. C **74**, 064004 (2006) [Erratum-ibid. C **75**, 059905 (2007)]. 51, 76

[99] S. R. Beane, P. F. Bedaque, M. J. Savage and U. van Kolck, Nucl. Phys. A **700**, 377 (2002). 51, 76

[100] S. R. Beane, D. B. Kaplan and A. Vuorinen, arXiv:0812.3938 [nucl-th]. 51, 73, 74, 76

[101] C. J. Yang, C. Elster and D. R. Phillips, arXiv:0901.2663 [nucl-th]. 51, 74, 76

[102] C. J. Yang, C. Elster and D. R. Phillips, arXiv:0905.4943 [nucl-th]. 51, 76

51, 76

[103] S. Durr *et al.*, Phys. Lett. B **701**, 265 (2011) [arXiv:1011.2403 [hep-lat]]. 99

[104] E. Epelbaum, U. G. Meissner and W. Gloeckle, Nucl. Phys. A **714**, 535 (2003) [arXiv:nucl-th/0207089]. 73, 74

[105] S. R. Beane and M. J. Savage, Nucl. Phys. A **717**, 91 (2003) [arXiv:nucl-th/0208021]. 73, 74

[106] M. Procura, T. R. Hemmert and W. Weise, Phys. Rev. D **69**, 034505 (2004) [arXiv:hep-lat/0309020]. 54

[107] M. Fukugita, Y. Kuramashi, H. Mino, M. Okawa and A. Ukawa, Phys. Rev. Lett. **73**, 2176 (1994) [arXiv:hep-lat/9407012]. 71

[108] M. Fukugita, Y. Kuramashi, M. Okawa, H. Mino and A. Ukawa, Phys. Rev. D **52**, 3003 (1995) [arXiv:hep-lat/9501024]. 71

[109] S. Aoki, T. Hatsuda and N. Ishii, Comput. Sci. Dis. **1**, 015009 (2008) [arXiv:0805.2462 [hep-ph]]. 72

[110] S. R. Beane, P. F. Bedaque, K. Orginos and M. J. Savage, Phys. Rev. Lett. **97**, 012001 (2006) [arXiv:hep-lat/0602010]. 72, 76

[111] S. R. Beane *et al.* [NPLQCD Collaboration], Phys. Rev. D **81**, 054505 (2010) [arXiv:0912.4243 [hep-lat]]. 72, 76

[112] M. R. Schindler and D. R. Phillips, Annals Phys. **324**, 682 (2009) [Erratum-ibid. **324**, 2051 (2009)] [arXiv:0808.3643 [hep-ph]]. 72, 94

[113] E. Epelbaum, U. G. Meissner and W. Gloeckle, arXiv:nucl-th/0208040. 73, 74

[114] J. -W. Chen, T. -K. Lee, C. -P. Liu and Y. -S. Liu, arXiv:1012.0453 [nucl-th]. 74

[115] G. Ecker, Prog. Part. Nucl. Phys. **36**, 71 (1996) [arXiv:hep-ph/9511412]. 83

[116] A. Dobado, M. J. Herrero and T. N. Truong, Phys. Lett. B **235**, 134 (1990). 79

[117] A. Dobado and J. R. Pelaez, Phys. Rev. D **56**, 3057 (1997) [arXiv:hep-ph/9604416]. 79

[118] J. A. Oller and E. Oset, Nucl. Phys. A **620**, 438 (1997) [Erratum-ibid. A **652**, 407 (1999)] [arXiv:hep-ph/9702314]. 79

[119] J. A. Oller, E. Oset and J. R. Pelaez, Phys. Rev. Lett. **80**, 3452 (1998) [arXiv:hep-ph/9803242]. 79

[120] J. A. Oller, E. Oset and J. R. Pelaez, Phys. Rev. D **59**, 074001 (1999) [Erratum-ibid. D **60**, 099906 (1999)] [Erratum-ibid. D **75**, 099903 (2007)] [arXiv:hep-ph/9804209]. 79

[121] I. Caprini, G. Colangelo and H. Leutwyler, Phys. Rev. Lett. **96**, 132001 (2006) [arXiv:hep-ph/0512364]. xx, 79, 91, 105

[122] H. Leutwyler, AIP Conf. Proc. **1030**, 46 (2008) [arXiv:0804.3182 [hep-ph]]. 79

[123] R. Garcia-Martin, R. Kaminski, J. R. Pelaez and J. Ruiz de Elvira, Phys. Rev. Lett. **107**, 072001 (2011) [arXiv:1107.1635 [hep-ph]]. 79

[124] S. Weinberg, Phys. Rev. **131**, 440 (1963). 79

[125] R. Baron *et al.* [ETM Collaboration], JHEP **1008**, 097 (2010) [arXiv:0911.5061 [hep-lat]]. xix, 80, 93, 96, 99, 102, 105

[126] G. Ecker, J. Gasser, A. Pich and E. de Rafael, Nucl. Phys. B **321**, 311 (1989). 81, 87, 96, 98

[127] V. Cirigliano, G. Ecker, M. Eidemuller, R. Kaiser, A. Pich and J. Portoles, Nucl. Phys. B **753** (2006) 139 [hep-ph/0603205]. 81

[128] I. Rosell, P. Ruiz-Femenia and J. Portoles, JHEP **0512** (2005) 020 [hep-ph/0510041]. 81, 87

[129] I. Rosell, J. J. Sanz-Cillero and A. Pich, JHEP **0701** (2007) 039 [hep-ph/0610290]. 87

[130] J. Portoles, I. Rosell and P. Ruiz-Femenia, Phys. Rev. D **75** (2007) 114011 [hep-ph/0611375]. 87

[131] I. Rosell, J. J. Sanz-Cillero and A. Pich, JHEP **0408** (2004) 042 [hep-ph/0407240]. 87

[132] M. Luscher and P. Weisz, Nucl. Phys. B **290**, 25 (1987). 81

[133] J. Frohlich, Nucl. Phys. B **200**, 281 (1982). 81

[134] M. Gell-Mann and M. Levy, Nuovo Cim. **16**, 705 (1960). 82

[135] S. Gasiorowicz and D. A. Geffen, Rev. Mod. Phys. **41**, 531 (1969). 82

[136] C. Hanhart, J. R. Pelaez and G. Rios, Phys. Rev. Lett. **100** (2008) 152001 [arXiv:0801.2871 [hep-ph]]. 91

[137] J. R. Pelaez and G. Rios, Phys. Rev. D **82** (2010) 114002 [arXiv:1010.6008 [hep-ph]]. 91

[138] G. Colangelo, J. Gasser and H. Leutwyler, Nucl. Phys. B **603**, 125 (2001) [arXiv:hep-ph/0103088]. 92, 93, 95, 100

[139] Z. Fu, Commun. Theor. Phys. **57**, 78 (2012) [arXiv:1110.3918 [hep-lat]]. 93, 99, 101, 102

[140] J. R. Batley *et al.* [NA48-2 Collaboration], Eur. Phys. J. C **70**, 635 (2010). 93

[141] T. Yamazaki *et al.* [CP-PACS Collaboration], Phys. Rev. D **70**, 074513 (2004) [arXiv:hep-lat/0402025]. 99

[142] J. W. Chen, D. O'Connell, R. S. Van de Water and A. Walker-Loud, Phys. Rev. D **73**, 074510 (2006) [arXiv:hep-lat/0510024]. 99

[143] S. R. Beane, T. C. Luu, K. Orginos, A. Parreno, M. J. Savage, A. Torok and A. Walker-Loud, Phys. Rev. D **77**, 014505 (2008) [arXiv:0706.3026 [hep-lat]]. 99

[144] X. Feng, K. Jansen and D. B. Renner, Phys. Lett. B **684**, 268 (2010) [arXiv:0909.3255 [hep-lat]]. 99

[145] J. J. Dudek, R. G. Edwards, M. J. Peardon, D. G. Richards and C. E. Thomas, Phys. Rev. D **83**, 071504 (2011) [arXiv:1011.6352 [hep-ph]]. 99

[146] S. R. Beane *et al.* [NPLQCD Collaboration], arXiv:1107.5023 [hep-lat]. 99

[147] T. Yagi, S. Hashimoto, O. Morimatsu and M. Ohtani, arXiv:1108.2970 [hep-lat]. 99

[148] G. Amoros, J. Bijnens and P. Talavera, Nucl. Phys. B **568**, 319 (2000) [arXiv:hep-ph/9907264]. 102

[149] R. Contino, C. Grojean, M. Moretti, F. Piccinini and R. Rattazzi, JHEP **1005**, 089 (2010) [arXiv:1002.1011 [hep-ph]]. 102, 105

[150] R. Machleidt, Phys. Rev. C **63**, 024001 (2001) [arXiv:nucl-th/0006014]. 102, 105